NTNU

Norwegian University of
Science and Technology

Photovoltaic Power Prediction and Control Strategies of the Local Storage Unit at Campus Evenstad

Lene Marie Hope Rognan

Master of Energy and Environmental Engineering
Submission date: July 2018
Supervisor: Olav B Fosso, IEL
Co-supervisor: Igor Sartori, SINTEF

Norwegian University of Science and Technology
Department of Electric Power Engineering

Abstract

This thesis represents a building block for future model predictive control of a battery connected to a complex energy system consisting of a photovoltaic (PV) system and a combined heat and power (CHP) plant. The complex energy system at Campus Evenstad in Norway is used a case study in this thesis. The aim of this thesis is bipartite: (1) the performance of the PV system is to be predicted, and (2) various control strategies of the battery will be investigated to see the flexibility that the battery may provide for the end-user. Two models have hence been developed: a PV model and an optimization model of the battery. Both models have been developed in Python with the help of the PVLIB and the Pyomo libraries.

Two approaches to estimate the plane-of-array (POA) irradiance on the PV array were tested in the PV model: the `dirindex` and the `erbs` irradiance decomposition methods, which are both built-in functions in the PVLIB library. Results showed that the `dirindex` decomposition method gave the most accurate results. However, results for winter months are highly inaccurate, and hence the PV model should be improved to better predict the PV performance in such months. The model was also tested with various overall PV system efficiencies and surface types indicating how much reflected solar radiation that hits the receiver. An overall system efficiency of 74% and surface type *asphalt* resulted in the most accurate PV estimation.

The optimization model was solved with three different objectives: (1) minimization of total import of electricity, (2) minimization of spot energy costs, and (3) peak shaving. In addition to analyzing the charge and discharge of the battery, the total cost of import was calculated for each control strategy. When using the battery to minimize the total import from the grid, the battery is not frequently used. The only recharging of the battery that takes place is a result of low demand in times of high PV production. The minimization of the spot energy cost control strategy reduces the energy cost of the imported electricity, but low spot prices lead to an increase in the import peak and hence an increase in the grid tariff cost. The total import cost of this control strategy comes out higher than the total cost of the other two control strategies. The variation in spot prices results in a rapid charge and discharge of the battery. Optimizing the utilization of the battery with the objective of performing peak shaving, the grid tariff, which is determined by the highest import peak in the last 12 months, is reduced. The grid tariff makes up the highest share of the total cost of import, and hence does this control strategy result in the lowest total cost.

Sammendrag

Denne masteroppgaven representerer en byggestein for å i framtiden oppnå model prediktiv regulering av et batteri koblet til et sammensatt energisystem bestående av et fotovoltaisk (PV) system og et kraftvarmeanlegg (CHP). Det sammensatte energisystemet på Campus Evenstad ved Høgskolen i Innlandet er brukt som et case-studie i denne masteroppgaven. Målet med denne oppgaven er todelt: (1) PV systemets ytelse skal forutsees, og (2) ulike kontrollstrategier av batteriet skal testes for å illustrere fleksibiliteten batteriet i et sammensatt energisystem representerer. To modeller har dermed blitt utviklet i denne masteroppgaven: en PV modell og en optimeringsmodell for batteriet. Begge modellene har blitt utviklet i Python, ved hjelp av de to bibliotekene PVLIB og Pyomo.

To tilnærminger for å estimere solinnstrålingen på et skrått plan ble testet i PV modellen: `dirindex` og `erbs` dekomposisjoneringsmetoder som begge er innebygde funksjoner i PVLIB. Resultatene viste at `dirindex` gav mer nøyaktige resultater. I vintermånedene ble PV produksjonen estimert til å være mye større enn historiske data tilsa, og PV modellen bør derfor forbedres for å forutsi PV prouksjonen på vinterstid mer nøyaktig. PV modellen ble kjørt med ulike systemvirkningsgrader og ulike typer jordoverflater som indikerer hvor mye reflektert solinnstråling som treffer PV panelene. En systemvirkningsgrad på 74% og overflate *asfalt* resulterte i mest nøyaktige estimater av PV produksjonen.

Optimeringsmodellen ble løst med tre ulike objektiver: (1) minimering av total import av strøm, (2) minimering av spot-energikostnad, og (3) peak shaving. I tillegg til å analysere oppladningen og utladningen av batteriet ble den totale kostnaden av import beregnet for hver kontrollstrategi. Ved minimering av total import av energi ble ikke batteri hyppig brukt. Den eneste oppladningen av batteriet fant sted da lasten var lav og PV produksjonen var høy. Ved minimering av spot-energikostnad ble energikostnaden av importert energy redusert, men lave spotpriser resulterte i økt import-peak, og dermed økt nettleie. Den totale kostnaden av import var derfor størst for denne kontrollstrategien. Variasjonene i spotpris førte til rask opp- og utladning av batteriet. Nettleien var lavest da peak shaving ble utført. Nettleien utgjør den største andelen av totalkostnadene for importert energi, og dermed resulterte peak shaving i lavest totale kostnader.

Preface

This master's thesis has been carried out at the Department of Electric Power Engineering during the spring semester of 2018, and marks the end of the five year master's programme in Energy and Environmental Engineering at the Norwegian University of Science and Technology (NTNU). The thesis has been supervised by Professor Olav Bjarte Fosso (NTNU) and Igor Sartori (SINTEF).

This thesis is thought to be a prework to future model predictive control of batteries implemented in existing electrical energy system. The complex energy system at Campus Evenstad at Inland Norway University of Applied Sciences (INN University) has been used as a case study in this thesis. However, the principles of the models developed in this thesis may also applied to other energy systems. In addition to optimizing the use of the battery based on selected control strategies, a model has been created to predict the performance of the photovoltaic (PV) system from measured solar radiation and ambient temperature.

Trondheim, July 23, 2018

Lene Marie Hope Rognan

Acknowledgment

The process of writing this thesis has indeed been a journey, and I owe many people my deepest gratitude for their valuable contributions. Firstly, I would like to thank my supervisor at NTNU, Professor Olav Bjarte Fosso, for his weekly supervision and guidance. He has been patient, and a great support for me in the process of writing this thesis. I am especially grateful for how he has let me be apart of the discussion when formulating the problem description of this thesis. I would also like to thank my co-supervisor at SINTEF, Igor Sartori, for agreeing to take me in and let me be apart of the on-going development at Campus Evenstad at the INN University on such short notice. Without him, conducting my thesis on a real-case complex energy system including a photovoltaic system with energy storage would not have been possible.

Through my co-supervisor, Igor Sartori, I have also been introduced to other people that became important when gathering necessary information for the specific case of Campus Evenstad. Among these are Tor Sveinar Rugsveen at Statsbygg who invited me to come visit Campus Evenstad, Ola Johansson at Solspesialisten, and Øystein Holm at Multiconsult. Both Ola Johanssen and Øystein Holm have given me valuable advise in relation to the modeling of the complex energy system at Campus Evenstad, and they have also provided me with necessary data on the existing photovoltaic system and battery system on campus. Further, I would like to thank Øyvind Kaaresen at Kinect Energy Group for providing hourly production data of the photovoltaic system at Campus Evenstad, and thus saving me from the time consuming job of downloading hourly data daily from the Sunny Portal.

Lastly, I have to thank everyone that has contributed to make my time at NTNU unforgettable, including professors, fellow students, friends, and family

Contents

List of Figures

List of Tables

Acronyms

AC Alternating Current

CHP Combined Heat and Power

DC Direct Current

DHI Diffuse Horizontal Irradiance

DNI Direct Normal Irradiance

DoD Depth-of-Discharge

GHI Global Horizontal Irradiance

MPP Maximum Power Point

MPPT Maximum Power Point Tracking

NOCT Nominal Operating Cell Temperature

NVE Norges Vassdrags- og Energidirektorat

POA Plane-of-Array

PV Photovoltaic

SOC State of Charge

STC Standard Test Conditions

Nomenclature

Greek Letters

β	Elevation angle	°
η_{sys}	Overall PV system efficiency	%
γ_T	Temperature coefficient	$\%/°C$
ϕ_s	Solar azimuth angle	°
θ_z	Zenith angle	°
δ	Declination angle	°

Roman Letters

I_0	Reverse saturation current	A
I_d	Diode current	A
I_{SC}	Short-circuit current	A
G	Irradiance	W/m^2
H	Hour angle	°
L	Latitude angle	°

Chapter 1

Introduction

1.1 Motivation

Power generation from renewables is increasing rapidly worldwide. Approximately 70% of the global power capacity added in the year 2017 was accounted for by renewable energy sources. Solar photovoltaic (PV) stands for the largest contribution with its 55%. As of the exit of 2017, 402 GW_p of solar PV DC capacity was installed globally. This represents an increase of 99 GW compared to values registered in 2016. China is the leading country when it comes to investment, capacity installment and production of solar PV power. [1]

At the exit of 2016, the total installed PV capacity in Norway was approximately 27 MW_p. Most of the PV systems installed in Norway are private off-grid systems at cabins. There has, however, been a significant increase in grid-connected PV systems in private and commercial buildings since 2013-2014. Grid-connected PV systems accounted for the majority of the installed PV capacity in Norway at the exit of 2016, with approximately 13.6 MW_p. The largest grid-connected PV system in Norway has an installed capacity of 3.38 MW_p. The PV power production is directly dependent on the solar irradiance. Although Norway is not known for its warm climate and long sunlight hours, measurements show that the solar irradiance values in the South of Norway are close to the level measured in parts of Germany. [2, 3]

Although solar PV is not yet economically attractive in Norway, mainly due to the low electricity prices, the use of solar PV is expected to increase with the continuously decreasing cost of PV technology, the expected increase in Norwegian electricity prices, and with the increasing consumer interest and awareness. [3]

The use of energy storage in combination with solar PV is becoming more common. The

global energy storage capacity as of 2017 is measured to be 158.9 GW, where electrochemical batteries accounted for 2.3 GW of the total. In 2017, lithium-ion batteries made up the majority of added battery capacity installment [1]. In addition to ensuring storage of energy, batteries also hold other important functions. For grid-connected systems, the main function of the battery is often to balance power fluctuations to meet the requirements of the connected grid. However, batteries can also be used for other purposes, such as peak shaving. Reducing power peaks potentially holds economical savings, both for end-users and grid operators [4]. Norwegian energy spot prices are expected to increase by 0.8 - 1.6 % annually towards 2030. Grid tariffs are also expected to increase in the coming years due to the planned investments for the modernization of the network infrastructure [5]. With the implementation of a battery system, the PV system owner achieves greater flexibility in how the energy system is managed and controlled in terms of both importation and exportation of electricity.

The motivation for writing this thesis is the continuous growth of solar PV systems and how the implementation of batteries in such systems improve the end user's flexibility when it comes to grid interaction. Campus Evenstad at the INN University in Norway holds a complex electrical energy system, consisting of a PV system, a combined heat and power (CHP) plant, and a battery system. The complex energy system at Campus Evenstad with the implemented battery system is used as a case study in this thesis.

1.2 Problem Formulation

This thesis represents a springboard for future model predictive control of a battery connected to a PV system. The aim of this thesis is divided into two parts:

1. The performance of the PV system is to be predicted based on site-specific meteorological data.
2. Various control strategies of the battery are tested and analyzed to recognize the flexibility that the battery provides for the end-user.

To meet the aims of the thesis, a PV model and an optimization model are developed. Various commercial programs for predicting PV performance exists. When using such programs, the user is often unaware of how the program actually works due to the many built-in functions and assumptions on which performance calculations are based. A motivation has been to develop skills within software programming while understanding the fundamentals of the PV model and the optimization model. Therefore, already existing PV performance estimation programs are not used in this thesis. Instead, a PV model is developed in Python by the author of this thesis. The PVLIB library is used as a tool in the decomposition and transposition of solar radiation. The optimization model for optimizing the use of the battery, provided the desired objective, is developed in Pyomo. The chosen control strategies that the battery utilization is optimized for are:

1. Minimization of total importation of electricity.
2. Minimization of spot energy costs.
3. Peak shaving.

The choice of using Python as programming language is based on the fact that many developers are starting to prefer Python over other programming languages as Python is free, open-source, and that it can easily be translated to other programming languages.

The complex energy system at Campus Evenstad at INN University in Norway is used as a case study in this thesis. With some adjustments, the developed PV model and the optimization model may in theory also be applied to other complex energy systems.

1.3 Limitations

Most of the limitations of this thesis are related to the access of data. The act of accessing good quality meteorological data is challenging, especially solar radiation data. In general, solar radiation is not well documented in Norway. The weather station at Evenstad is one of the many weather stations in Norway where solar radiation is not measured. The access to other relevant data, such as historical data on PV production and electricity demand at Campus Evenstad, is also limited. The CHP plant at Campus Evenstad is heat-driven, and as the heat demand on campus is considered to be out-of-scope in this thesis, the CHP plant's contribution to on-site electricity generation is not well accounted for in this thesis. In lack of historical data on the CHP's electricity production, simplifications are made when modeling the CHP plant.

1.4 Structure of the Thesis

Chapter 1 An introduction to the thesis is given in Chapter 1. The background and motivation for writing the thesis are given. The problem formulation is described, and limitations related to the thesis are addressed.

Chapter 2 Chapter 2 gives a brief introduction to Campus Evenstad at INN University, and why Campus Evenstad has become a field of interest for many parties.

Chapter 3 An introduction to the solar resource and the theory behind solar energy is given in this chapter. This chapter is, to a great extent, based on the specialization project [6] written by the author of this thesis and fellow student Maren Haugland Hansen conducted in the autumn semester of 2017.

Chapter 4 In Chapter 4, the technological operation principles of the main system components of the energy system at Campus Evenstad are explained. This chapter is necessary in order to understand the modulation of the complex energy system in question.

Chapter 5 In this chapter, relevant data for performing the modulation is presented. This includes site-specific meteorological data, historical data of the PV production and the imported electricity, and system specific data of the PV panel and the battery. An introduction to grid tariffs and energy prices is also given.

Chapter 6 Chapter 6 provides a short introduction to the programming theory of the modeling performed in this thesis.

Chapter 7 This chapter gives a detailed presentation of the functions and equations used in the system modeling, both in the PV model and in the optimization model. The different control strategies used in the optimization model are well explained and exemplified.

Chapter 8 The results of the developed PV model and the optimization model are presented and discussed in chapter 9. Results are mainly presented in tables and plots.

Chapter 9 A short conclusion is made in this chapter based on the results and discussion presented in Chapter 8.

Chapter 10 Chapter 10 includes suggestions to further work.

Chapter 2

Campus Evenstad

Campus Evenstad is one of three campuses at Inland Norway University of Applied Sciences (INN University). The campus is owned by Statsbygg, which is a state-owned management company under the Ministry of Local Government and Modernisation. An overview of Campus Evenstad is given in Fig. 2.1.

FIGURE 2.1: Overview of Evenstad Campus. Photo provided by SINTEF.

Over the years, Campus Evenstad has become a field of interest, and many parties are involved in the continuous development of the campus. Through a collaboration with SINTEF, one of Europe's largest independent research institutes, and the Norwegian National

Research Centre on Zero Emission Buildings (ZEB), a ZEB-COM (ZEB - Construction, Operation, Materials) building was built on campus in 2016. This building was the first of its kind in Norway. A roof-mounted PV system was installed in 2013. In 2016, a CHP plant was installed. Thermal solar collectors are also present on campus, and in time of writing this thesis (June 2018), a battery system is installed. [7]

Campus Evenstad is currently self-sufficient with heat. The long-term aim of Statsbygg is, however, that the campus also will become 100% self-sufficient with electricity. With today's electricity situation, this is far from the reality, but the installation of the battery system is considered to be a step in the right direction. As the focus of this thesis is the complex electrical energy system at Campus Evenstad, the heat production on campus will not be considered in this thesis.

Chapter 3

Solar Resource and Photovoltaic Systems

The majority of the theory presented in this chapter is taken from the specialization project [6] conducted in autumn 2017 by the author of this thesis and fellow student Maren Haugland Hansen. The specialization project is unpublished but can be made available by NTNU on request.

3.1 The Solar Resource

The sun is the earth's most significant source to energy. Earth receives on average $1.2 \times 10^{17} W$ of power from the sun [8]. Although the sun emits more power than the human population can use, the availability of solar energy is dependent on the characteristics of the sun. [6]

3.1.1 The Solar Spectrum

All objects emit a certain amount of radiant energy at a given temperature. The sun behaves almost like a blackbody at 5800 K, i.e., it behaves as a perfect emitter and absorber. Figure 3.1 shows the extraterrestrial solar spectrum, the spectrum just outside the earth's atmosphere, and a blackbody at 5800 K in the same graph. Irradiance, measured in W/m^2, is a measure of the power density of solar radiation, while irradiation, is a measure of energy, indicating the amount of irradiance over time, viewed as the area under the blackbody curve in Fig. 3.1. Only 47% of the solar spectrum is visible, as illustrated in the Fig. 3.1. [6, 9]

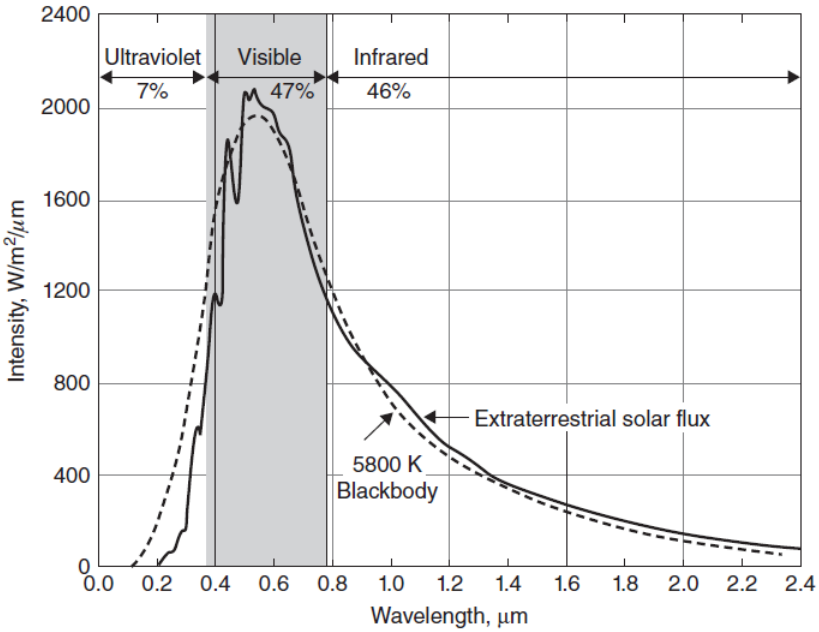

FIGURE 3.1: Comparison of the solar spectrum with a blackbody at 5800 K. Figure from [9].

Air mass (AM) is a measure of how much power that is lost due to the absorption of radiation in the atmosphere. The air mass ratio, m, provides a relation between the actual path that sunlight takes to reach a certain point on the earth's surface and the shortest possible path it, in theory, could take. This relation is given in Eq. (3.1), where θ_z is the zenith angle [6, 8]. The zenith angle is explained in Section 3.1.3.

$$m = \frac{1}{\cos(\theta_z)} \tag{3.1}$$

The air mass ratio hence depends on the relative position of the sun. When the sun is directly overhead, $m = 1$, which abbreviates to AM1. AM1.5 is generally assumed to be the solar spectrum at the earth's surface on a regular day [9]. AM1.5 corresponds to a zenith angle of 48.2° and an irradiance of 1 kW/m^2 on a clear day. [6, 8]

3.1.2 Solar Radiation

Site-specific solar radiation must be assessed when designing PV systems. Not all of the radiation that the sun emits reaches the surface of the earth; some is scattered in the atmosphere. Direct radiation, also called beam radiation, is the radiation that directly hits a receiver without any impact from the atmosphere. If the direction has been affected by the atmosphere, i.e., scattered by clouds or other molecules, the radiation is referred to as diffuse radiation.

Radiation that reaches a receiver due to reflection is called albedo radiation. Albedo is only considered for tilted planes, i.e., albedo is neglected for horizontal planes. The total solar radiation is known as the global radiation. The sunlight's components are illustrated in Fig. 3.2. [6, 10, 11]

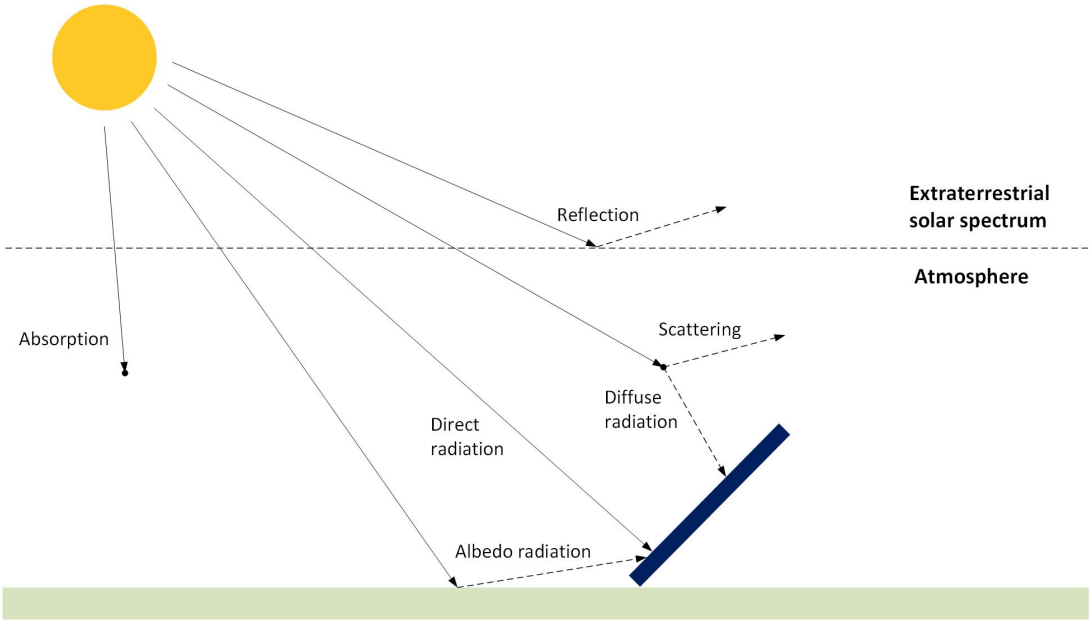

FIGURE 3.2: The components of the sun.

For a horizontal plane, global horizontal irradiance (GHI) may be decomposed into its direct normal irradiance (DNI) and diffuse horizontal irradiance (DHI) components. GHI is given as the sum of DHI and DNI multiplied with the zenith angle, θ_z, as shown in Eq. (3.2). [12]

$$GHI = DNI \cdot \cos\theta_z + DHI \tag{3.2}$$

The DHI is found from Eq. (3.3), where DF is the diffuse radiation fraction. The diffuse radiation on a tilted surface can be calculated using either analytic models or empirical models [13]. The DNI can further be found by substituting Eq. (3.3) into Eq. (3.2) and solve for DNI.

$$DHI = DF \cdot GHI \tag{3.3}$$

For a tilted surface, the plane-of-array (POA) global irradiance is given by Eq. (3.4), where POA_{dir} is the direct irradiance incident on the plane-of-array, and $POA_{diff,refl}$ and $POA_{diff,sky}$ are the ground reflected diffuse and the sky diffuse irradiance, respectively [14].

$$POA = POA_{dir} + POA_{diff,refl} + POA_{diff,sky} \tag{3.4}$$

The conversion from GHI on a horizontal surface to POA irradiance on a tilted surface is done through the use of transposition models. Several transposition models are in use. Different models require various input data, and hence is the availability of data a limiting factor when choosing transposition method. A comparison of some of the transposition models in use, conducted in [14], shows that estimations of the POA irradiance vary depending on the transposition model used when providing all models with the same GHI as input. [14]

3.1.3 Solar Position

The distribution of solar radiation is dependent on the geometric relationship between the earth and the sun. When size, location, and orientation of solar modules are to be determined, knowledge about solar angles and the position of the sun is important.

Solar elevation and zenith The solar elevation angle, β, and the zenith angle, θ_z, are complementary angles. β is the angle between a horizontal plane and the rays of the sun, i.e., it describes the angular height of the sun seen from the horizon. θ_z is the angle between the sunlight and an axis perpendicular to the site where the sunlight hits [10]. The two angles can be found from Eq. (3.5), where L represents the geographical latitude and δ is the declination angle. [6]

$$\sin\beta = \sin\delta \sin L + \cos\delta \cos L \cos H = \cos\theta_z \tag{3.5}$$

As the elevation angle and the zenith angle are complementary angles, the relation between them can alternatively be expressed as in Eq. (3.6). The two angles are illustrated in Fig. 3.3.

$$\theta_z = 90° - \beta \tag{3.6}$$

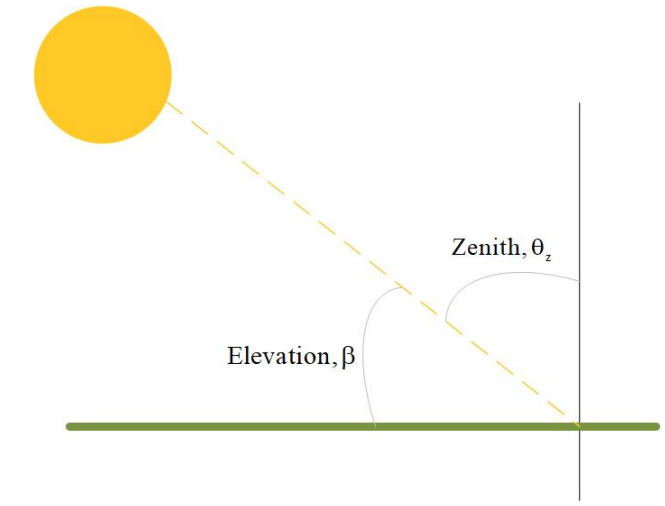

FIGURE 3.3: Solar elevation and zenith angle.

Solar azimuth The direction of the sun is defined by the solar azimuth angle, ϕ_s, and is dependent on the specific latitude, day number, and time of day. The solar azimuth angle is defined as zero at solar noon. The solar azimuth angle can be found using Eq. (3.7),

$$\sin\phi_s = \frac{\cos\delta \sin H}{\cos\beta} \tag{3.7}$$

where H is the hour angle describing the angular displacement of the sun. The hour angle can also be used to calculate the time of sunrise and sunset [6, 8]. The solar azimuth angle is illustrated in Fig. 3.4.

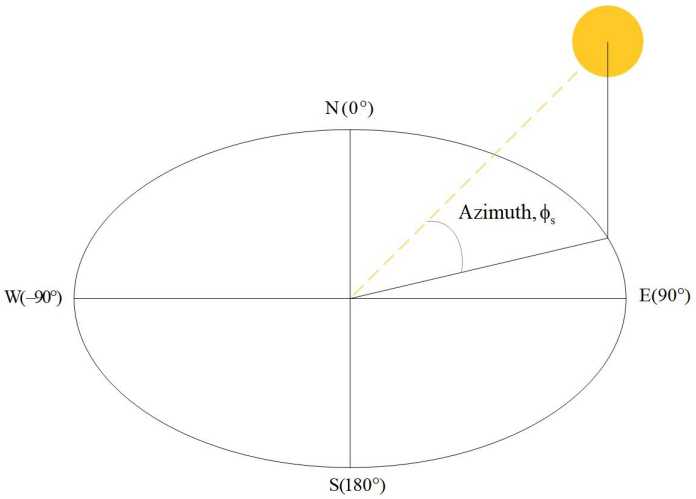

FIGURE 3.4: Solar azimuth angle.

Solar declination The declination angle, δ, illustrated in Fig. 3.5, is the angle between the equatorial plane and the line drawn between the center of the sun and the center of the earth. The declination angle ranges from +23.45° to -23.45° at the summer and winter solstice respectively, and can be calculated from Eq. (3.8), where N is the N^{th} day of the year. The summer solstice is defined as the day of the year with the highest amount of daytime hours and is set to June 21. The winter solstice occurs on December 21. [6, 9]

$$\delta = 23.45 \sin\left[\frac{360}{365}(284 + N)\right] \tag{3.8}$$

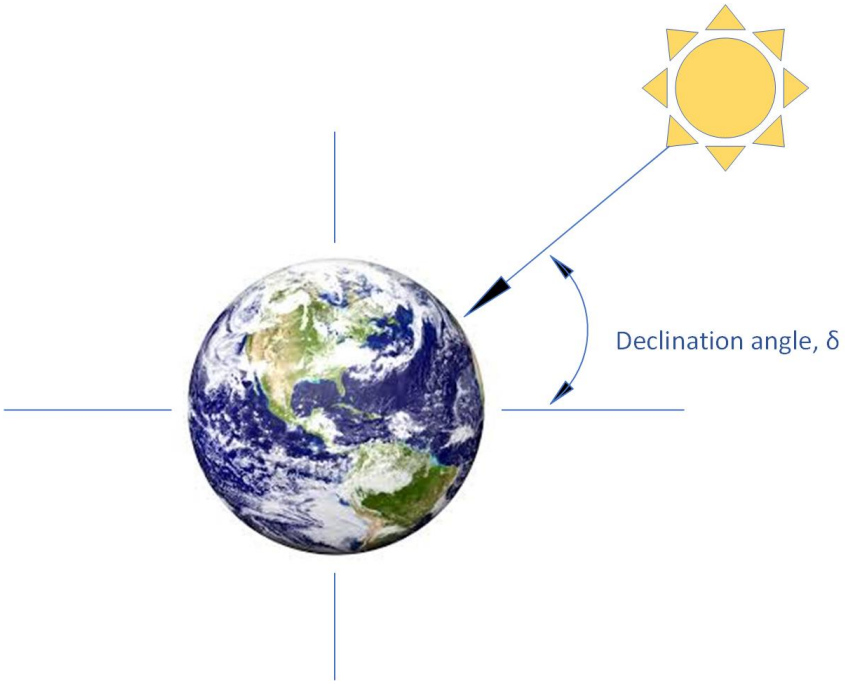

FIGURE 3.5: Solar declination angle.

Chapter 4

Energy System Components at Campus Evenstad

Figure 4.1 shows the components of the complex electrical energy system at Campus Evenstad. The theory behind PV systems, converters, batteries and CHP plants is introduced in the following sections of this chapter.

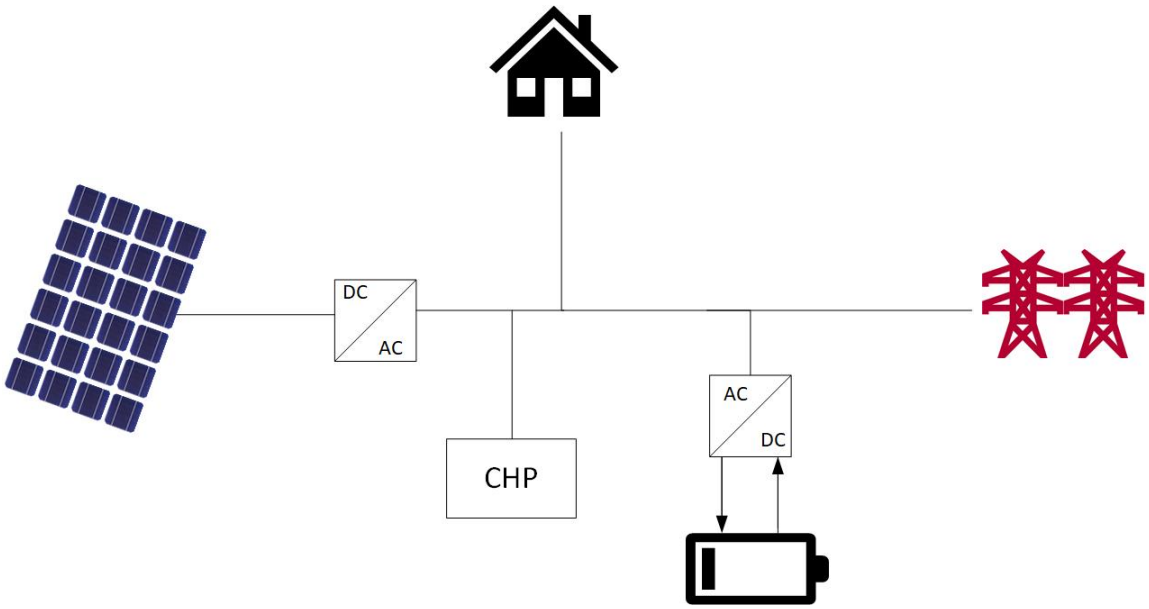

FIGURE 4.1: System components at Campus Evenstad.

Large parts of the theory presented in this chapter are taken from the specialization project [6] written by the author of this thesis and fellow student Maren Haugland Hansen in autumn 2017. The specialization project is unpublished but can be made available by NTNU on request.

4.1 The Photovoltaic System

There are two overall categories when it comes to PV systems: grid-connected PV systems and stand-alone PV systems. The main difference between grid-connected systems and stand-alone systems is that the grid-connected system is connected to a utility grid and can hence import electricity in times when the PV system is not able to generate the required amount of energy demanded by the load. In times of overproduction, the grid-connected PV system may export excess energy to the grid, thus preventing the generated energy from going to waste. Stand-alone PV systems may be connected to a backup generator which can provide power when the PV production is insufficient. In Norway, stand-alone PV systems are typically found in cabins. The PV system at Campus Evenstad is a grid-connected system. [6, 9, 15]

4.1.1 The Photovoltaic Cell

The simplest representation of a PV cell is through an equivalent circuit consisting of a real diode in parallel with an ideal current source, as illustrated in Fig. 4.2.

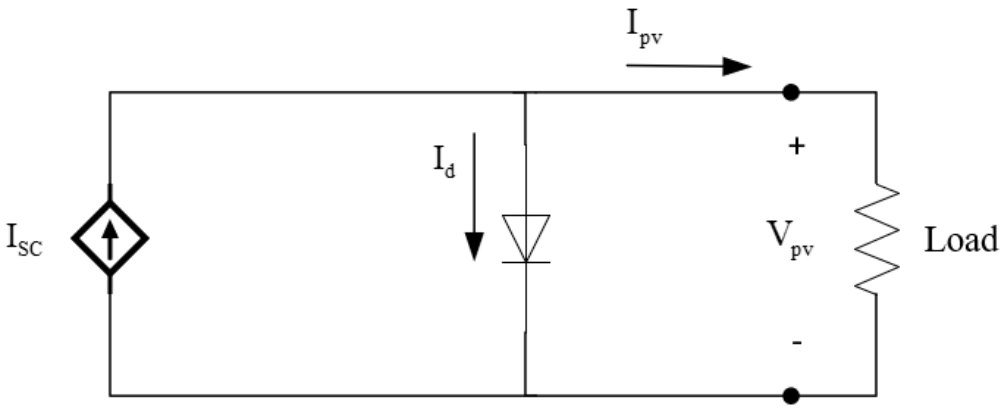

FIGURE 4.2: Equivalent circuit of a PV cell.

The output current of the PV cell, I, is given in Eq. (4.1) according to Kirchhoff's current law (KCL).

$$I = I_{SC} - I_d \tag{4.1}$$

The current passing through the diode, I_d, is given by the Shockley diode equation. By substituting I_d in Eq. (4.1) with the Shockley diode equation, the PV cell's output current

can be expressed as in Eq. (4.2), where $q = 1.602 \times 10^{-19} C$ is the electron charge and $k = 1.38 \times 10^{-23} J/K$ is the Boltzmann's constant. I_0 is the reverse saturation current, while T represents the temperature at the junction measured in Kelvin. [6, 9]

$$I = I_{SC} - I_0(e^{qV_{pv}/kT} - 1) \tag{4.2}$$

The PV cell can be modeled more accurately by adding a parallel leakage resistance, R_p, and a series resistance, R_s, to the equivalent circuit. The parallel and series resistances are added to achieve a better indication of the power generated when for instance the PV cell is exposed to shading. The modified equivalent circuit is given in Fig. 4.3.

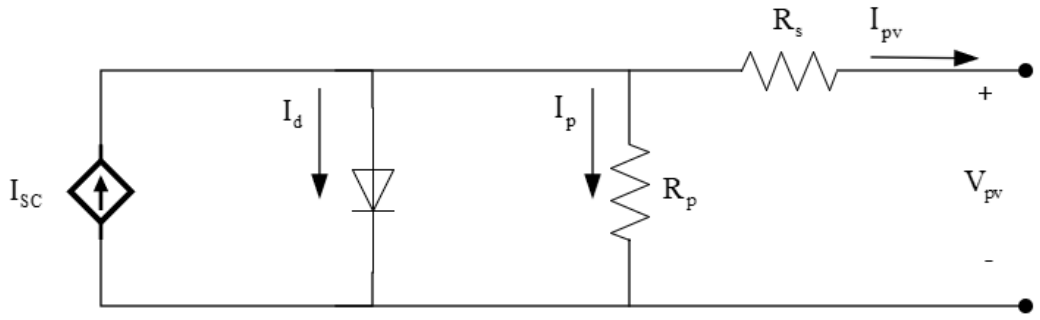

FIGURE 4.3: A more accurate approximation to the equivalent circuit of a PV cell.

Including the parallel leakage resistance and the series resistance, the PV output current drops $\frac{V}{R_p}$ and the voltage decreases with a factor of $\Delta V = IR_s$. The resulting expression for the PV output current is given in Eq. (4.3). [6, 9]

$$I = I_{SC} - I_0(e^{\frac{q(V_{pv}+I_{pv}R_s)}{kT}} - 1) - \frac{V_{pv} + I_{pv}R_s}{R_p} \tag{4.3}$$

The power generated by a solar cell is the product of the current and the voltage. Ideally, low currents and high voltages are preferable to achieve desired power output, and hence the parallel leakage resistance should be high while the series resistance should be low in order to improve the performance of the PV cell. Figure 4.4 shows the I-V curve of a solar cell and the power output. The Maximum Power Point (MPP), marked in the graph, represents the product of current, I_R, and voltage, V_R, that gives the highest output power of the PV cell. Temperature and irradiance severely impacts the I-V curve of a solar cell. When temperatures increase, the voltage decreases, while the current increases with increasing irradiance. A Maximum Power Point Tracker (MPPT) is used to track the MPP, and hence ensure maxi-

mum power operation of the PV cell for the continuously changing temperatures and irradiance levels. The MPPT is included in the DC-DC converter, which is often integrated into the inverter [6, 9]. Inverters are explained in Section 4.2. More on the electrical characteristics of a PV cell, along with common material technologies, can be found in [6, p. 11-22].

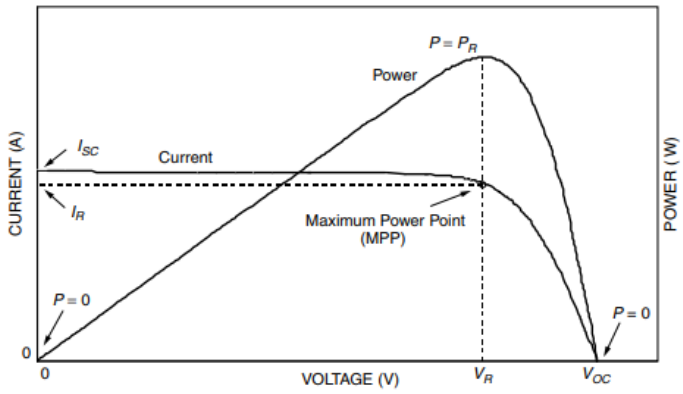

FIGURE 4.4: The I-V curve and power output of a PV cell, showing the MPP. Figure from [9].

4.1.2 The Photovoltaic Array

Electric energy is generated when sunlight hits a PV cell, and a current starts to flow. The PV system is built up by multiple PV cells connected in series and parallel forming a PV module. Several modules may be connected in series to form a PV string, and the PV strings may further be connected in parallel to form a PV array. The formation of a PV module is illustrated in Fig. 4.5, while the formation of the PV array is illustrated in Fig. 4.6. The number of series connected PV modules in a string determines the output voltage of the PV system, while PV strings are connected in parallel to obtain the desired output current. [6, 9, 16]

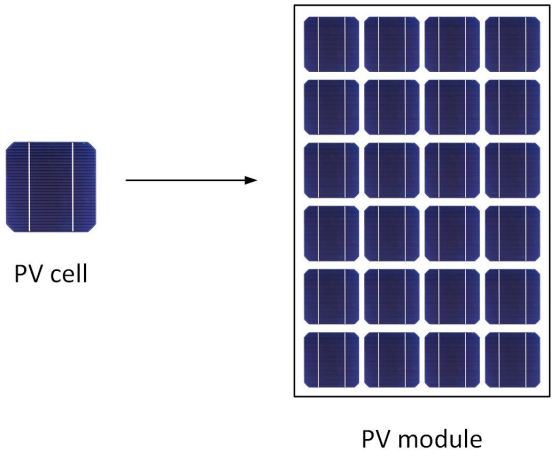

FIGURE 4.5: Illustration of a PV cell and a PV module.

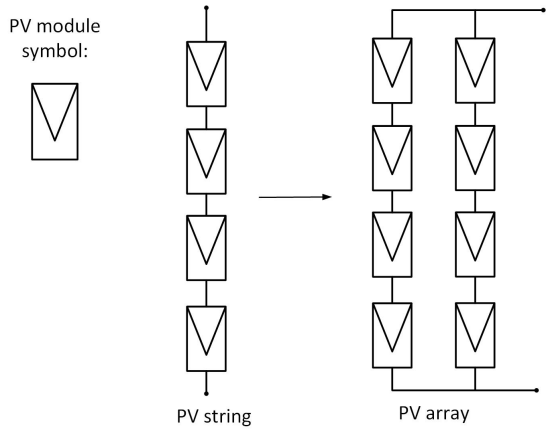

FIGURE 4.6: PV modules forming a PV array.

4.1.3 Photovoltaic Production Model

The PV panel produces DC power. The conversion from DC to AC power for a PV panel is given in Eq. (4.4), where P_{dc0} is the PV nameplate DC rating in kW. The overall system efficiency, η_{sys}, in the conversion from DC to AC power under real field conditions, includes losses in wiring, shading, module mismatch, inverter, etc. Temperature and irradiance impacts on the PV performance are, however, not included in η_{sys}. [9]

$$P_{ac} = P_{dc0} \cdot \eta_{sys} \tag{4.4}$$

The amount of power that can be produced by a PV panel is highly dependent on temperature and irradiance levels. Output PV power increases with increasing irradiance. The temperature coefficient of the voltage is negative, and the voltage hence decreases with increasing temperatures, implying that lower temperatures are preferable to optimize the PV system's performance. Equation (4.5) gives a more accurate estimation of the PV production, including irradiance and temperature impacts. G_{poa} is the global plane-of-array irradiance on the PV panels in W/m^2, and γ_T is the PV temperature coefficient measured in $\%/°C$. $G_{STC} = 1000 W/m^2$ and $T_{cell,STC} = 25°C$ represents the solar irradiance and the PV cell temperature under Standard Test Conditions (STC). [17]

$$P_{ac} = P_{dc0} \cdot \eta_{sys} \cdot \frac{G_{poa}}{G_{STC}} [1 + \gamma_T \cdot (T_{cell} - T_{cell,STC})] \tag{4.5}$$

The solar cell temperature may be calculated for varying ambient temperatures using Eq. (4.6). The Nominal Operating Cell Temperature (NOCT) is the predicted temperature

of a solar cell provided by the manufacturer given an ambient temperature of 20°C, a solar irradiance of 800 W/m^2 and wind speed of 1 m/s. [6, 9]

$$T_{cell} = T_{amb} + \frac{NOCT - 20°C}{0.8} \cdot G \tag{4.6}$$

4.2 Inverters

For simplifying reasons, the inverters in the complex energy system at Campus Evenstad will not be modelled in this thesis. The loss that these inverters represent will simply be included in the PV model and the battery model respectively. Only a short introduction to the theory behind inverters is hence given in this section.

As previously mentioned, the PV array generates DC power. Most equipment runs on AC power, and hence the power generated in the PV array must be converted into AC power. The conversion from DC to AC power is done using a DC-AC converter, also called an inverter. First, the DC voltage generated in the PV array must be converted into a suitable voltage level for the load which is to be supplied. This is referred to as DC-DC conversion. When the voltage is at a suitable level, the DC power is converted into AC power. At Campus Evenstad, the DC-DC converter is integrated into the inverter, but the two converters may be separate. This is normally the case if some loads are DC loads, and hence it is unnecessary to convert all the DC power into AC power. Batteries run on DC power. When the battery is located on the AC side, which is the case at Campus Evenstad, a bidirectional inverter is necessary to charge and discharge the battery. The bidirectional inverter converts AC to DC at charge, and the reverse operation is carried out at discharge. [6, 15, 16, 18]

Figure 4.7 illustrates the fundamental circuit of a DC-AC inverter. The fundamental circuit includes two switches, T_+ and T_-, and two associated diodes, D_+ and D_-. The two switches can never be on or off simultaneously. Which device, the switch or the corresponding diode, that conducts the current depends on the direction of the output current. When T_+ is on, T_+ is conducting when the output current is positive, and D_+ is conducting for negative output current. The output voltage of the inverter does not depend on which device, i.e., the switch or the diode, is conducting; it only depends on the operating state of the switches. [6, 18]

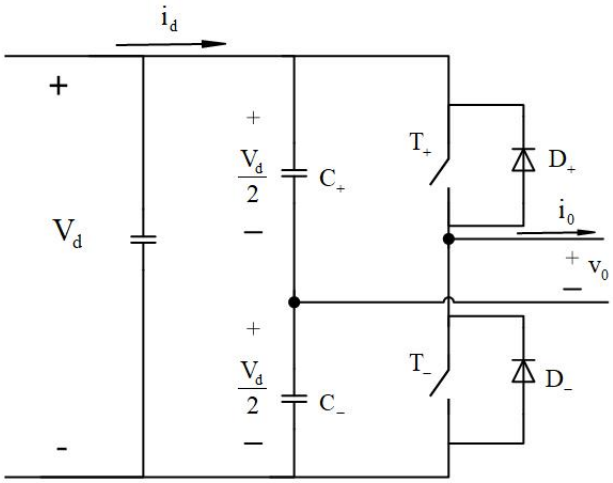

FIGURE 4.7: Fundamental inverter circuit.

The inverter must ensure that characteristics like frequency, voltage, and power are controlled and regulated to meet the standards and the requirements of the load to which power is supplied. Ideally, the inverter produces a sinusoidal waveform output. This can be achieved using Pulse-Width Modulation (PWM). The original output voltage waveform of the inverter is a square-wave. Inverters that use PWM can rapidly switch between on- and off-state, resulting in a better approximation to a sinusoidal output voltage waveform. As previously explained, the MPPT is included in the DC-DC converter. When the DC-DC converter is integrated into the inverter, as it is at Campus Evenstad, it hence becomes the inverter's task to ensure optimal operation of the PV array at all times. In the case of Campus Evenstad, each inverter has two MPPT inputs which allows the inverter to perform MPP tracking of two separate PV strings simultaneously [6, 18]. More on inverters and MPPT can be found in [6, p. 25-36].

The inverter efficiency is not constant; it changes based on the DC output power of the PV array and the PV voltage. Figure 4.8 shows the efficiency curve of the Sunny Boy 5000TL inverter, which is the inverter connected to the PV system at Campus Evenstad. As seen in Fig. 4.8, the inverter efficiency ranges between 95% and 97% depending on the PV output voltage. For low output power, the inverter efficiency is significantly reduced. The inverter is often undersized, meaning that the inverter limits the maximum AC power that the PV system can deliver. This is typically due to the high cost of inverters, and the fact that, most of the time, the PV system is generating less power than its maximum installed capacity.

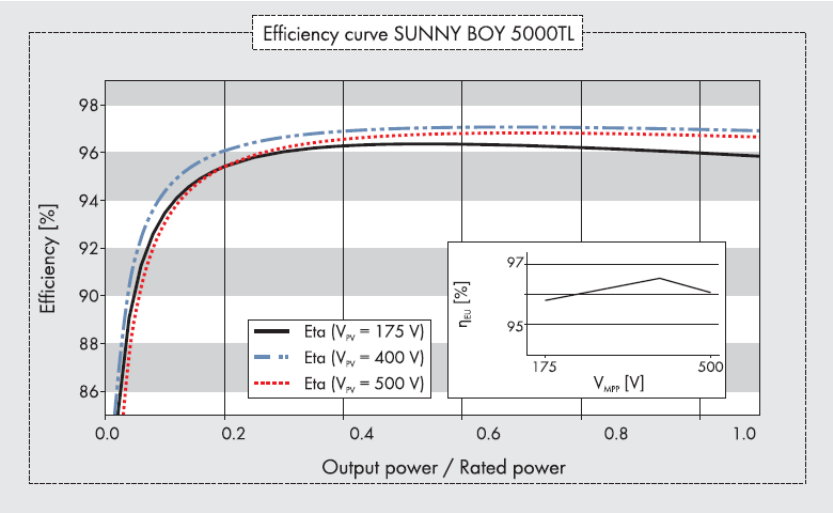

FIGURE 4.8: Inverter efficiency curve. Figure from SMA's inverter datasheet in [19].

4.3 Battery System

One of the greatest challenges related to the use of renewable energy sources in electricity generation is that the energy generation is dependent on uncontrollable weather conditions. There are no guarantees that the sun shines when you need energy the most, and hence a solution in order to store energy may be beneficial.

Energy may be stored in many forms. For PV systems, rechargeable batteries, also called secondary batteries, are normally used as the storage unit. Batteries are electrochemical devices that use chemical reactions to generate power through the acceptation and donation of electrons at the positive and negative electrodes [20, 21]. A battery bank can consist of multiple batteries, where each battery is made up of many series connected battery cells. Each battery cell generally has a nominal voltage of 2 V [6, 15]. Batteries are connected in series to achieve the desired output voltage, and in parallel to achieve higher battery capacity. Generally, higher voltage and lower current are desirable to achieve the desired power capacity since higher current leads to greater losses. However, the parallel connection of batteries ensures system reliability as the entire battery bank shuts down if a battery fails in a system with only series connected batteries. Hence, the system design is always a trade-off between battery capacity, losses, and reliability. The lifetime of a battery is measured looking at how many charge and discharge cycles the battery is capable of, and is highly dependent on the depth of discharge (DoD), i.e., to which level the battery is discharged with respect to the power capacity of the battery. The deeper the discharge, the more battery capacity is lost and hence the resulting lifetime of the battery becomes shorter. [6, 9, 22]

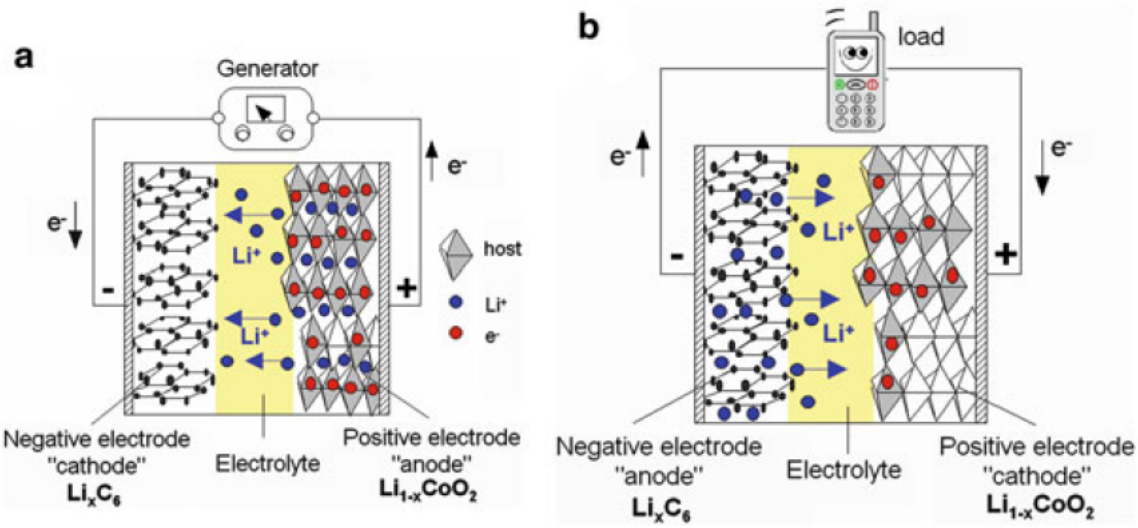

FIGURE 4.9: Illustration of a lithium-ion battery cell. (a) shows the charging process, and (b) shows the discharge process of the battery. Figure from [20].

Lead-acid batteries are the most commonly used rechargeable batteries. The battery installed at Campus Evenstad is a lithium-ion battery. Lithium-ion batteries hold many advantages over lead-acid batteries, e.g., higher energy density, higher efficiency, longer lifetime capacity, and they are made up of lighter material, making it easier and cheaper to transport the batteries [21, 22]. A lithium-ion battery cell is illustrated in Fig. 4.9. Li^+ ions are transferred from the positive to the negative electrode during charge, and from negative to positive during discharge. Notice in Fig. 4.9 that the anode and cathode changes from the charging process to the discharge process. This is due to the fact that ions always flow from anode to cathode, and hence are the positive and negative electrode referred to as anode and cathode during charge, and vice versa during discharge [20]. The equivalent circuit of a battery is given in Fig. 4.10.

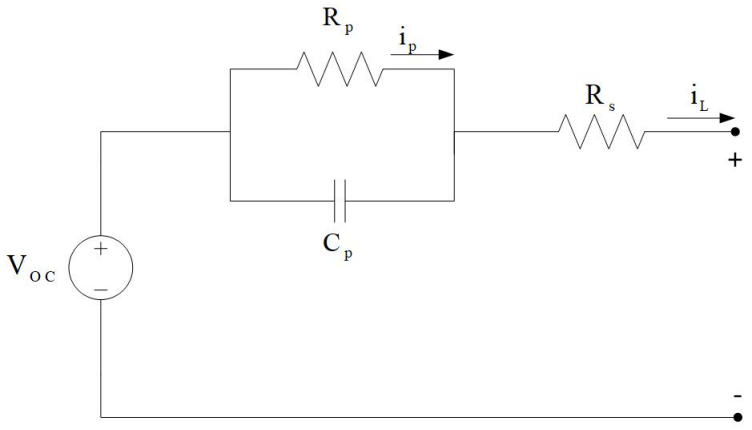

FIGURE 4.10: Equivalent circuit of a battery.

4.3.1 Energy Storage Model

As the installation of the battery at Campus Evenstad took place while writing this thesis, no information on the battery performance or the use of the battery is available. The battery will, in this thesis, hence be modeled as a box that will be charged at a charge efficiency η_{ch} and discharged at a discharge efficiency η_{dch}. The charge efficiency, η_{ch}, of the battery is the ratio of energy gained by the battery during charge, while the discharge efficiency, η_{dch}, is the ratio of discharged energy from the battery. The roundtrip efficiency of a battery is a term that describes the ratio of discharged energy from the battery to the energy charged into the battery. The roundtrip efficiency is hence equal to η_{ch}/η_{dch} [22]. According to IRENA in [22], the roundtrip efficiency of lithum-ion batteries is 85% - 95%. The roundtrip efficiency includes losses in the battery and in the battery inverter. Both the charge- and discharge efficiency depends on the State of Charge (SOC) of the battery. The SOC describes the available charge capacity of the maximum battery capacity in %, hence does the charge- and discharge efficiency change over time depending on the energy content in the battery. [20, 23]

4.4 Combined Heat and Power

The CHP plant produces power and heat simultaneously. The CHP plant can be steam turbine-based, gas turbine-based, fuel cell-based or engine-based [24]. The CHP at Campus Evenstad is gas engine-based. It uses locally produced wood chips which are gasified into biogas and further burnt in a combustion engine. For small-scale CHP plants, gas engines generally achieve high power efficiencies [24]. The small-scale and wood chip based CHP plant at Campus Evenstad was the first of its kind in Norway when installed in 2016.

As the CHP plant at Campus Evenstad is heat driven, it is necessary to consider the heat demand on campus to model the CHP plant accurately. This is considered out-of-scope for this thesis, and the CHP is hence modeled as only having two operation modes in this thesis; running on maximum in winter and being completely shut off during summer. Therefore, further theory on the operation of a CHP plant will not be given.

Chapter 5

Site-Specific Data for Campus Evenstad

5.1 Meteorological Data

The performance of a PV module is directly dependent on solar radiation and site-specific weather conditions. The collection of meteorological data, therefore, becomes important when modeling a PV system. A high level of uncertainty is to be expected in measurements of solar irradiance due to the difficulty of performing such measurements. Hence, the availability of irradiance measurements, along with the quality of these measurements, varies. [12, 25]

Various equipment to measure the solar resource exists. Such equipment is either based on surface observations, satellite data or meteorological models. Among surface observation equipment, pyranometers and reference cells are often used to measure global radiation. The pyranometer is a thermopile sensor where the measured temperature difference generates a voltage proportional to the radiation that hits the instrument. The pyranometer is the most commonly used instrument for measuring global radiation. Reference cells have similar characteristics to the PV panel. For a reference cell sensor, a voltage is generated when the sensor captures incoming photons. [11, 26]

5.1.1 Meteorological Data for Campus Evenstad

In this thesis, meteorological data from the Norwegian Meteorological Institute has been used. The Norwegian Meteorological Institute has in total 70 weather stations equipped with sunshine duration sensors or pyranometers measuring global radiation [11]. Hourly data can be accessed from their database, eklima. Data is logged using the Norwegian Mean Time

(NMT) which is equivalent to UTC+1. The time is not changed for summertime, which is creating a timeshift in the results for simulations performed during the summer months. More on this in Section 8.1.

The Norwegian Meteorological Institute does not measure solar radiation at the weather station at Evenstad, *8140 EVENSTAD*. The closest weather station to campus where the global radiation is measured is *7420 RENA*, which is located approximately 23 km from Evenstad. Table 5.1 gives an overview of weather stations close to Evenstad where global irradiance is measured.

TABLE 5.1: Overview of the Norwegian Meteorological Institute's weather stations close to Evenstad

Nr.	*Station Name*	*Altitude*	*Latitude*	*Longitude*	*Distance in km*
8140	EVENSTAD	257	61.4255	11.0803	-
7420	RENA	872	61.3763	11.4992	23
13030	GAUSDAL	375	61.2247	10.2588	49
13150	FÅVANG	200	61.4582	10.1872	48

Hourly data on global radiation (W/m^2) and air temperature are downloaded from eklima in *.xls files from the weather stations listed in Table 5.1. Hourly values of the GHI measured at Rena, Gausdal, and Fåvang are plotted in Fig. 5.1 for the year 2017. Out of the three weather stations, Rena is closest in distance from Evenstad. It could hence be reasonable to use GHI values measured at Rena in the simulation of the PV system at Evenstad. However, as seen in Fig. 5.1a, the GHI measured at Rena exceeds 1000 W/m^2 on several occasions. According to Norsk Solenergiforening in [2], the GHI in Norway is typically between 700 W/m^2 and 1000 W/m^2. GHI values above 1000 W/m^2 may, therefore, be considered suspiciously high for this location. Hourly GHI values for Rena, Gausdal, and Fåvang was downloaded for a more extended time period to see if such high values had also occurred previous years. Values for years 2015 to 2017 are plotted in Fig. 5.2. As observed in Fig. 5.2, 2017 is the only year where GHI values exceed 1000 W/m^2. It may hence be concluded that the GHI values measured in 2017 are irregularly high at times. These irregularities mostly apply to Rena, as measurements for the two other stations seems to be more stable.

Taking a closer look at the location parameters of Evenstad, Rena, Gausdal and Fåvang weather station listed in Table 5.1, it becomes evident that the altitude at which the weather stations are located differs from one another to a great extent. Rena weather station may be the closest in distance, but it is located at a much higher altitude than Evenstad weather sta-

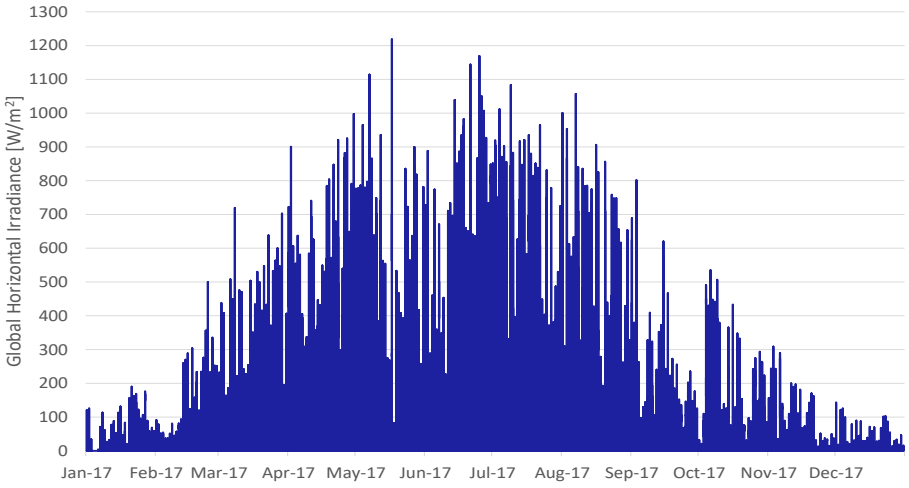

(A) Rena

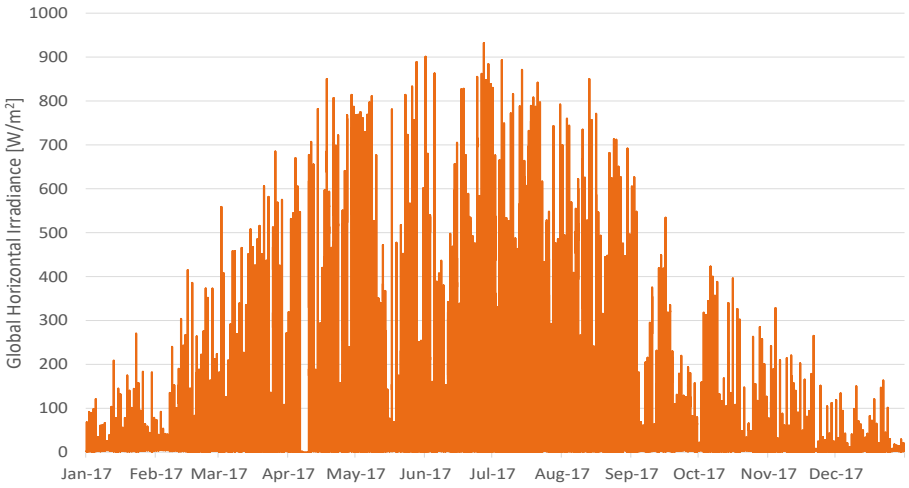

(B) Gausdal

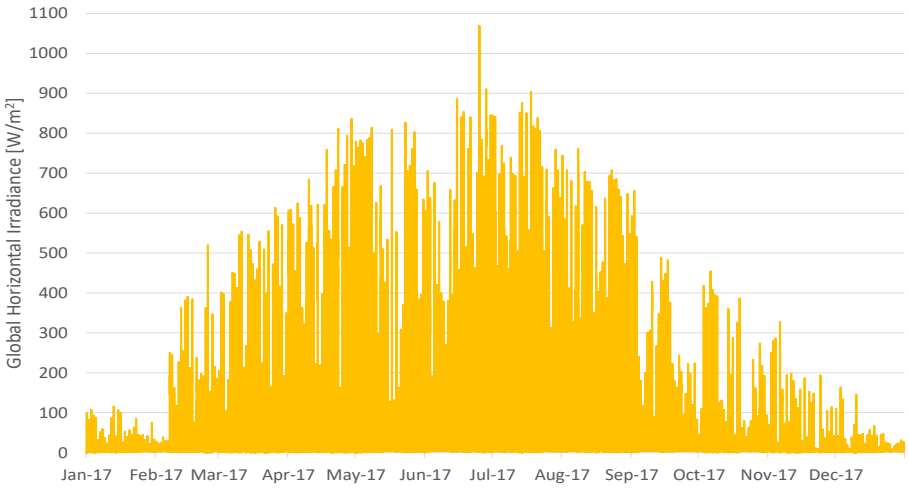

(C) Fåvang

FIGURE 5.1: Hourly GHI values for 2017,downloaded from eklima.

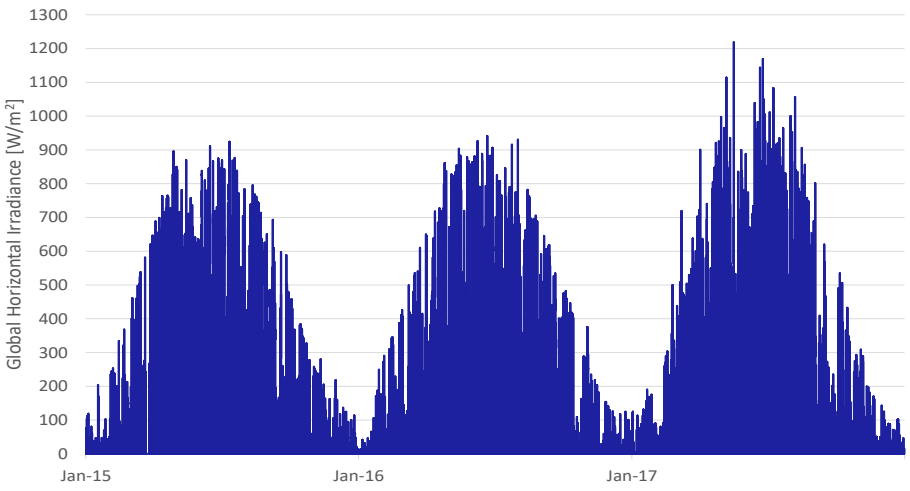

(A) Rena

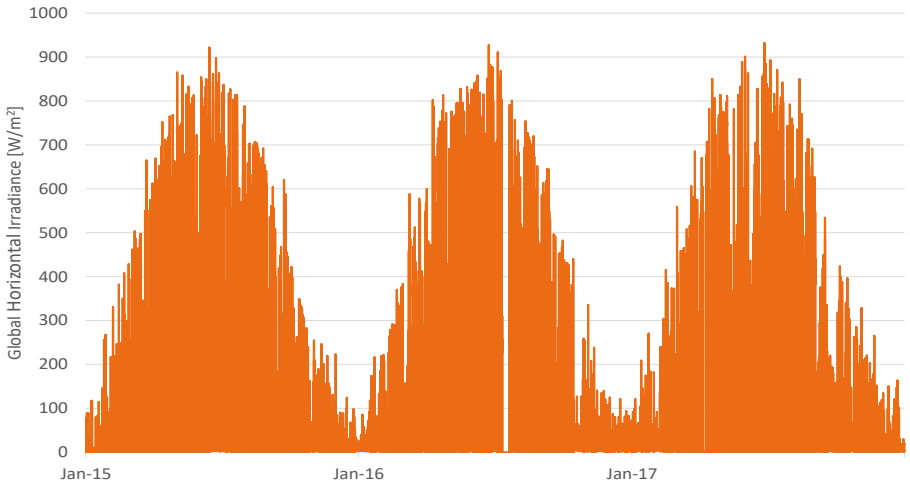

(B) Gausdal

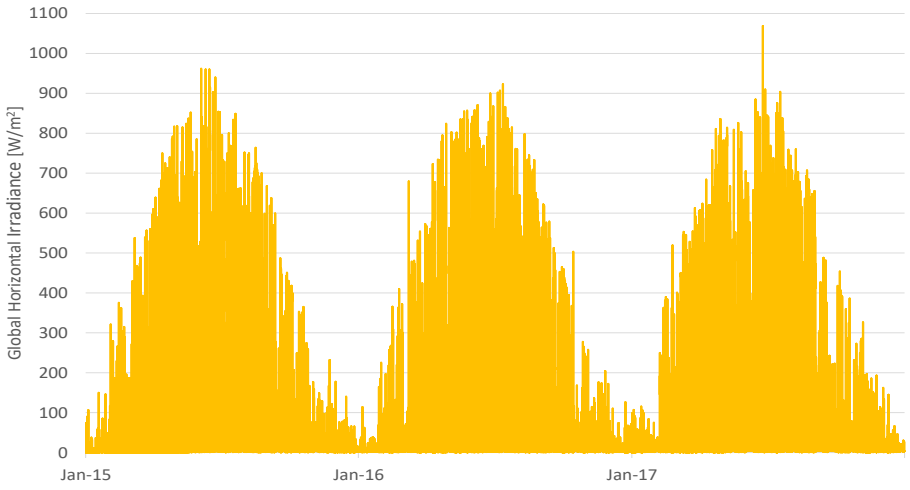

(C) Fåvang

FIGURE 5.2: Hourly GHI values for 2015-2017 downloaded from eklima.

tion. Solar radiation tends to increase with increasing altitude since sunlight has a shorter path to reach a surface at higher altitudes, and hence is the radiation exposed to less scattering and absorption in the atmosphere. The altitudes effect on the solar radiation is referred to as the altitude effect [27]. The difference in altitude between Rena and Evenstad is 615 meters, which may account for a significant differentiation in solar irradiance at the two locations.

Based on the previously mentioned observations, it is concluded that using global radiation measured at Rena weather station in the simulation of a PV system located at Evenstad is not ideal, both due to the high GHI values observed at Rena in 2017 and due to the massive altitude difference of the two stations. Therefore, it was decided to manipulate the global radiation data to be used as input to the PV model. There are several ways to manipulate data. As the main problem seems to be unrealistically high values of global radiation in certain time periods, one could, for instance, replace these values with interpolated values. After studying the global radiation data more closely, this was considered not to be a good solution, as there are also uncertainties related to low values of measured global radiation. Additionally, it is difficult to interpolate data when there are multiple occurrences of irregular data in series. Therefore, it was considered to be more accurate to operate with average values. Both Gausdal and Fåvang weather stations are located East of Evenstad, while Rena weather station is located West of Evenstad. Hourly average GHI values of Gausdal and Fåvang weather stations were hence averaged with hourly GHI values for Rena. The obtained approximation of the GHI at Evenstad in 2017 is plotted in Fig. 5.3.

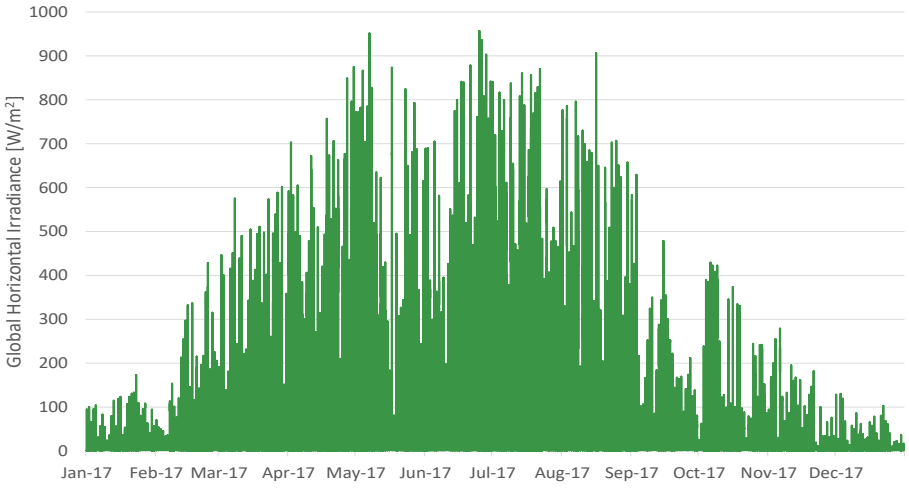

FIGURE 5.3: Estimated hourly GHI values for Evenstad in 2017.

In the simulations of the PV system at Campus Evenstad, air temperature measured at Evenstad weather station were used. At some occasions, measurements were missing, and in these cases, the temperature was estimated in the same way as the global radiation.

5.2 Photovoltaic Production at Campus Evenstad

The PV system at Campus Evenstad was installed in late 2013 by the Norwegian company FUSen. The system consists of 276 REC 255PE PV modules and 12 Sunny Boy 5000TL-21 inverters. The system is roof-mounted, south-faced, and tilted 35°. The installed capacity of the PV system is 70.38 kW_p, meaning that a maximum of 70.38 kW_{dc} can be produced under ideal conditions. The annual production on site is approximately 60 034 kWh [28]. On days with high levels of isolation, the PV system at Campus Evenstad can produce approximately 500 kWh/day [7]. Figure 5.4 shows the installed PV system at Evenstad.

FIGURE 5.4: South-faced roof-mounted PV system at Campus Evenstad.

At SMA's Sunny Portal measured data from the PV system at Evenstad is available for download. Power production together with POA irradiance, PV module temperature, and wind speed values can be accessed from Sunny Portal. The POA irradiance logged in the Sunny Portal is measured using a reference cell. Figure 5.5 shows an annual comparison of the PV production at Campus Evenstad.

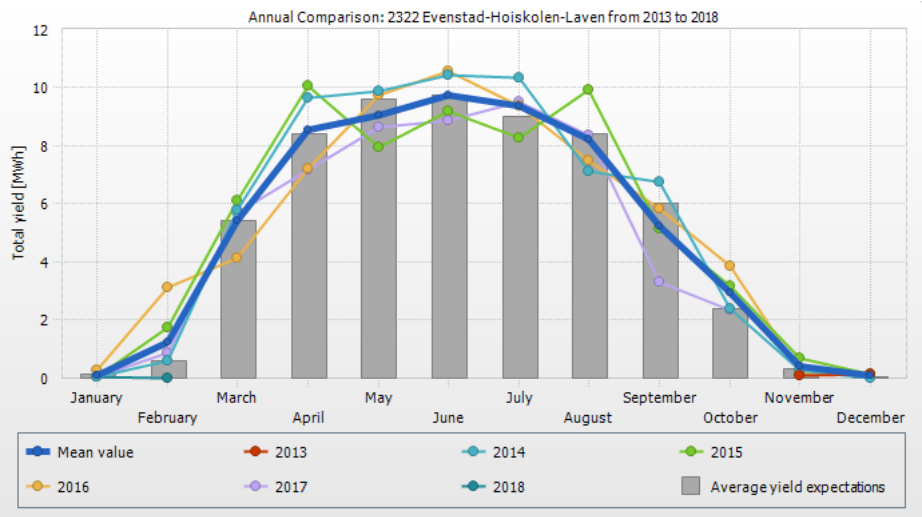

FIGURE 5.5: Comparison of the annual PV production at Campus Evenstad. Figure from [28].

Hourly, daily, monthly, and yearly data are logged at the Sunny Portal. For the PV production, a 15-minute time resolution is available. The 15-minute time resolution is easily converted into hourly data, which is the time interval used in the modeling in this thesis. However, data with such high time resolution is only available for day-by-day download. This makes the process of collecting hourly data from the Sunny Portal extremely time-consuming. The prediction of the hourly PV production cannot be executed accurately with daily or monthly values of radiation and temperature, simply since irradiance and temperature varies continuously throughout the day. A PV production prediction based on daily or monthly values would hence be inaccurate and useless when determining the hourly operation of the battery.

Kinect Energy Group is responsible for calculating the electricity certificate for Campus Evenstad. An electricity certificate is a subsidy scheme for power produced from renewable energy sources. As renewable energy is generated at Campus Evenstad, the INN University receives electricity certificates which they can further sell to electricity suppliers which are obliged to buy such certificates [29]. Kinect Energy Group, therefore, has measuring equipment on campus, measuring the hourly PV production. Figure 5.6 illustrates the monthly PV production at Campus Evenstad from September 2016 to April 2018 provided by Øyvind Kaaresen at Kinect Energy Group. Kinect Energy Group does not store hourly PV production data after a certain period of time, and hence the access to historical hourly production data is limited. Data on PV production provided by Kinect Energy Group is rounded to the closest kWh/h.

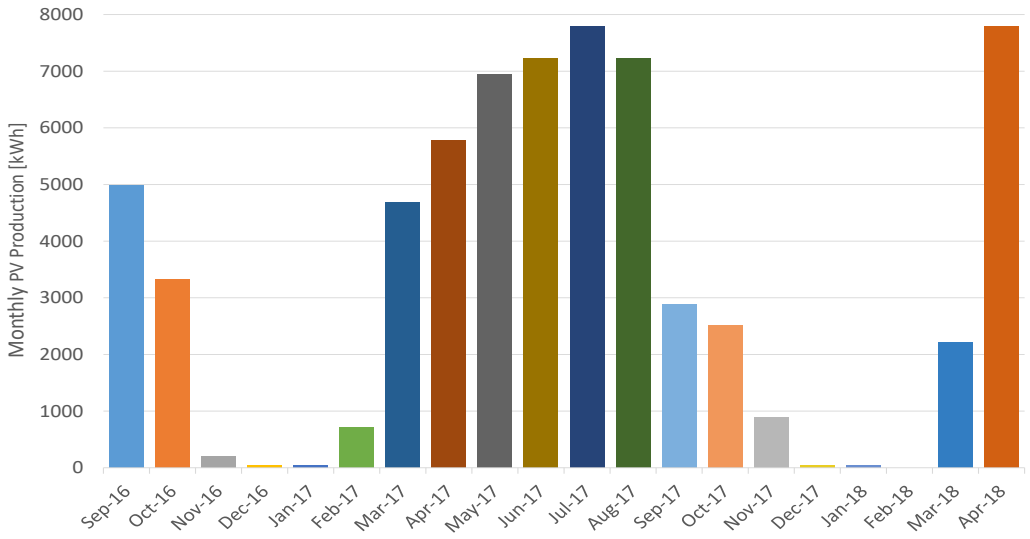

FIGURE 5.6: Monthly PV production at Campus Evenstad from September 2016 to April 2018 based on data provided by Kinect Energy Group.

The estimated PV production at Campus Evenstad, obtained through simulations of the developed PV model in this thesis, will, in Section 8.1, be compared to the measured PV production data provided by Kinect Energy Group.

5.3 CHP Electricity Production

A CHP plant, installed in 2016 as the first of its kind in Norway, ensures local energy production from locally produced wood chippings that are gasified and burnt, and hence produces both electricity and heat. The CHP plant has a capacity of 40 kW_{el} and 100 kW_{heat}. The expected annual production is 325 MWh/year heat and 133 MWh/year electricity [7]. Historical data of the CHP electricity production at Campus Evenstad is normally logged at Sauter Vision Center. However, due to recent upgrades in the Vision Center, historical data on the CHP electricity production is only available from April 10, 2018.

The CHP plant at Evenstad is heat driven, i.e., the operation of the plant is determined by the heat demand on campus. The electricity generated by the CHP is merely considered a by-product. As the CHP is heat driven, it is impossible to make an accurate estimation of the electricity production from the CHP without considering the heat demand on campus. As this thesis solely focuses on the electricity management of the complex energy system at Campus Evenstad, simplifications are made regarding the CHP plant. The CHP is therefore assumed to be operating at maximum (40 kW_{el}) between October and April when it is cold

outside and students are living on campus. From May to September, the CHP is assumed to be shut completely off as the weather is warmer, and the majority of students are assumed not to be living on campus during these months.

5.4 Battery Specifications

Campus Evenstad has, from time to time, suffered from power failure, mainly due to weather conditions and trees falling over power transmission lines in the area. Without access to power, the CHP plant is unable to start up. As the CHP plant is the main source to heat on campus, this can be critical, especially during the winter months, as the majority of students live in dorms on campus. Based on this, Statsbygg decided to invest in a battery system. The battery was installed in June 2018, i.e., in times of writing this thesis, by Solcellespesialisten, the leading vendor of solar cells in Norway. The battery installed is a lithium-ion battery, more specifically lithium nickel manganese cobalt oxide, and holds a capacity of 108 kW/204 kWh. The battery capacity describes the useful discharge capacity of the battery, not the total amount of energy that may be stored in the battery [23]. The functions of the battery system are listed below, in prioritized order as specified by Statsbygg [7].

1. Uninterrupted power supply
2. Start battery for the CHP plant
3. Energy storage for the PV system (maximize self-consumption)
4. Reduce the need for imported electricity from the grid

The minimum requirement for operation in island mode is 50 kW/100 kWh [7]. This is considered sufficient to ensure backup power supply, including starting current for the CHP, at times of power failure. The capacity of 50 kW/100 kWh must hence be available at any given time. Additional capacity may be used as energy storage for excess energy produced by the PV system and the CHP plant. The installed battery system may be expanded in the future depending on demand.

5.5 Historical Data on Grid Exchange

Imported and exported electricity at Campus Evenstad is measured by the local grid company, Eidsiva. Øystein Holm at Multiconsult provided hourly values of imported and exported electricity in 2016 and 2017. The *.xlsx for 2016 contained several timestamp duplicates. Where the values of the duplicates did not correspond, the highest value of imported electricity was consistently selected.

The estimated annual electricity consumption at Campus Evenstad is 750 MWh/year [7]. Figure 5.7a shows the electricity imported from and exported to the grid at Campus Evenstad for the year 2016. In total, 1.06 GWh was imported while only 157.59 kWh was exported in 2016. According to Multiconsult [7], the high electricity consumption in 2016 can be explained by construction work on campus and the fact that the actual electricity consumption in new buildings is typically higher than the estimated consumption. The highest hourly imported electricity in 2016 was 479.46 kWh and occurred on the 7th of March. Figure 5.7b shows the imported electricity from the grid in 2017, from February 8 to December 31. The highest hourly imported energy in this period was 467.70 kWh and occurred on the 22nd of November. The total import sums up to 904.18 MWh, i.e., also higher than the estimated annual electricity consumption. Data on exported electricity is not available for 2017.

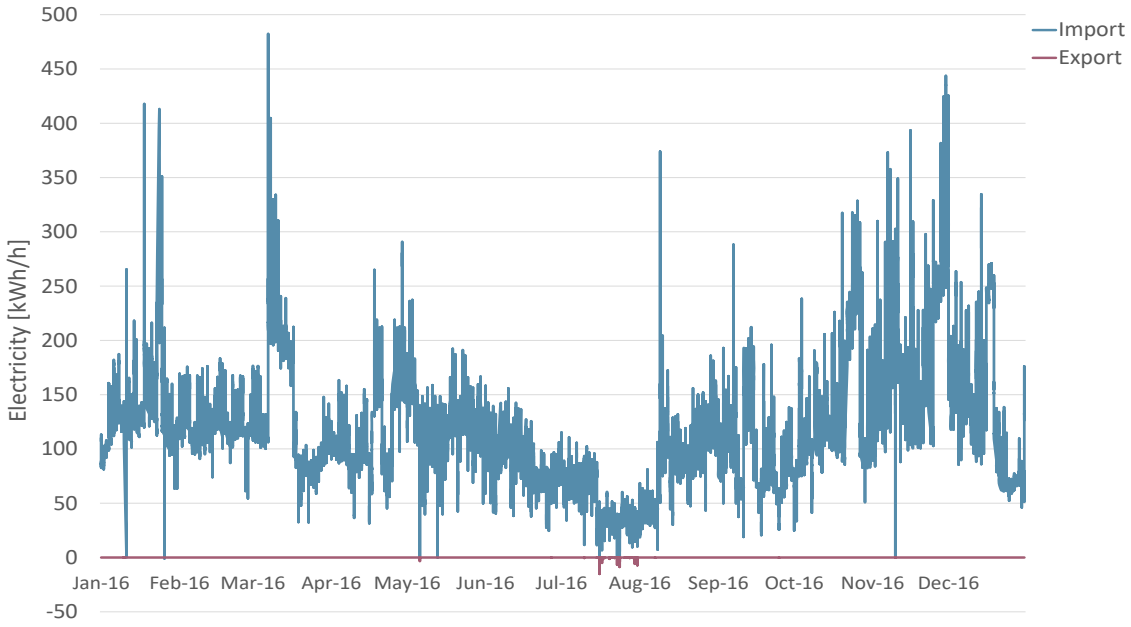

(A) Import and export 2016.

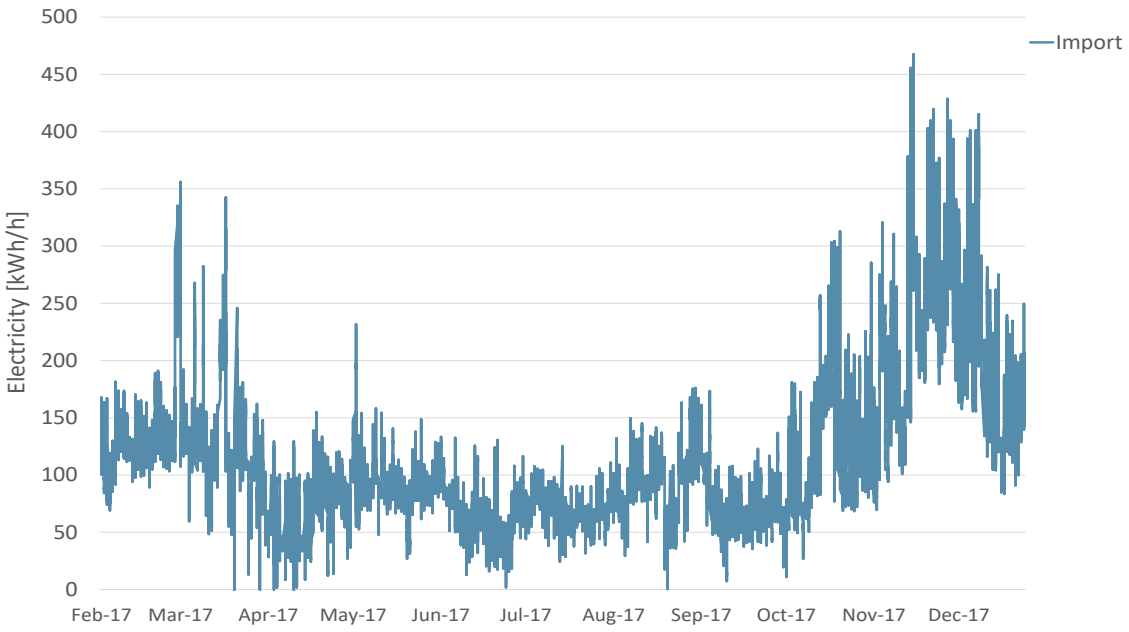

(B) Import from 08.02.2017 to 31.12.2017.

FIGURE 5.7: Imported electricity at Campus Evenstad.

5.6 Cost of Import

The total cost of the energy imported from the grid is divided into two:

1. The cost of the actual amount of electricity that is imported, and
2. The cost of the grid tariff.

The company that distributes the energy is not necessarily the same company that supplies the energy. The supplier charges the customer for the electricity supplied, while the distributor charges the customer for the distribution, i.e., the transportation, of the supplied energy.

5.6.1 Grid Tariff Structure

Tariff designs are controlled and regulated by Norwegian Water Resources and Energy Directorate, Norges Vassdrags- og Energidirektorat (NVE).

Current Tariff Structure

Although NVE provides guidelines and regulations to how grid companies may design tariffs, they are to some extent free to design grid tariffs as they please. It is common among grid companies to differentiate customers depending on annual consumption or installed capacity, and set the tariff thereafter. The tariff for residential customers consist of a fixed annual charge and an energy charge based on how much energy they consume. In addition to the fixed charge and the energy charge, commercial customers are charged with a capacity charge. As Campus Evenstad at INN university annually imports more than 100 MWh, it is considered to be a commercial customer. [30]

Future Tariff Structure

Lately, there has been an increasing focus on the grid tariff structure in Norway. The constantly increasing electricity consumption is putting pressure on the grid companies. In many cases, an expansion of the existing grid has become, or is becoming, necessary. High investment costs are related to such expansions. In the report *Status of NVE's work on network tariffs in the electricity distribution system* [30], NVE suggests that future tariff structures should ensure that customers are rewarded for reducing their demand during peak hours. Reducing demand during peak load decreases the installed capacity demand, and thus costs related to grid building and grid extension will decrease. The grid is built based on the demand of capacity, not energy. This implies that, with today's tariff design, the grid holds unused capacity large parts of the day when demand is lower than the maximum installed capacity. If consumers manage to change their consumption behavior such that the load profile is more evenly distributed throughout the day, the grid would be used more efficiently. [30]

NVE stresses that the grid tariff structure highly influences the usage of the grid. Within the year of 2018, smart meters will replace conventional meters for measuring electricity in Norway. Smart meters provide consumers with more detailed information regarding their electricity consumption and the cost of the energy they consume. These smart meters are expected to cause consumers to become more conscious of their energy consumption, and potentially make consumers distribute their load in a more efficient way such that the demand in specific periods is reduced. If this is the case, a potential need for expansion of the grid may be reduced or postponed, lowering the overall cost for the consumer. [30]

Grid Tariff for Campus Evenstad

Eidsiva is the local grid company at Evenstad. Campus Evenstad is considered to be a commercial customer, and hence, in addition to paying for the energy that they consume, they are also charged for the power they draw from the grid. Eidsiva base their power tariff on the highest hourly consumption over the last 12 months. As the future grid structure is uncertain, the current tariff structure is used as a basis in this thesis. The expression for calculating the grid tariff is given in Eq. (5.1).

$$C_{tariff} = C_{fixed,yearly} + C_{power} \cdot y^{imp,peak} + C_{energy} \cdot \sum_{t=1}^{8760} y_t^{imp} \tag{5.1}$$

Eidsiva's tariff prices for commercial customers for 2017 are given in Table 5.2. If the power peak exceeds 200 kW, the highest power price listed in Table 5.2 apply to the first 200 kW while the lowest power price is multiplied with the remaining power in kW.

TABLE 5.2: Eidsiva's tariff prices for commercial customers, including VAT and customer fee, for 2017. Prices from [31]

Grid level	Fixed [NOK/yr]	Energy [NOK/kWh]	Power [NOK/kW]
Low voltage	20 500	0.279	
Power < 200 kW			620
Power > 200 kW			470

5.6.2 Energy Prices

All residences are assigned a grid company responsible for the power grid and for making sure that electricity is delivered to the consumer. Each grid company has the monopoly in their assigned geographical area, meaning that the consumer cannot freely choose a grid company. Consumers are, on the other hand, free to choose the energy distribution company of their preference.

Energy distribution companies operate with different prices, price structures and terms of agreements. Most energy distribution companies offer a spot price structure. The spot price structure is widely used among consumers. The spot price structure, given in Eq. (5.2), consists of a fixed monthly charge, a price for each kWh consumed according to Nord Pool

power market spot prices, and an additional cost per kWh including an electricity certificate fee decreed by law. The price of energy per kWh is generally higher during peak hours.

$$C_{spot} = 12 \cdot C_{fixed,monthly} + \sum_{t=1}^{8760} (C_t^{nordpool} + C_{GC}) \cdot y_t^{imp} \tag{5.2}$$

In the system modeling, Eidsiva is assumed to be the energy distribution company at Campus Evenstad, and the spot price structure is assumed to be the price structure in use. The fixed monthly charge of Eidsiva's spot price structure is 45 NOK, and the electricity certificate fee is 0.045 NOK/kWh [32]. Historical data on the hourly spot prices in different regions may be downloaded from Nord Pools's database [33]. Spot prices, including VAT, for Oslo in 2017 are plotted in Fig. 5.8.

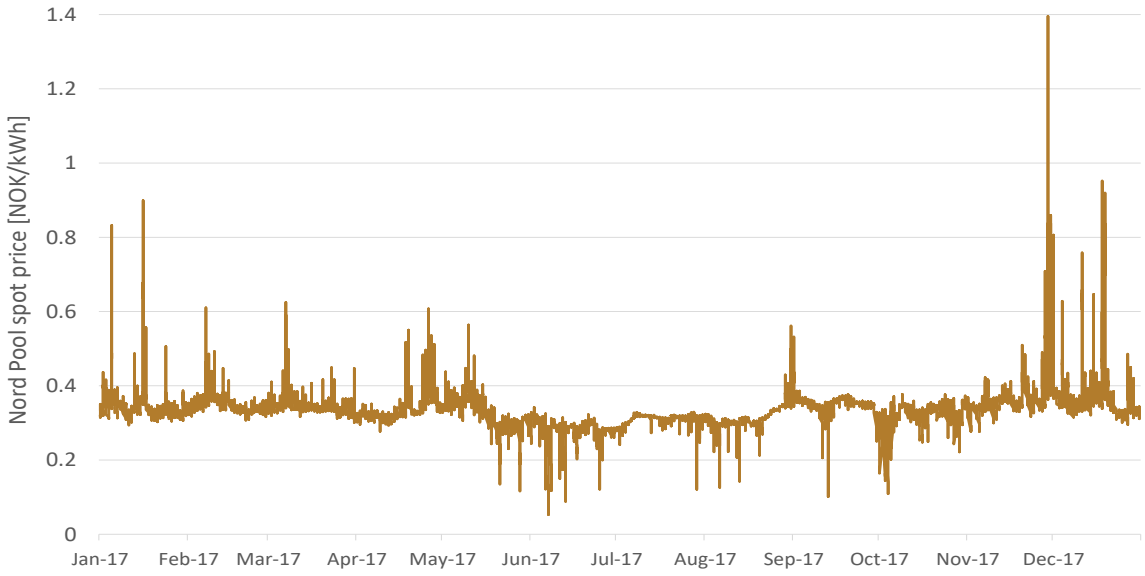

FIGURE 5.8: Hourly spot prices including VAT for 2017. Data from [33].

5.7 Electricity Load

Several factors affect the electricity demand and load profile of the consumer. Time, economy and social behavior represent some factors [34]. The energy consumption in Norway is naturally higher in winter than in summer due to the cold climate. The daily load curve of residences generally has two power peaks; one in the morning and one in the evening. The industry is often divided into primary, secondary and tertiary industry depending on what kind of operations and services the industry provides. Campus Evenstad goes under

the tertiary industry category. In the tertiary industry, the daily load profile is smoother and doesn't contain the typical power peaks expected in the load profile of residences [35]. Social behavior and customer awareness affect the load profile, and it is expected to do so to an even greater extent in the future as the structure of the grid tariff changes as described in Section 5.6.1.

Many methods for predicting or forecasting the load profile exists. The different methods use different approaches in the prediction process. Some methods are based on historical data of the load with respect to weather data, while others also require information about user behavior and specific information of the building construction [36]. For simplifying reasons, historical data are, in this thesis, used to determine the electricity demand at Campus Evenstad. As the battery was installed in June 2018, and hence no data on the use of the battery was accessible at the time of writing this thesis, the demand is determined by the simple relation given in Eq. (5.3). The estimated load demand at Campus Evenstad in 2017 is plotted in Fig. 5.9. Note that the load estimation for 2017 is inaccurate as historical data on export was unavailable for 2017 and the electricity generation from the CHP plant is estimated as explained in Section 5.3.

$$Demand = PV + CHP_{el} + Import - Export \tag{5.3}$$

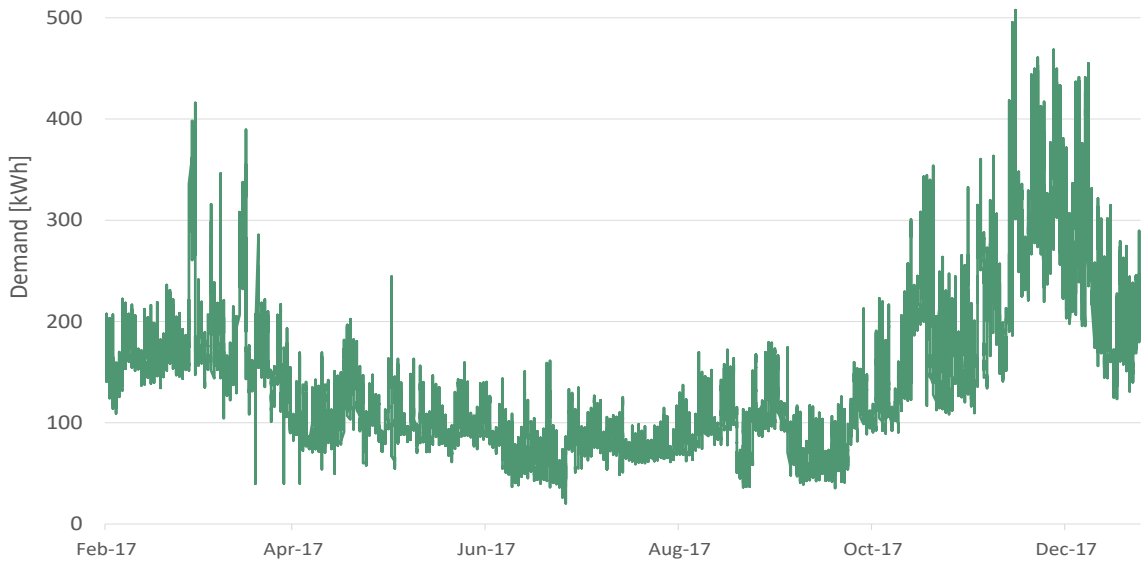

FIGURE 5.9: Estimated demand at Campus Evenstad in 2017.

Chapter 6

Programming Theory

Python is chosen as the programming language in this thesis. Python is open-source, and hence it is free to use, and information and examples can easily be accessed online. In addition, Python plays well with other programming languages such as R and C.

6.1 PV System Modeling

Various software packages for predicting the performance of PV systems exists. PVsyst, SAM, and PVWatts represent some of the most well-known software packages available on the market. Such commercial software packages are great for performance prediction, system sizing, and loss factor analysis, but they generally lack simulation flexibility as they are created and designed based on integrated tools and assumptions that the user of the software is unaware of. PVLIB, a fairly young open-source environment developed for PV modeling, represents an alternative to the well-established PV system softwares mentioned above. [37, 38]

6.1.1 PVLIB

PVLIB is a fairly young PV modeling environment. It started as an in-house project at Sandia National Laboratories in 2009 with the aim to collect and standardize PV modeling functions. As has been mentioned on several occasions in this thesis, the system performance of a PV system depends on many factors. The system performance modeling consists of many steps, and there are various methods for completing each step. Through PVLIB, developed algorithms for PV system performance is published in one place, giving the software user the

flexibility and ability to customize, modify, and compare algorithms based on the specific PV system in question. The PVLIB environment includes algorithms for weather forecasting, weather data conversion and handling, and PV performance forecasting. [37, 38]

As stated in Section 1.2, one of the motivations for writing this thesis was to develop skills within software programming while understanding how the software packages work. In relation to this, it was decided to use a combination of the built-in functions that PVLIB provides for the PV performance prediction and well-accepted functions described in Section 4.1. As the model constructed in this thesis is meant to be a prework for future model predictive control of the battery, the forecast weather functions that PVLIB provides, may be implemented in the model at a later time.

There are some limitations to the use of PVLIB for PV system performance modeling, especially for PV systems located in Northern countries. Several of the built-in functions used in this thesis enables the user to specify optional input parameters that will ensure a more accurate performance estimation. Some of these optional input parameters are unknown values for the specific case of this thesis, and hence the functions default settings are used in such cases. In other cases, none of the possible input parameters fit the description of the specific case used in this thesis due to a mismatch between the site locations used in the documentation of the built-in functions and the specific site location of this thesis. This primarily applies for the transposition function from irradiance components on a horizontal plane to POA irradiance components, which is based on Perez coefficients. Perez coefficients are only determined for a handful of sites around the world, most of them situated in the United States and with climatic conditions which differ from Norwegian climate conditions. [39]

6.1.2 Validation of the PV Model

The predicted PV performance of the constructed PV model is validated using historical data on the PV production. The goodness of the PV model is, in this thesis, determined by using two different methods. Firstly, the error of the total amount of estimated PV production is compared to the total amount of measured PV production is calculated for each test period using the simple relation given in Eq. (6.1). Note that the error does not account for hourly differences between estimated and measured production; only the total error is found.

$$error = \frac{|PV_{measured} - PV_{estimated}|}{PV_{measured}} \cdot 100\% \tag{6.1}$$

Secondly, the coefficient of determination, also known as R^2, is calculated for each test period. R^2 holds a value between 0 and 1, and indicated how much of the variations in the predicted value, $\hat{y}$, are explained by the variations in the measured value, y [40]. In other words, R^2 describes how similar two datasets are; not necessarily in value, but in variation. In this thesis, R^2 is used to indicate to what degree the daily curve of the predicted PV production follows the daily curve of the measured PV production, i.e, how much of the hourly variation in the predicted PV production ($\hat{y}$) can be explained by the hourly variations in the measured PV production (y). Several expressions for calculating R^2 exist [41]. The mathematical expression used in this thesis is given in Eq. (6.2), where $\bar{y}$ is the mean of y. Note that, for this expression, R^2 may, in fact, be negative if the two datasets are not at all a good fit [41].

$$\begin{aligned} R^2 &= 1 - \frac{SS_{Res}}{SS_T} \\ &= 1 - \frac{\sum_{i=1}^{n}(y_i - \hat{y}_i)^2}{\sum_{i=1}^{n}(y_i - \bar{y})^2} \end{aligned} \tag{6.2}$$

6.2 Optimization

The act of optimization is performed in order to find the solution to a problem that gives the best outcome under specified conditions. Various optimization modeling tools exist. Pyomo has been chosen for the optimization of the use of the battery in this thesis.

6.2.1 Pyomo

Pyomo is an open-source library, supported by Python, commonly used to handle optimization problems. Tools to formulate the problem, solve and analyze the results are included in the Pyomo software. Various problem types can be optimized using Pyomo, including linear, quadratic, nonlinear, and stochastic programming. [42]

In pyomo, parameters and variables included in the model must be declared. Parameters represent values that must be provided in order for the model to be solved and optimized. Variables, on the other hand, represents changing or unfixed values that will be determined

during the solving of the model depending on the optimal solution. Problem restrictions are modeled as constraints, and finally, the objective of the optimization model is declared.

The optimization problem formulation is performed in Pyomo, but in order to obtain the optimal solution to the problem, a third-party solver must be specified. Pyomo supports a wide range of solvers, including ASL solvers, cplex, glpk and gurobi [42]. Gurobi is widely used in industries due to its fast run-time and its capability of solving a wide range of optimization problem types. Gurobi is not open-source, but offer a free license for academic users. Although it is a drawback that gurobi is not an open-source solver, and many free, open-source solvers exist on the market, it is concluded that a robust, fast solver is preferred over a less robust open-source solver, and hence gurobi is chosen as the solver in this thesis. Gurobi also supports interfaces for other programming languages. [43]

Chapter 7

System Modeling

In this section, equations used in the modelling process are given. Parameters and variables used in the modelling are listed below.

	Model Parameters
D_{el}	Electricity demand at time t [kWh]
X^{ba}	Installed battery capacity [kWh]
η_{ch}	Charge efficiency [%]
η_{dch}	Discharge efficiency [%]
	Model Variables
y_t^{PV}	PV production at time t [kWh]
y_t^{CHP}	CHP_{el} production at time t [kWh]
y_t^{imp}	Imported electricity at time t [kWh]
y_t^{exp}	Exported electricity at time t [kWh]
y_t^{ch}	Energy charge of battery at time t [kWh]
y_t^{dch}	Energy discharge of battery at time t [kWh]
z_t^{ba}	Energy content of battery at time t [kWh]

7.1 PVLib

Built-in functions from the PVLIB library are used to perform the PV modelling in this thesis. The functions used are listen in Table 7.1. All functions are accessed through the PVLIB online documentation [44].

TABLE 7.1: Built-in functions in PVLIB used for the PV modelling

Solar Position Function	
`pvlib.solarposition.spa_python`(lat, ..)	Calculate the solar position
Clear Sky Function	
`pvlib.location.get_clearsky`(times,..)	Clear sky GHI, DNI and DHI
Irradiance Decomposition Function	
`pvlib.irradiance.erbs`(ghi, zenith, doy)	Estimate DNI and DHI from GHI
`pvlib.irradiance.dirindex`(ghi, zenith,..)	Determine DNI from GHI
Irradiance Transposition Function	
`pvlib.irradiance.total_irrad`(tilt, ..)	Determine total POA irradiance
Cell Temperature Function	
`pvlib.pvsystem.sapm_celltemp`(gPOA, ..)	Estimate cell temperature

Solar position function The solar position function is based on the National Renewable Energy Laboratory's (NREL) Solar Position Algorithm (SPA) described in [45]. The solar position function is used to calculate the apparent zenith, the solar zenith, and the solar azimuth angles in degrees for a specific location. These angles are further used as input to the decomposition and transposition functions. The site-specific parameters for Evenstad, listed in Table 7.2, were given as input to the solar position function. The air pressure in Table 7.2, is the average air pressure measured at Evenstad weather station in 2017, based on data downloaded from eklima.

TABLE 7.2: Input parameters for the solar position function

Location Parameters	Evenstad
Longitude [°]	11.0803
Latitude [°]	61.4255
Altitude [m a.s.l.]	257
Pressure [kPa]	980

Irradiance decomposition and transposition functions The irradiance decomposition function decompose the measured GHI into its DNI and DHI components, while the transposition function transpose these components into POA components for a given surface tilt. As previously mentioned, multiple decomposition and transposition models exists. PVLIB includes various built-in decomposition methods. Based on available data for Campus Even-

stad, only two of the built-in decomposition methods could be used in the PV model developed in this thesis:

1. The `erbs` irradiance decomposition model, and
2. The `dirindex` irradiance decomposition model.

Both were implemented in the model to see if the choice of decomposition model would significantly impact the results. The `erbs` decomposition model is described in [46], and has its name from one of the authors of the article, D.G. Erbs. The `erbs` decomposition model estimates both the DNI and the DHI based on input GHI, where the diffuse fraction is estimated through an empirical relationship between the diffuse fraction and the ratio of GHI to extraterrestrial irradiance [46]. The `dirindex` decomposition model is based on [47]. This decomposition method determines the DNI using clear-sky values of the GHI and the DNI. The corresponding DHI is calculated using Eq. (3.2) described in Section 3.1.2. Clear-sky values of the GHI and the DNI are estimated using `get_clearsky`. The `get_clearsky` function takes in the time and the solar position angles, and returns the GHI and DNI that can be expected on a clear-sky day for the specific site in question.

TABLE 7.3: PV panel input parameters for the transposition function

PV panel parameters	
Tilt angle	35 °
PV azimuth	170 °
Albedo	0.2

The transposition function takes in the PV panel's tilt angle, the panel's azimuth from North, and the surface albedo. The values of the mentioned parameters are listed in Table 7.3. The approximation of the PV azimuth and the albedo is supported by a master's thesis [25], conducted spring 2017, analyzing the PV system at Campus Evenstad, though in [25], the azimuth was approximated to be -10° from South. The `total_irrad` transposition function overrides the albedo if the user specifies the surface type on which the sunlight is reflected. Among the possible surface types are *grass*, *snow*, and *asphalt*. According to the references [48, 49, 50] provided for `total_irrad` in [44], surface type *grass* is equivalent to an albedo of 0.15 - 0.25. Surface types *snow* and *asphalt* represents an albedo of 0.80 - 0.90 and 0.04-0.18, respectively. Based on the big difference in albedo for the different surface types, the selected surface type is expected to have a great impact on the resulting PV pro-

duction estimation. Therefore, `total_irrad`, will be run with the different surface types mentioned above, including *none* which implies that the specified albedo of 0.2 is used.

The transposition function chosen for this thesis provides a list of six irradiance models to choose from. Required input vary from model to model, which in turn limits the choice of irradiance model. The *isotropic* irradiance model was selected as the preferred irradiance model. A perez model also needed to be specified in the transposition function. Most of the available perez models are based on observations from the United States, at locations with distinct climate conditions from those expected in Norway [39, 51, 52, 53]. The *allsitecomposite1990* perez model was hence selected, as this model includes an average over all sites investigated.

PV production Equation (4.5) from Section 4.1.3 is used to estimate the PV production at Campus Evenstad. The overall PV system efficiency, η_{sys}, is suggested to be 77%, excluding temperature impacts, on p. 323 in [9]. Knowing that the AC capacity of the PV system at Campus Evenstad is approximately 60 kW_{ac} [7], η_{sys} is calculated to be 85% from Eq. (4.4). Investigating the measured data of the PV production provided by Kinect Energy Group, the highest hourly PV production was found to be 52 kWh/h, which suggests an overall system efficiency of 74%. The PV production of Campus Evenstad will hence be estimated using three values of η_{sys}: 0.74, 0.77 and 0.85. The cell temperature, T_{cell}, is calculated using Eq. (4.6). The remaining parameters are listed in Table 7.4.

TABLE 7.4: Input parameters to the PV production model

PV production parameters	
P_{dc0} [kW]	70.38
γ_T [%/°C]	-0.4
G_{STC} [W/m^2]	1000
$T_{cell,STC}$ [°C]	25

7.2 Pyomo

7.2.1 Battery Model

As mentioned in Section 4.3.1, the battery is in this thesis modeled as a box that will be charged at an efficiency η_{ch} and discharged at an efficiency η_{dch}. As the installation of the battery took place while writing this thesis, no information on the battery performance is available. Based on [22], the roundtrip efficiency of the battery is assumed to be 90%. Further, η_{ch} and η_{dch} are assumed to be equal and constant at 95% for simplifying reasons. The battery is initially assumed to fully charged.

The energy content of the battery at time t is given by Eq. (7.1), where z_{t-1}^{ba} represents the energy content prior to time t. The energy drawn from the energy system at time t to charge the battery is denoted as y_t^{ch}, while y_t^{dch} is the energy that becomes available from discharging the battery at time t. Imported electricity along with locally generated electricity from the PV system and the CHP plant may be used to charge the battery.

$$z_t^{ba} = z_{t-1}^{ba} + y_t^{ch} \cdot \eta_{ch} - \frac{y_t^{dch}}{\eta_{dch}} \tag{7.1}$$

The energy content of the battery must at all times, given grid access, have at least 100 kWh usable energy available in case of operation in island mode. This restriction is expressed in Eq. (7.2). On the other hand, the energy content of the battery cannot surpass the installed capacity of the battery. This constraint is given in Eq. (7.3).

$$z_t^{ba} \geq \frac{100kWh}{\eta_{dch}} \tag{7.2}$$

$$z_t^{ba} \leq \frac{204kWh}{\eta_{dch}} = X^{ba} \tag{7.3}$$

To ensure that the energy charged to the battery does not exceed the remaining capacity of the battery, Eq. (7.4) is introduced. Likewise, Eq. (7.5) is introduced to ensure that the energy discharged from the battery does not exceed the available amount of energy stored in the battery at time *t*.

$$y_t^{ch} \leq \frac{X^{ba} - z_{t-1}^{ba}}{\eta_{ch}} \tag{7.4}$$

$$y_t^{dch} \leq z_{t-1}^{ba} \cdot \eta_{dch} \tag{7.5}$$

7.2.2 CHP Model

As explained in Section 5.3, the CHP will be modelled to have two modes of operation:

1. Completely shut off in months October to April, and
2. Operating at maximum (40 kW_{el}) in months May to September.

7.2.3 Electricity Balance

Based on the previous definitions, the electricity demand of Campus Evestad is given in Eq. (7.6). The electricity demand is modelled as a parameter as it, in this thesis, is assumed to be known.

$$D_t^{el} = y_t^{PV} + y_t^{CHP} + y_t^{imp} - y_t^{exp} - y_t^{ch} + y_t^{dch} \tag{7.6}$$

The system is modelled as a single node for simplifying reasons, meaning that it is not considered how the electricity demand is distributed within the campus.

7.2.4 Control Strategies

Three control strategies of the battery are defined in this thesis:

1. Minimization of total import,
2. Minimization of spot energy cost, and
3. Peak shaving.

Minimization of total import As Statsbygg has a long-term vision that Campus Evenstad will become 100% self-sufficient with electricity, an obvious control strategy of the battery would be to minimize the total imported electricity from the grid. Previous to the battery system installation on campus, there were no possibility to control the amount of imported electricity, except creating awareness of the consumption behaviour among students and employees. With the installed battery system, one can, to a greater extent, control the amount of energy imported. As the total import is minimized with this control strategy, the optimization model does not consider at which hours throughout the day it would be more, or less, beneficial to import electricity. From Eq. (7.6), Eq. (7.7) gives the expression to minimize the total amount of imported electricity.

$$Min \sum_{t \in T} y_t^{imp} = \sum_{t \in T} (D_t^{el} - Y_t^{PV} - y_t^{CHP} + y_t^{exp} + y_t^{ch} - y_t^{dch}) \tag{7.7}$$

Minimization of spot energy cost As explained in Section 5.6, the total cost of import is given by the cost of energy and the grid tariff. The minimization of the spot energy cost control strategy takes into consideration the hourly spot price from Nord Pool. The grid tariff is not included in this control strategy. Historical spot prices for 2017, downloaded from Nord Pool, are used in the simulations when implementing this control strategy. The expression for calculating the spot energy cost is given in Eq. (5.2) in Section 5.6.2.

Peak shaving The integration of an energy storage unit is, according to [54] the strategy for peak shaving that holds the most potential. Using the battery to perform peak shaving includes shifting the load from peak periods to off-peak periods, i.e. to charge the battery when demand is low and to discharge the battery in times when the demand is high [54]. It is important to differentiate between grid peak and consumer peak, as the two may not correlate. Shifting the load from grid peak periods to off-peak periods could benefit the grid

as it may reduce the risk of necessary grid expansion. Note that peak shaving at Campus Evenstad solely in grid peak periods is insignificant due to the size of electricity consumption at Campus Evenstad compared to the size of the grid. For the grid to experience effects of the grid peak shaving, other customers must also shift their consumption. In the specific case of Campus Evenstad, there is another reason why peak shaving would be beneficial; reducing the grid tariff. As Campus Evenstad is categorized as a commercial customer when it comes to the grid tariff, the campus is charged for power drawn from the grid in addition to the energy consumed. Eidsiva's grid tariff for commercial customers is calculated based on the hour with the highest amount of power drawn from the grid the last 12 months. Minimizing the local import peak would therefore reduce the grid tariff for Campus Evenstad. There are different approached to reduce the peak power in the optimization problem. The approach chosen in this thesis is to introduce a fictitious penalty cost for power peak.

One could differentiate between two ways of performing peak shaving; minimize the absolute highest import peak, and minimize the sum of imported power above a certain kW. If the objective is to minimize the grid tariff, the highest import peak must be minimized. Minimizing the highest import peak is considered to be the preferred peak shaving strategy for Campus Evenstad.

Minimizing the highest import peak is a quite complicated optimization problem that calls for several iterations. First, the initial import is determined by running the minimization of total import control strategy. In the result, the second highest import value, $y^{imp,2peak}$, is located. The bounds of $y_t^{imp,low}$ are set to this value. The total import is now defined as in Eq. (7.8), differentiating between imports lower and higher than $y^{imp,2peak}$.

$$y_t^{imp} = y_t^{imp,low} + y_t^{imp,high} \tag{7.8}$$

Further, fictitious penalty costs are introduced for $y^{imp,low}$ and $y^{imp,high}$. The optimization model is then run with the objective of peak shaving. In practice, this is carried out by minimizing the total fictitious penalty cost of the imported electricity as expressed in Eq. (7.9). The value of $y^{imp,2peak}$ is adjusted according to the obtained results, and the simulations are repeated.

$$\min C_{penalty} = \sum_{t \in T} (C_{low} \cdot y_t^{imp,low} + C_{high} \cdot y_t^{imp,high}) \tag{7.9}$$

In theory, it would also be beneficial to minimize the export power peak. Per definition, Campus Evenstad is a prosumer. A prosumer is an end-use customer that generates electricity for self consumption. At times when the self-generated electricicty surpass the demand, the prosumer may sell the surplus electricity to the local grid company. The self-generated electricity exported to the grid must not exceed 100 kW at any given time for the end-user to be a prosumer. If the exported electricity exceeds 100 kW, the end-user is categorized as a power supplier and additional costs apply [55]. With today's complex energy system, Campus Evenstad will not exceed 100 kW of self-generated electricity at any given time as the maximum production of the PV system is approximately 60 kW while the maximum electricity production of the CHP is 40 kW. In relation to this, the minimization of the export power peak is therefore not relevant for Campus Evenstad with today's complex energy system. In the future, if the PV system is expanded or additional electrical energy sources are installed, this may become an interesting problem to address.

7.2.5 Minimization of Import Costs

For each control strategy, the total import cost is calculated to see how the choice of control strategy impacts the total cost of import. The total yearly cost of import is given in Eq. (7.10) from Eqs. (5.1) and (5.2) in Section 5.6.

$$\begin{aligned} C_{tot,yearly} = 12 \cdot C_{fixed,monthly} + \sum_{t=1}^{8760} (C_t^{nordpool} + C_{GC}) \cdot y_t^{imp} \\ + C_{fixed,yearly} + C_{power} \cdot y^{imp,peak} + C_{energy} \cdot \sum_{t=1}^{8760} y_t^{imp} \end{aligned} \tag{7.10}$$

The grid tariff is assumed to amount to the highest cost for the customer, and the largest savings potential therefore lies in reducing the grid tariff. In 2017, the highest hourly value of imported electricity was 467.70 kWh. Based on the size of the battery, power peak can as a maximum be reduced by 104 kW. In theory, the grid tariff could therefore be reduced by 104 kW $\cdot$ 470 NOK/kW = 48 880 NOK. In reality, savings of this size would require low demand the following hours and high levels of on-site electricity production.

Chapter 8

Results & Discussion

In this chapter, the obtained results are presented and discussed. Firstly, results from the PV model simulations are given, and lastly, the results of the optimization model with the different control strategies of the battery are presented. Tables and plots are mainly used to present the results. A short recap of some of the terms used to present and discuss the results in this chapter is given below. All terms have been explained in previous chapters, and hence they are only included for fast access.

dirindex	A PVLIB built-in function that decomposes measured GHI into its DNI component based on site-spesific clear-sky values.
erbs	A PVLIB built-in function that decomposes measured GHI into its DNI and DHI components.
R^2	Coefficient of determination. A factor used to describe the goodness of fit between two datasets. $R^2 = 1$ indicates a perfect fit. Note that R^2 may be negative if the two datasets are incompatible.
Albedo	Radiation that reaches a reciever due to reflection.
Pyranometer	Surface observation measuring equipment used to measure global radiation.
Reference cell	Measuring equipment used to measure POA irradiance on the same tilt angle as the PV panel.
DoD	Depth-of-Discharge of the battery, i.e., to which level the battery is discharged with respect to the power capacity of the battery.

8.1 Photovoltaic Model

The PV model constructed in PVLIB is thought to be used to predict future PV production at Campus Evenstad given the weather forecast for a specific day. Although the weather forecast usually changes from hour to hour, it was considered necessary to validate the constructed PV model for longer time periods. Historical meteorological data downloaded from eklima and historical data on the PV production provided by Kinect Energy Group are used to validate the PV model. A manually adjusted timeshift is included to account for Norwegian summertime in the downloaded meteorological data.

The limited available data on historical PV production, and the quality of the historical meteorological data, limit the time periods possible for validation and also the credibility of the result. All simulations were run with the two irradiance decomposition methods, `erbs` and `dirindex`, and various surface types as explained in Section 7.1. When running the simulations, it became clear from the results that an albedo of 0.2 was used for the surface type *grass*, i.e. surface types *grass* and *none* gave the same result in all cases. Surface type *grass* is therefore excluded from the results.

Firstly, it was desirable to run simulations for a whole year to compare the estimated annual PV production with the measured and expected annual production. Based on available data, 2017 was chosen. Further, it was interesting to split the test period into summer and winter to see if the different methods worked better or worse in periods with low temperatures and irradiance values compared to high temperatures and irradiance values. An obvious way to separate summer from winter is to differentiate Norwegian summertime from wintertime. In 2017, Norwegian summertime was from the 26th of March at 02:00 to the 29th of October at 03:00. For simplifying reasons, summertime was modelled from 26.03.2017 00:00 to 28.10.2017 23:00. Hence, 2017 is divided into the following three test periods:

1. **1st Wintertime Period**: 01.01.2017 - 25.03.2017
2. **Summertime Period**: 26.03.2017 - 28.10.2017
3. **2nd Wintertime Period**: 29.10.2017 - 31.12.2017

Due to the time-consuming process of downloading measured POA irradiance from Sunny Portal as explained in Section 5.1.1, the estimated POA irradiance is not presented nor compared to measured POA irradiance in these three test periods.

As Norwegian summertime and wintertime represent quite long time periods, the model was also tested for shorter periods of time. Two additional time periods were selected based on the quality of the meteorological data. The two time periods are listed below.

1. **May & June 2017**: 01.05.2017 - 30.06.2017
2. **October 2016**: 01.10.2016 - 31.10.2016

For these two time periods, hourly values of the measured POA irradiance were downloaded from Sunny Portal. Both the estimated POA irradiance and the estimated PV production are hence compared to measured data for May & June 2017 and for October 2016.

The following subsections present the results obtained for the different test periods. The POA irradiance is given in kW/m^2, while the PV production is given in kW. All results are rounded to the nearest kW. The error of the estimations, compared to measured data, is given in %. Both the calculated error and R^2 are given in separate columns for each result.

8.1.1 Results 2017

The total PV production measured in 2017 by Kinect Energy Group is 46 770 kW. The PV model results are listed in Table 8.1, including the calculated error and R^2 of each PV estimate. The combination of overall system efficiency, irradiance decomposition method and surface type that gives the best estimation of the measured PV production is highlighted in Table 8.1.

TABLE 8.1: Estimated PV production 2017

η_{sys}	**PV$_{\text{dirindex}}$**	*error*	R^2	**PV$_{\text{erbs}}$**	*error*	R^2
Surface type = none						
0.74	52 304	11.83 %	0.76	54 175	15.83 %	0.64
0.77	54 424	16.37 %	0.75	56 371	20.53 %	0.61
0.85	60 079	28.46 %	0.70	62 228	33.05 %	0.52
Surface type = snow						
0.74	54 093	15.66 %	0.76	55 962	19.65 %	0.63
0.77	56 286	20.35 %	0.74	58 231	24.51 %	0.60
0.85	62 134	32.85 %	0.68	64 281	37.44 %	0.50
Surface type = asphalt						
0.74	51 985	11.15 %	0.77	53 856	15.15 %	0.64
0.77	54 092	15.66 %	0.75	56 040	19.82 %	0.61
0.85	59 712	27.67 %	0.70	61 862	32.27 %	0.53

As seen from Table 8.1, the calculated R^2 correlates to the calculated error, i.e., the combination of η_{sys}, irradiance decomposition method and surface type that gives the smallest error is also the best fit of the measured PV production according to R^2. Using `dirindex` to decompose the GHI into its DNI and DHI components gives the best approximation of the total PV production for all combinations of η_{sys} and surface type. The difference in calculated error for surface type *none* and *asphalt* is small, while surface type *snow* accounts for a larger error.

The hourly variation in the estimated PV production is plotted in Fig. 8.1 using the `dirindex` irradiance decomposition method and a system efficiency of 74%. The measured PV production is included in the figure for comparison. As seen in Fig. 8.1, PV_{erbs} exceeds the installed capacity of the PV system on some occasions. The scaling of the graph makes it difficult to see how the hourly variations of PV_{erbs} fit the hourly variations of the measured PV production, but it may seem like the PV production is somewhat flat throughout the whole year compared to the measured PV production which clearly is lower the first three and the last two months of the year. Although $PV_{dirindex}$ clearly is a better fit to the hourly variations in the measured PV production, it is evident from Fig. 8.1 that the estimated PV production in winter is higher than the measured PV production.

1st Wintertime Period

The total measured PV production in the first wintertime period, from the 1st of January to the 25th of March, is 4 416 kW. Simulated results for this time period are listed in Table 8.2. The combination of overall system efficiency, irradiance decomposition method and surface type that gives the estimated PV production closest to the measured PV production is highlighted in the table.

In the first wintertime period of 2017, $PV_{dirindex}$ gives the smallest error of the estimated PV production as seen in Table 8.2, although the error is unacceptably high. Using the `erbs` irradiance decomposition method gives an error over 100% for all combinations of η_{sys} and surface type. Notice that the calculated R^2 is negative for PV_{erbs}, indicating that estimated values and the measured values are incompatible. As the estimated PV production is clearly an overestimation of the measured PV production, the lowest overall system efficiency and the lowest albedo value results in the most accurate PV estimation. Recall from Section 7.1 that surface type *asphalt* indicates an albedo between 0.04 - 0.18.

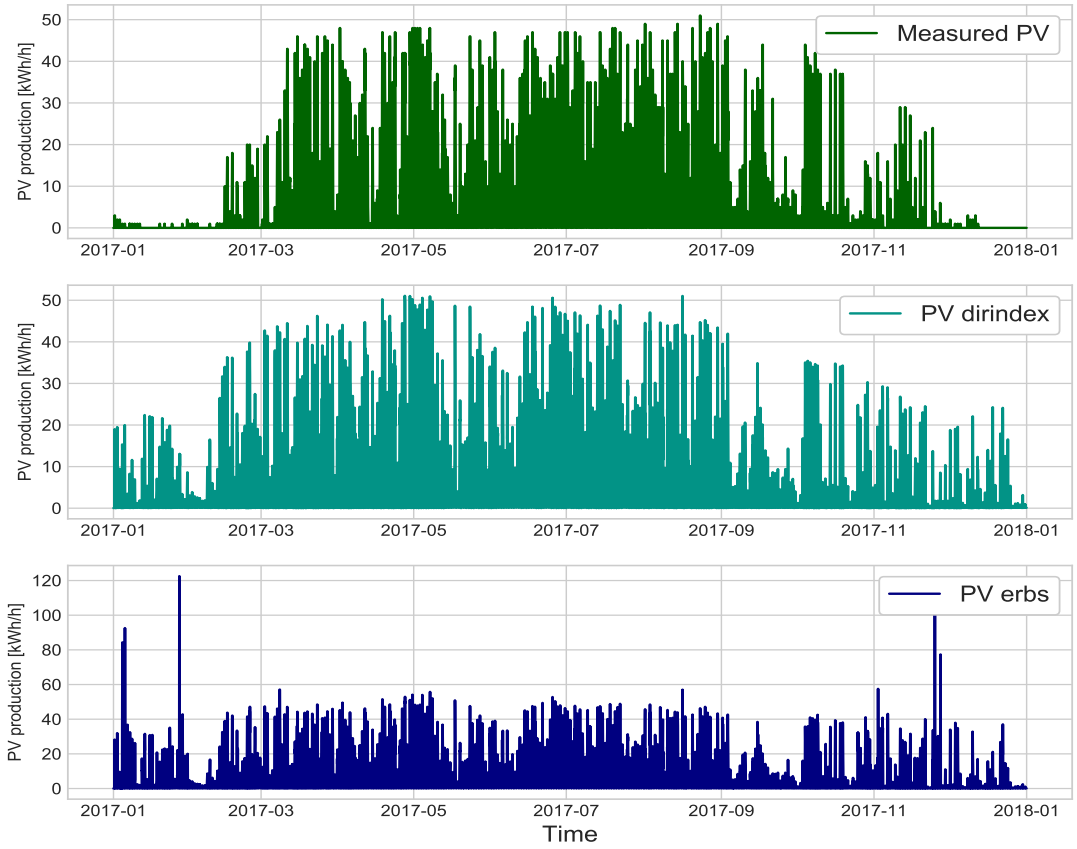

FIGURE 8.1: Hourly variations in the 2017 PV production.

TABLE 8.2: Estimated PV production in the 1st wintertime period

η_{sys}	$\mathbf{PV_{dirindex}}$	*error*	R^2	$\mathbf{PV_{erbs}}$	*error*	R^2
Surface type = none						
0.74	8 106	83.56 %	0.39	9 437	113.70 %	-0.28
0.77	8 435	91.01 %	0.33	9 820	122.37 %	-0.40
0.85	9 311	110.85 %	0.13	10 840	145.47 %	-0.77
Surface type = snow						
0.74	8 310	88.18 %	0.36	9 640	118.30 %	-0.31
0.77	8 647	95.81 %	0.30	10 030	127.13 %	-0.44
0.85	9 546	116.17 %	0.09	11 073	150.75 %	-0.83
Surface type = asphalt						
0.74	8 070	82.74 %	0.40	9 401	112.88 %	-0.27
0.77	8 397	90.15 %	0.34	9 782	121.51 %	-0.39
0.85	9 269	109.90 %	0.14	10 799	144.54 %	-0.76

Figure 8.2 gives a closeup of the measured and the estimated PV production in the first three months of 2017. Looking at the graph of the measured PV production in this time period, hardly any energy is generated the first month and a half. It is questionable whether these are realistic measurements of the PV production. Although the PV system is expected

to generate less energy in winter due to less solar radiation and fewer sunlight hours, low temperatures and the reflection of sunlight from the snow should contribute to a higher PV production than what is visualized in Fig. 8.2. The $PV_{dirindex}$ production is also lower the first month and a half compared to the rest of the time period, although significantly higher than the measured PV production. As commented in the 2017 results, the `erbs` irradiance decomposition method is, on some occasions, resulting in a much higher PV production than the installed capacity of the PV system corresponds to. From the plot of the PV_{erbs} production, it is clearer that, apart from the extremely high values mentioned, the hourly variations in the PV production are smaller than the hourly variations in the measured and the estimated $PV_{dirindex}$ production. The extreme overestimation may explain the negative R^2 of the estimated PV_{erbs} production.

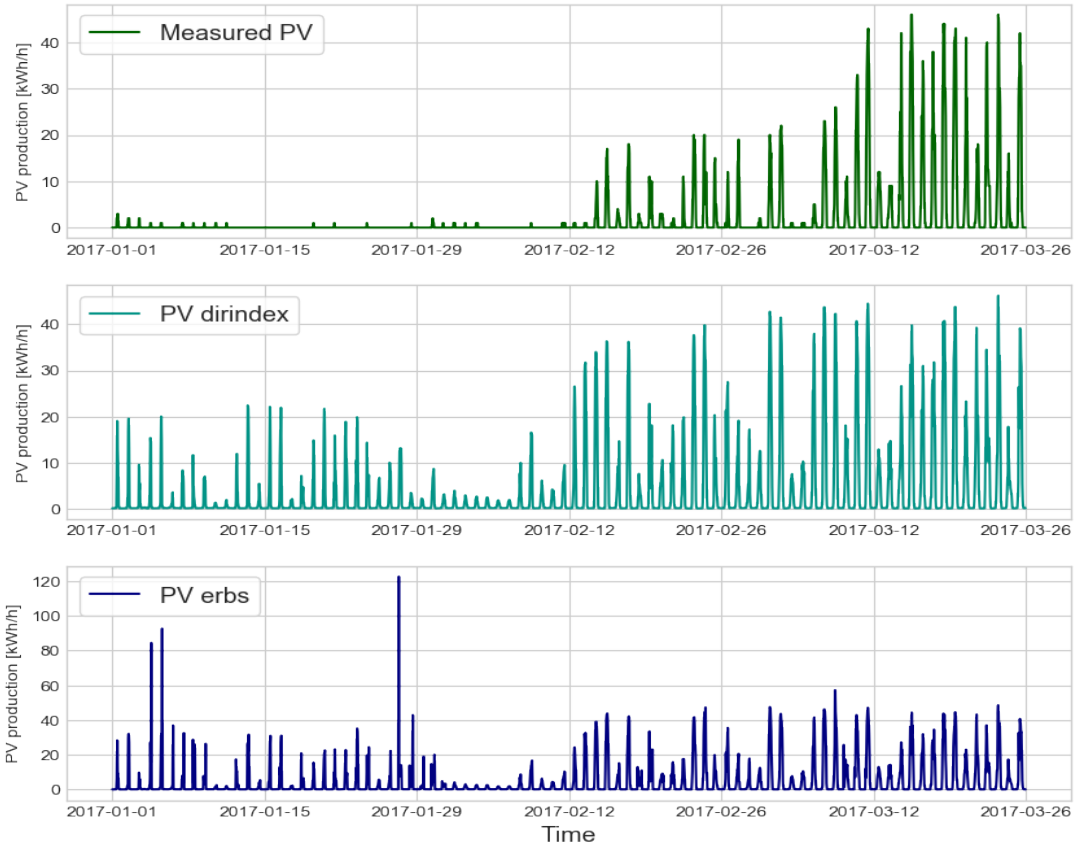

FIGURE 8.2: Hourly variation in the PV production during the 1st wintertime period.

Summertime Period

Table 8.3 includes the obtained results for the summertime period in 2017. As it is unlikely that there is snow in this time period, simulations were not run for surface type *snow*. The

total measured PV production in this time period is 41 325 kW. The combination of η_{sys}, irradiance decomposition method and surface type that gives the most accurate result compared to measured PV production is highlighted in the table.

TABLE 8.3: Estimated PV production in the 2017 summertime period

η_{sys}	$\mathbf{PV_{dirindex}}$	*error*	R^2	$\mathbf{PV_{erbs}}$	*error*	R^2
Surface type = none						
0.74	41 680	0.86 %	0.80	41 009	0.76 %	0.79
0.77	43 369	4.95 %	0.80	42 672	3.26 %	0.78
0.85	47 875	15.85 %	0.76	47 105	13.99 %	0.74
Surface type = asphalt						
0.74	41 406	0.20 %	0.80	40 736	1.43 %	0.79
0.77	43 085	4.26 %	0.80	42 387	2.57 %	0.78
0.85	47 561	15.09 %	0.77	46 791	13.23 %	0.75

As seen from Table 8.3, the calculated error of the estimated PV production in much smaller in the summertime period compared to the error found in the 1st wintertime period. It is not unlikely that the built-in functions in PVLIB are calibrated to work better in summer as PV systems are expected to produce more energy in summer than in winter due to solar radiation levels. The smallest error, 0.20%, is found for $PV_{dirindex}$ with surface type *asphalt* and an overall system efficiency of 74%. For an insignificant error of 0.20% one could expect that the R^2 would be higher than 0.80. A goodness of fit of 80% when the error is only 0.20% indicates that the estimated PV production might be overestimated some hours and underestimated other hours. The overestimation and underestimation of the PV production add up to a total estimated production of low error compared to total measured PV production. The difference in the $PV_{dirindex}$ and the PV_{erbs} production estimations are very small, and much smaller than the differences found in the 1st wintertime period results.

The hourly variations in the PV production are plotted in Fig. 8.3 using η_{sys} = 74% and surface type *asphalt*. Unlike in the 1st wintertime periods, there are no PV production values that exceeds the installed capacity of the PV system. However, as seen in Fig. 8.3, the highest estimated PV_{erbs} value is higher than the highest estimated $PV_{dirindex}$ value. Comparing the three plots in Fig. 8.3, there is a small deviation between the hourly variation in the estimated PV production and the hourly variations in the measured PV production. From Table 8.3, the R^2 of the $PV_{dirindex}$ estimation is 0.80 while the R^2 of the PV_{erbs} estimation is 0.79. 80% of the variations in the $PV_{dirindex}$ estimation and 79% of the variations in the PV_{erbs} can hence be accounted for in the hourly variations of the measured PV production.

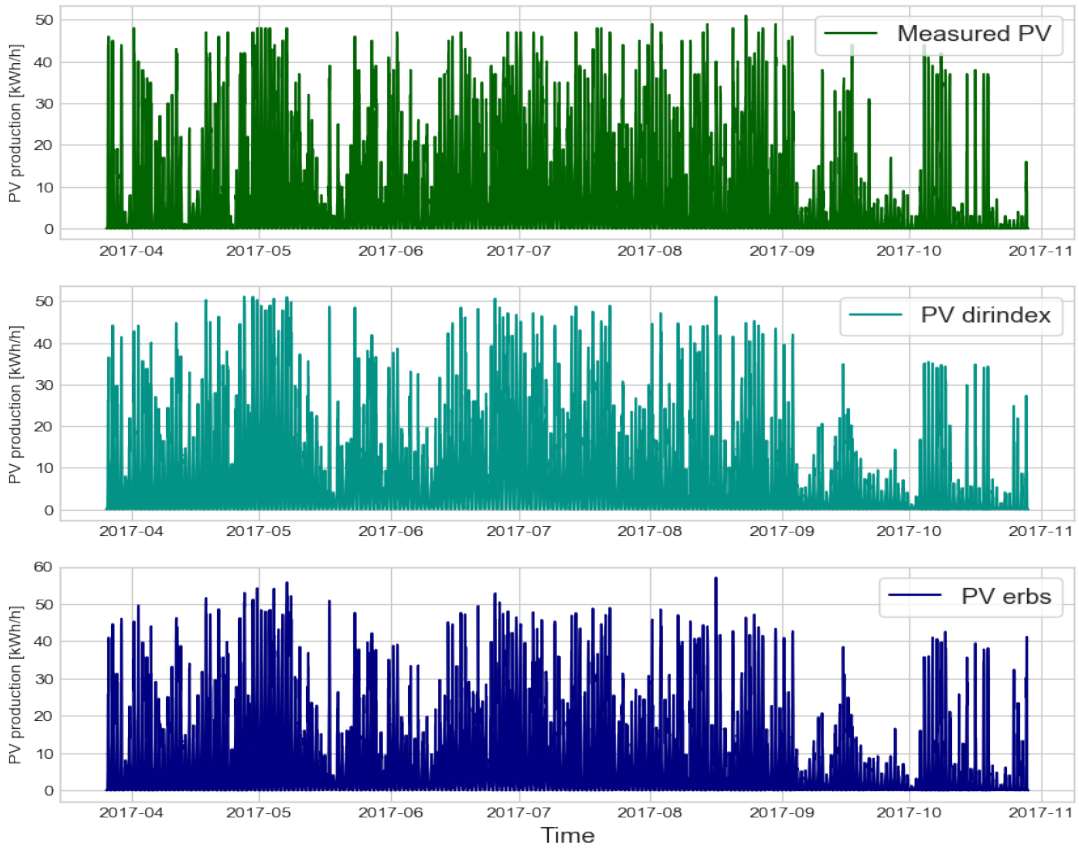

FIGURE 8.3: Hourly variations in the PV production in summertime 2017.

2nd Wintertime Period

The total measured PV production in the 2nd wintertime period in 2017 is 1 029 kW. The estimated results obtained from the PV model are presented in Table 8.4, where the combination of η_{sys}, irradiance decomposition method and surface type that gives the best approximation of the PV production is highlighted.

As in the first two time periods of 2017, an overall system efficiency of 74% and using the `dirindex` irradiance decomposition method gives the best PV approximation. However, the error of the PV estimation is 143.8% which is significantly bigger than the error found in the 1st wintertime period and in the summertime period. Both irradiance decomposition methods result in negative R^2, but as seen from Table 8.4, the calculated R^2 is much poorer for PV_{erbs}.

Looking at the PV plots in Fig. 8.4, the case is similar to that in the 1st wintertime period. In December, hardly any PV production is registered in the measured data provided by Kinect Energy Group. As discussed earlier, it seems unlikely that the PV production is zero or close to zero even though irradiance levels are low. Also in the first half of the time period, the

TABLE 8.4: Estimated PV production in the 2nd wintertime period of 2017

η_{sys}	**PV$_{\text{dirindex}}$**	*error*	R^2	**PV$_{\text{erbs}}$**	*error*	R^2
Surface type = none						
0.74	2 518	144.70 %	-0.43	3 728	262.29 %	-4.32
0.77	2 620	154.62 %	-0.57	3 880	277.07 %	-4.80
0.85	2 892	181.05 %	-0.98	4 283	316.23 %	-6.19
Surface type = snow						
0.74	2 570	149.76 %	-0.48	3 779	267.25 %	-4.40
0.77	2 674	159.86 %	-0.63	3 933	282.22 %	-4.88
0.85	2 952	186.88 %	-1.05	4 341	321.87 %	-6.30
Surface type = asphalt						
0.74	2 509	143.83 %	-0.42	3 719	261.42 %	-4.31
0.77	2 610	153.64 %	-0.56	3 870	276.09 %	-4.79
0.85	2 882	180.08 %	-0.97	4 272	315.16 %	-6.17

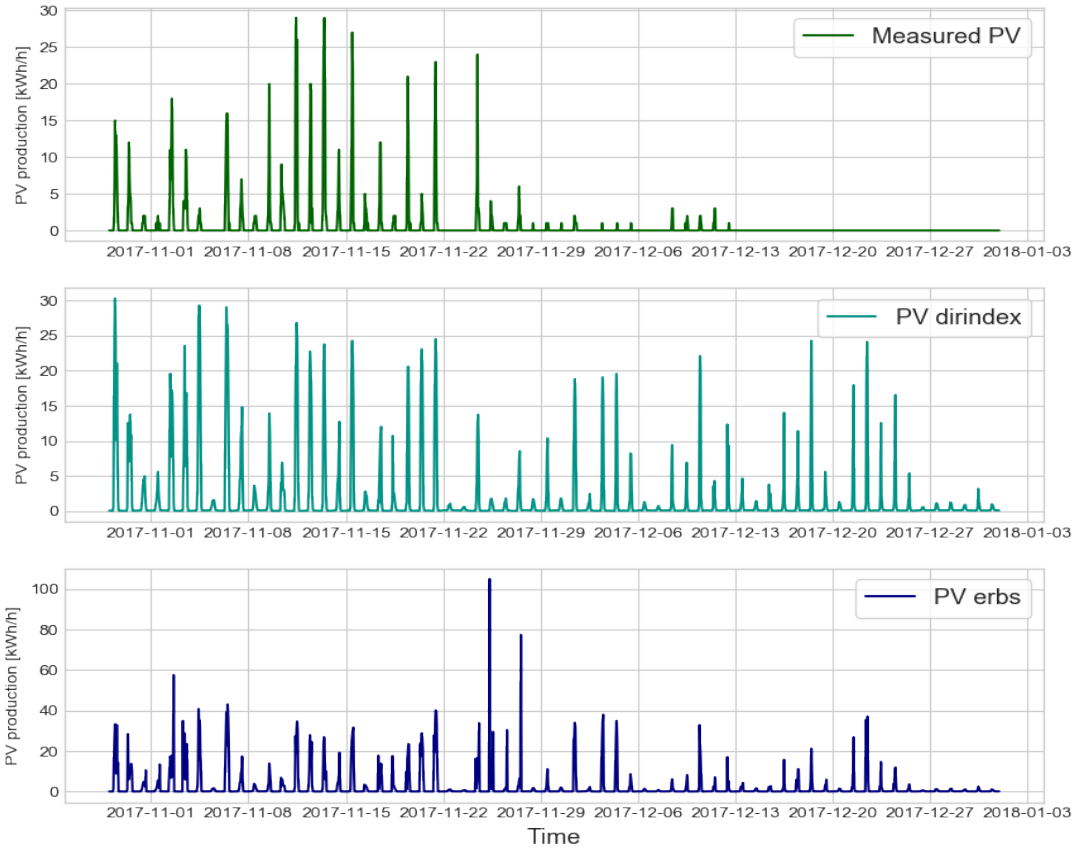

FIGURE 8.4: Hourly variations in the PV production during the 2nd wintertime period.

estimated PV production is higher than the measured PV production. In the hourly variation plot for the whole year of 2017 in Fig. 8.1, a peak was seen in the estimated PV$_{\text{erbs}}$ production. In Fig. 8.4 it is evident that the PV$_{\text{erbs}}$ estimate exceeds the installed PV capacity on two occasions in the 2nd wintertime period. Even the lower values of PV$_{\text{erbs}}$ are higher than the

$PV_{dirindex}$ estimations. The hourly variation plots of the estimated $PV_{dirindex}$ production and the PV_{erbs} production reflects the negative R^2 in Table 8.4.

8.1.2 May & June 2017

Due to weather conditions, the highest PV production is expected to take place during the summer months. Good irradiance values in Norway are normally detected in May and June, and therefore these two months were selected for further validation of the PV model in summer. Figures 8.1 and 8.3 in Section 8.1.1 confirms high levels of measured PV production at Campus Evenstad in May and June 2017. Surface type *snow* is excluded from the simulations as it is considered unsuitable and unrealistic for this time period. Hourly data of the measured POA irradiance, downloaded from Sunny Portal, are used to compare the measured and the estimated POA irradiance. The total measured POA irradiance in May & June 2017 is 301.66 kW/m^2. The results of the estimated POA irradiance are presented in Table 8.5. It is self-explanatory that the overall PV system efficiency does not impact the results of the POA irradiance estimates as the PV performance is dependent on the solar radiation, but not vice versa. The best estimation of the measured POA irradiance is highlighted in Table 8.5.

TABLE 8.5: Estimated POA irradiance May & June 2017

Surface type	$\mathbf{G_{dirindex}}$	*error*	R^2	$\mathbf{G_{erbs}}$	*error*	R^2
none	287.64	4.65 %	0.81	277.18	8.12 %	0.81
asphalt	285.56	5.34 %	0.81	275.10	8.80 %	0.81

The total estimated POA irradiance in May & June 2017 is lower than the measured POA irradiance in all cases. $G_{dirindex}$ gives an error of 4.65% when surface type *none* is applied. This is a very small error considering the following factors:

1. The GHI data used as input in the PV model for Campus Evenstad is estimated based on GHI measurements from close-by weather stations. As stated in Section 5.1, the solar radiation is site dependent, which implies that the Evenstad GHI estimate itself may be inaccurate. Apart from the large distances between the close-by weather stations and Evenstad weather station, the variation in altitude of the different weather stations is significant. Recall from Section 5.1 that locations at higher altitudes tend to experience higher levels of solar radiation due to the path that the sunlight takes before it reaches the surface is shorter.

2. The estimated GHI at Evenstad is further decomposed into its DNI and DHI components using built-in functions in PVLIB that are mainly tested for sites with distinct climate conditions from what is expected in Northern countries.
3. Ultimately, POA irradiance estimated from estimated GHI values measured with a pyranometer is compared to POA irradiance measured on a reference cell.

From the estimated POA irradiance, the estimated PV production is found. According to data provided by Kinect Energy Group, the total PV production in May & June 2017 is 14 160 kW. The results of the PV estimates are presented in Table 8.6. The combination of overall system efficiency, irradiance decomposition method and surface type that gives the best estimation of the measure PV production is highlighted.

TABLE 8.6: Estimated PV production May & June 2017

η_{sys}	**$PV_{dirindex}$**	*error*	R^2	**PV_{erbs}**	*error*	R^2
Surface type = none						
0.74	14 661	3.54 %	0.83	14 099	0.43 %	0.83
0.77	15 255	7.73 %	0.82	14 670	3.60 %	0.83
0.85	16 840	18.93 %	0.77	16 194	14.36 %	0.78
Surface type = asphalt						
0.74	14 561	2.83 %	0.83	13 999	1.14 %	0.83
0.77	15 151	7.00 %	0.83	14 566	2.87 %	0.83
0.85	16 725	18.11 %	0.78	16 079	13.55 %	0.78

The PV_{erbs} estimation gives the smallest error as seen from Table 8.6. This is the first test period where the `erbs` irradiance decomposition method resulted in the best PV estimation. However, the difference in the calculated $PV_{dirindex}$ and PV_{erbs} errors with η_{sys} = 74% is so small that $PV_{dirindex}$ estimate can also be considered to be a good estimate of the measured PV production. R^2 for the two irradiance decomposition methods are equal, implying that $PV_{dirindex}$ and PV_{erbs} are an equally good fit of the measured PV production. Compared to the results of the summertime period in 2017 in Section 8.1.1, the error is slightly higher but the goodness of fit is better. This simply implies that the hourly variations of the PV estimation are better accounted for in the May & June test period although the deviation of the total PV production is slightly higher.

The hourly variations of the estimated POA irradiance and the estimated PV production are plotted in Fig. 8.5. For consistency, an overall system efficiency of 74% and surface type *asphalt* is applied in the plots. The accuracy of the obtained results in Tables 8.5 and 8.6 are confirmed by the plots in Fig. 8.5.

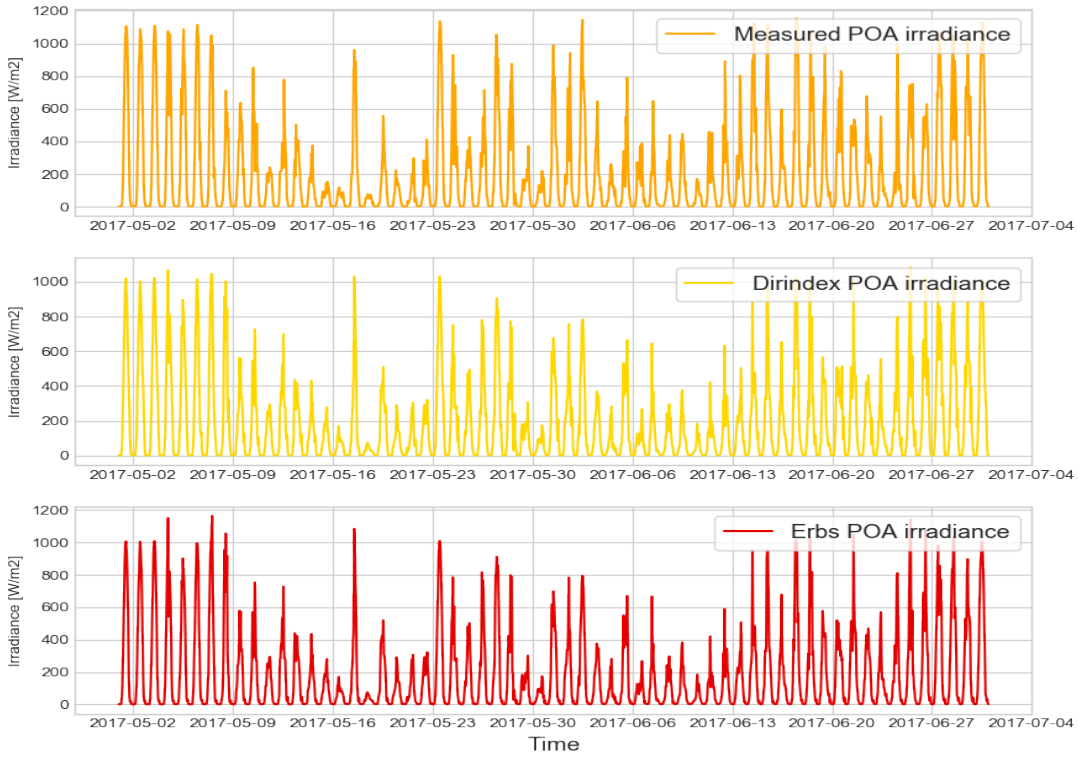

(A) POA irradiance

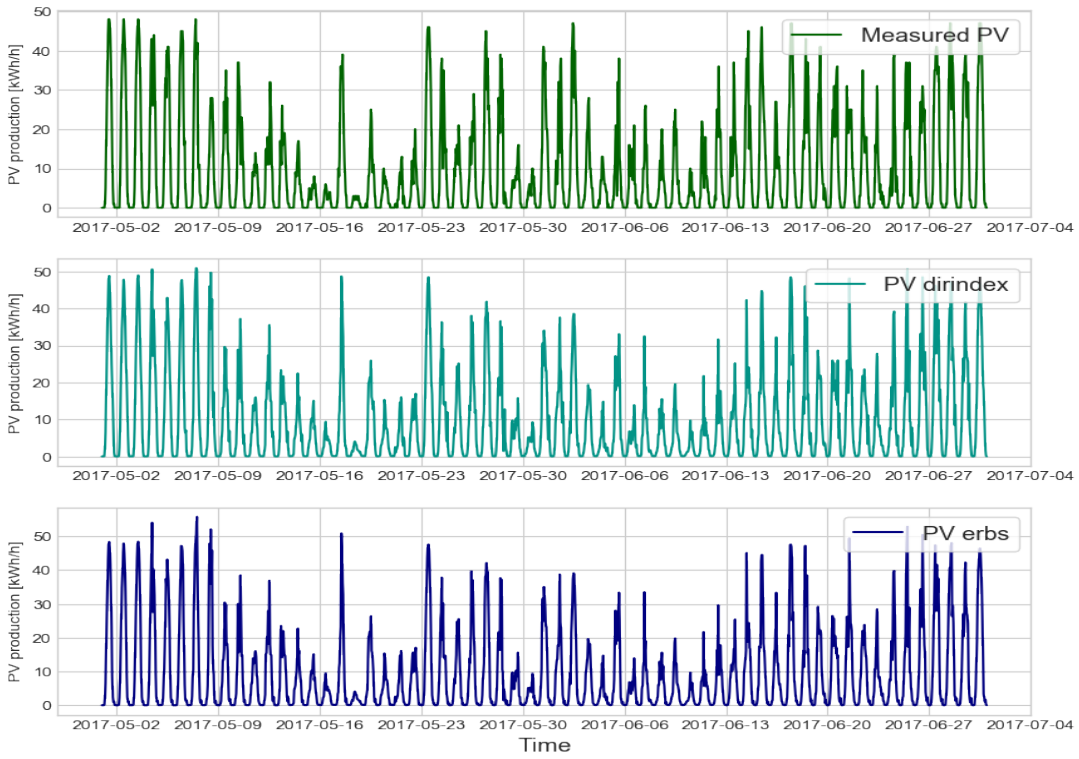

(B) PV production

FIGURE 8.5: Hourly variations in POA irradiance and PV production in May & June 2017.

8.1.3 October 2016

Although October is per definition summertime in Norway, the month is generally considered to represent the transition between summer and winter. The climate conditions may vary from one extreme to another, which makes October an interesting month to analyze. Surface type *snow* is included in the simulations as October is a month where the first snowfall may occur.

The results of the estimated POA irradiance are presented in Table 8.7 and compared to measured POA irradiance downloaded from Sunny Portal. As mentioned in Section 5.2, no data is logged on the Sunny Portal after October 19, 2017. Therefore, October 2016 is modelled. The total measured POA irradiance in October 2016 is 59.24 kW/m^2. The most accurate POA irradiance estimation is highlighted in Table 8.7.

TABLE 8.7: Estimated POA irradiance October 2016

Surface type	**$G_{dirindex}$**	*error*	R^2	**G_{erbs}**	*error*	R^2
none	54.76	7.56 %	0.86	76.61	29.33 %	-0.00
snow	56.42	4.76 %	0.87	78.27	32.12 %	-0.02
asphalt	54.47	8.05 %	0.86	76.32	28.83 %	-0.00

Compared to the POA irradiance results found for May & June 2017, the difference in error between $G_{dirindex}$ and G_{erbs} is significantly larger in the results of October 2016. The `dirindex` irradiance decomposition method gives the most accurate estimation of the POA irradiance. The calculated R^2 of G_{erbs} ranges from -0.02 to -0.00, i.e., the estimated POA irradiance from `erbs` is a bad fit of the measured POA irradiance. $G_{dirindex}$, on the other hand, represents a fit of approximately 86%-87%. What is surprising about the POA irradiance results is that surface type *snow* gives the best estimation of the measured POA irradiance. As described in Section 7.1, surface type *snow* is equivalent to an albedo of 0.80 - 0.90, while the approximated albedo, i.e., the albedo for surface type *none*, is 0.20. The higher albedo, the larger amounts of solar radiation is reflected onto the PV panel, and the more energy is generated by the PV array. Even with an albedo of 0.80 - 0.90, the $G_{dirindex}$ POA irradiance is underestimated compared to the measured POA irradiance.

The PV production measured at Campus Evenstad in October 2016 is 3 319 kW. The total estimated PV production based on estimated POA irradiance is presented in Table 8.8. The combination of overall system efficiency, irradiance decomposition method and surface type that estimated the total PV production to be closest to the measured PV production is

highlighted in the table.

TABLE 8.8: Estimated PV production October 2016

η_{sys}	$\mathbf{PV_{dirindex}}$	*error*	R^2	$\mathbf{PV_{erbs}}$	*error*	R^2
Surface type = none						
0.74	2 923	11.93 %	0.74	3 894	17.32 %	0.66
0.77	3 041	8.38 %	0.74	4 052	22.08 %	0.62
0.85	3 357	1.14 %	0.74	4 472	34.74 %	0.51
Surface type = snow						
0.74	3 007	9.40 %	0.75	3 976	19.80 %	0.65
0.77	3 129	5.72 %	0.75	4 137	24.65 %	0.62
0.85	3 454	4.07 %	0.74	4 567	37.60 %	0.49
Surface type = asphalt						
0.74	2 908	12.38 %	0.74	3 879	16.87 %	0.66
0.77	3 025	8.86 %	0.74	4 036	21.60 %	0.62
0.85	3 340	0.63 %	0.74	4 456	34.26 %	0.51

Unlike the results of the POA irradiance, the best estimation of the PV production is found for surface type *asphalt*. In all other test periods presented in this chapter, η_{sys} = 74% gave the best result. The October 2016 results show that η_{sys} = 85% gives the best estimation of the PV production. In fact, for all other test periods, the estimation of the PV production is less accurate with increasing overall system efficiency without exception, both when the estimated PV production is based on the `dirindex` and when it is based on the `erbs` irradiance decomposition method. For October 2016, the accuracy of the estimated $PV_{dirindex}$ production increases with increasing η_{sys}. Assuming surface type *asphalt* and η_{sys} = 74%, both the resulting POA irradiance and the PV production are underestimated compared to the measured data. The high albedo of the best POA irradiance estimation and the high overall PV system efficiency of the optimal PV production estimate may be a cause of several things:

1. The estimated GHI values used as an input to the PV model may be underestimated. Underestimated GHI values would cause the estimated POA irradiance to be too low compared to the measured POA irradiance, which would explain the high albedo. Low POA irradiance estimations will in turn result in an underestimate of the PV production, which would explain the high overall system efficiency.
2. The measured PV production used for comparison may be inaccurately high. As stated in Section 5.2, the measured data on the historical hourly PV production provided by Kinect Energy Group is rounded to the nearest kWh/h. Information on how the PV

production values are rounded to the nearest kW is not given, but it is a reasonable assumption that the values are rounded up if .5 or higher and down otherwise. The hourly PV production may be reduced or increased by 1 kW as a consequence of this. This itself is an insignificant number, but in the long run this might impact the total PV production significantly. Hypothetically, the total PV production in October could be reduced or increased by 744 kW as a consequence of this rounding, i.e., the measured PV production in October 2016 would lie in the range of 2 575 kW - 4063 kW. Assuming that actual PV production in October 2016 is lower than the data provided by Kinect Energy Group implies, the accuracy of the estimated PV production would possibly be better than the current results show.

3. The PV model itself may be underestimating the POA irradiance and hence also the PV production. As discussed previously, the built-in functions in PVLIB used to decompose and transpose GHI into POA irradiance are not tested and validated for high latitudes and cold climates. An inaccurate decomposition and transposition of the GHI causes an inaccurate estimation of the POA irradiance, and hence an even more inaccurate estimation of the PV production as the POA irradiance is also used to calculate the PV cell temperature that impacts the estimated performance of the PV system.
4. As previously stated, October represents the transition between summer and winter in Norway, and hence varying weather conditions may occur. Uncertain and unstable weather conditions may have had an impact on both meteorological data, the POA irradiance measurements, and the measurements of the historical PV production.

The hourly variations in the POA irradiance and the PV production are plotted in Fig. 8.6, using surface type *asphalt* and η_{sys} = 74% for consistency. As for the estimated PV production in the two wintertime periods in 2017, PV_{erbs} exceeds the installed PV capacity on some occasions. As seen from Fig. 8.6a, the high PV_{erbs} values are caused by extremely high estimated G_{erbs} values. The highest POA irradiance value exceeds 4 kW/m^2. Such high values of irradiance are impossible to reach, and the estimation is hence fundamentally wrong for this time point. The quality of input data may to some extent cause too high estimations of the POA irradiance, however, the main reason why the estimated POA irradiance is so high is without a doubt due to the decomposition and the transposition of input GHI data. It is difficult to tell whether the error is caused by the decomposition or by the transposition of GHI, but most likely it is a combination of both as many uncertain factors are involved. Apart from

(A) POA irradiance

(B) PV production

FIGURE 8.6: Hourly variations in POA irradiance and PV production for October 2016.

the POA irradiance peak, G_{erbs} exceeds 1 kW/m^2 on three occasions as seen in Fig. 8.6a. The maximum POA irradiance found in the measured data and in the estimated POA irradiance

based on the `dirindex` irradiance decomposition method is around 800 W/m^2.

8.1.4 Notes and Comparison of the PV Model Results

Some general observations can be made when comparing the results of the PV model for the different test periods:

- The developed PV model in this thesis is more accurate in summertime periods than in wintertime periods, i.e., when expected solar radiation is higher.
- The `dirindex` irradiance decomposition method proved to give more accurate estimations of POA irradiance and PV production. The exception is the test period in May & June 2017, where the PV_{erbs} estimation was closest to the measured PV production. However, the difference in error between $PV_{dirindex}$ and PV_{erbs} is so small that `dirindex` can be considered to be the preferred irradiance decomposition method.
- An overall system efficiency of 74% gave the best results for all test periods, except in October 2016. The irregularity in the October 2016 results may be caused by multiple factors as discussed in Section 8.1.3. $\eta_{sys} = 74\%$ was the overall system efficiency found based on the maximum measured PV production.
- Generally, a low albedo, i.e., low levels of reflected solar radiation, resulted in the most accurate results. Again, October 2016 results were the exception.
- The calculated R^2 is not always consistent with the calculated error. For instance, the results of the summertime period in 2017 had an error of 0.20% and a R^2 value of 0.80, while the estimated PV production in for the May & June 2017 test period, the error was higher (0.43%) but it still resulted in a higher goodness of fit to the measured PV production (0.83). This indicates that although the total error is low, there might be some points where the estimated results are shifted from the measured results, i.e., the estimated PV production decreasing when the measured production is rising or vice versa.
- May & June 2017 results and October 2016 results verify that the largest source to error lies in the decomposition and transposition of GHI into POA irradiance. Other sources to error in the PV model have been discussed throughout Section 8.1, but are briefly recapped here:
  - The GHI values used as input to the PV model are estimated.

- The chosen built-in functions to decompose and transpose GHI into POA irradiance may be inappropriate or even inaccurate. As described in Section 6.1.1, PVLIB is developed and tested for geographical locations that are very distinct from that of Evenstad.
- Input GHI is measured using a pyranometer, while measured POA irradiance is measured on a reference cell.
- Data on historical PV production was rounded to the nearest kW. In the worst-case scenario, the actual annual PV production could be 8760 kW higher or lower than the provided data indicate.

As the results of the two wintertime period in 2017 were bad, one could argue that more validation of the developed PV model should have been performed for winter months. However, as discussed in Section 8.1.1, the measured PV production that the estimated values are compared to are questionable. If the model had given accurate results of inaccurate measurements, the model would still be wrong. It was attempted to run the PV model for additional winter months. However, due to the lack of access to good quality meteorological data and measured PV data in winter, it was concluded that presenting the results would be both improper and erroneous.

8.2 Optimization Model

The optimization model created in Pyomo was solved with the three battery control strategies explained in Section 7.2.4:

1. Minimization of total imported electricity.
2. Minimization of spot energy cost.
3. Peak shaving of the highest import peak.

When minimizing the spot energy cost, the fixed monthly charge of the spot energy cost is excluded from Eq. (5.2) in the optimization model. Excluding the fixed charge from the simulations will not affect the use of the battery since the fixed charge remains constant in all months. The modified expression for total spot energy cost is given in Eq. (8.1).

$$C_{spot} = \sum_{t=1}^{n} (C_t^{nordpool} + C_{GC}) \cdot y_t^{imp} \tag{8.1}$$

The use of the battery is dependent on the hourly load demand and the hourly electricity generation on site. In this thesis, as the CHP electricity generation is assumed to be known, the PV production accounts for the hourly variations in the on-site electricity generation. The model created in this thesis is supposed to be a building block to perform model predictive control of the battery in the future. The PV production is, as previously discussed, highly dependent on the variations in solar radiation and air temperature. The weather forecast changes continuously, and to account for the changing forecast of solar radiation and air temperature, it makes sense to optimize the use of the battery for shorter time periods. A 48-hour optimization period of the battery is chosen as the simulation time period in this thesis. As it is desirable to see how much savings potential the battery holds, the optimization model is also applied to the whole year of 2017. Based on the results of the 2017 simulations, the total cost of import is calculated, including the monthly fixed cost of the spot price and the yearly fixed cost of the grid tariff.

In addition to applying the control strategies to the actual complex energy system at Campus Evenstad, two additional cases were added:

1. The estimated PV production was doubled to see how an expansion of the PV system would affect the use of the battery, and
2. The installed capacity of the battery was doubled to see how the size of the battery would affect its use.

8.2.1 48h Optimization Results

It was desirable to test time periods of high load demand and periods of high PV production. Four 48-hour time periods were chosen: two in May due to the high PV production, and two in November due to the high load demand. The results are presented graphically for each test period.

The peak shave control strategy is not applied to the 48-hour test periods as the cost-benefit of peak shaving at the specific case of Campus Evenstad is to reduce the grid tariff, and looking at an isolated 48-hour time period does not give a good indication of whether the peak in this period is also the yearly peak.

May 2017

May holds high solar radiation levels in Norway and hence high PV production. From Fig. 8.5b in Section 8.1.2, it is visible that the PV production on May 17 is especially high compared to the day before and the day after. Therefore, the following two 48-hour time periods were chosen:

1. May 16 to 17
2. May 17 to 18

Figure 8.7 shows the optimization results for these two 48-hour time periods in May 2017. The spot price is plotted using a secondary axis to see the correlation between the spot price and the imported energy for the minimization of spot energy cost control strategy.

Naturally, when the objective is to minimize the total import of electricity, energy is not imported to recharge the battery. Hence, does only the on-site PV production contribute to the recharging of the battery. As seen from Figs. 8.7a and 8.7b, recharging of the battery only occurs when the PV production is assumed doubled for both 48-hour time periods in May, and even then, only a small recharge of the battery takes place. Doubling the installed battery capacity leads to the discharging of the battery being distributed over some time, as the available discharge capacity of the battery is higher than the load demand.

When optimizing with the objective of minimizing the spot energy cost, the battery is used more actively since low spot prices leads to full recharging of the battery. For both 48-hour time periods in May, the spot price decreases drastically between hours 24 and 30, as seen in Figs. 8.7a and 8.7b, resulting in a full recharge of the battery. The low spot price in this time period results in a significant increase of the import peak, and the peak also takes place at a time where the load demand is not at its highest. When doubling the installed battery capacity for this control strategy, the import peak exceeds 400 kW. The results hence show that applying the minimization of spot energy cost control strategy may lead to a peak shift and also a peak increase. The peak is no longer determined by the load demand; it is determined by the spot price and the available storage capacity of the battery.

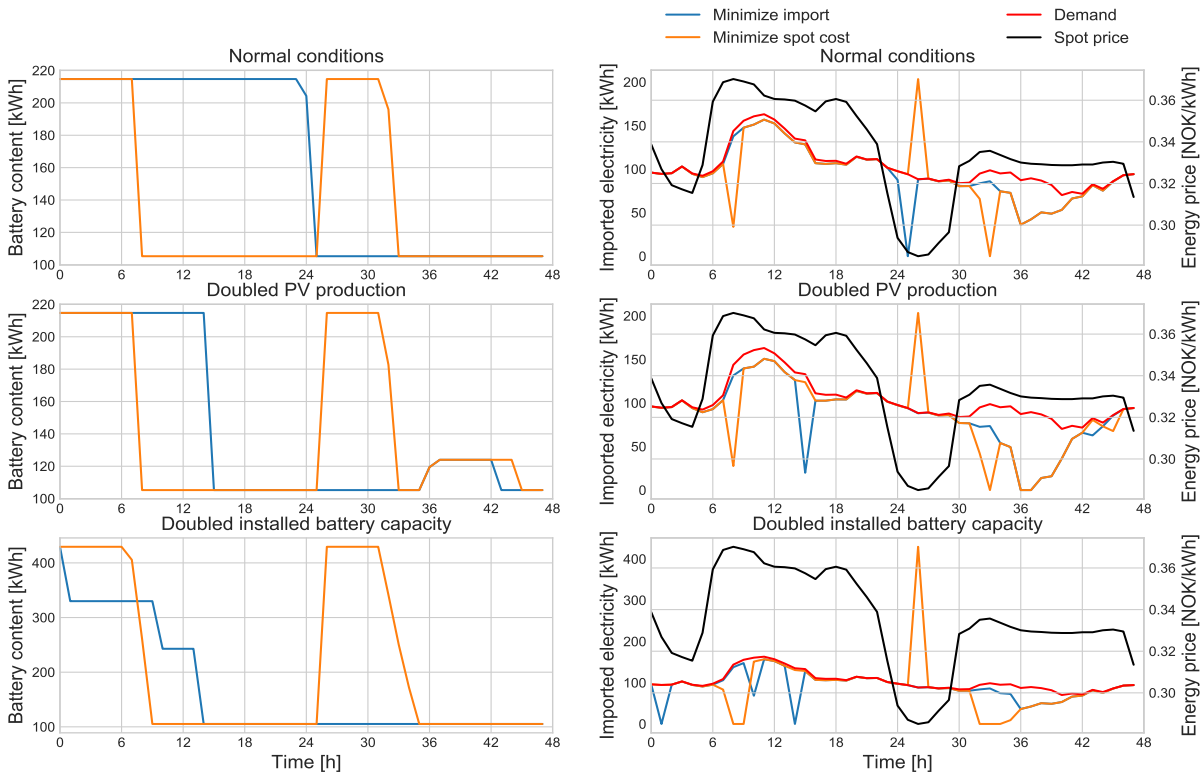

(A) 16th and 17th of May

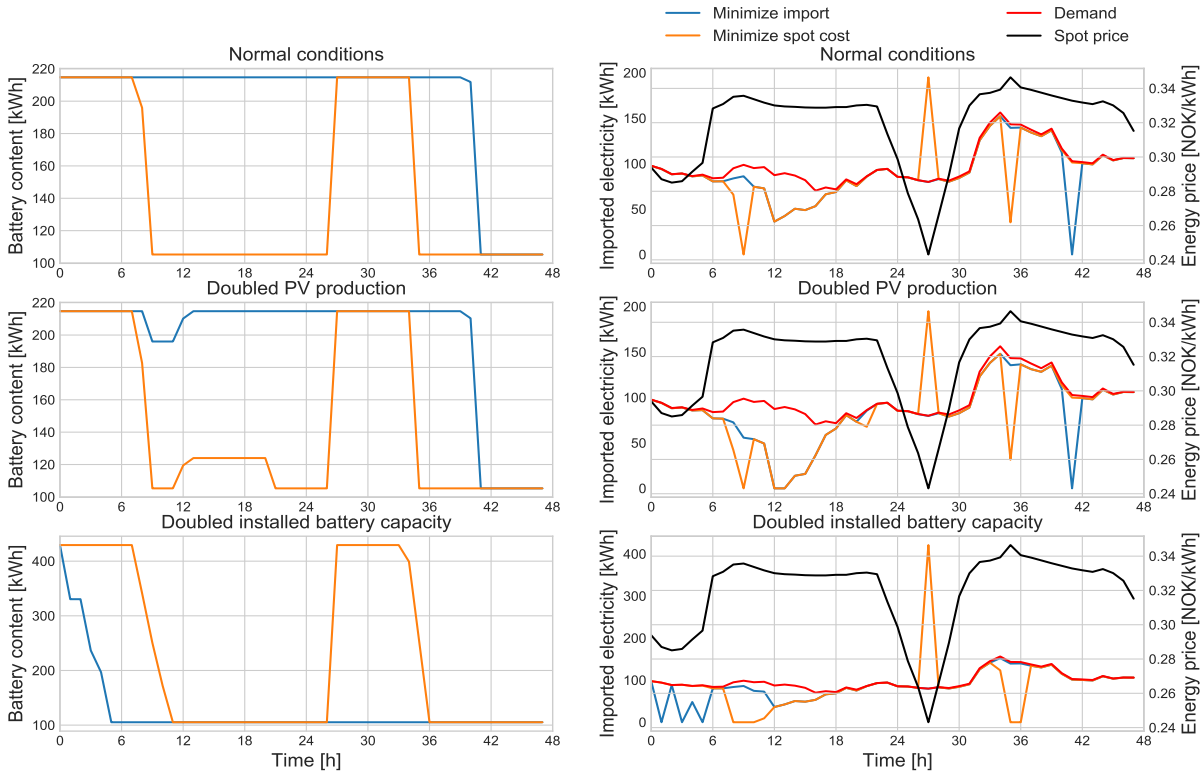

(B) 17th and 18th of May

FIGURE 8.7: Optimization results of the 48-hour time periods in May 2017.

November 2017

November is chosen due to the historical high import peaks in both 2016 and 2017, as seen from Fig. 5.7 in Section 5.5. The import peak in 2017 from the historical data provided by Multiconsult is 467.70 kW and occurred on November 22. Since the days prior to November 22 also showed high values of imported electricity, the following 48-hour time periods were selected for November 2017:

1. November 20 to 21
2. November 21 to 22

The results of the optimization model for the two 48-hour time periods in November 2017 are illustrated in Fig. 8.8. The main findings in the 48-hour time periods in May also apply in the 48-hour time periods in November:

1. When minimizing the total imported electricity, the battery is only discharged once.
2. When applying the minimization of spot energy cost control strategy, the battery is fully recharged as a result of low spot prices.

However, unlike in the May optimization results, doubling the PV production does not lead to small recharging of the battery. The PV production in November is much smaller than in May, while the load demand is higher, and hence a recharge of the battery is unlikely. Also, when doubling the installed battery capacity, the discharge of the battery is not spread over time, like it was in May for the minimization of total import control strategy, due to the high load demand.

In the two 48-hour time periods in May, the import peak increased and changed its occurrence when the control strategy of minimizing the energy spot cost was applied. In the November results, for the same control strategy, the peak is increased and shifted only when the installed battery capacity is assumed doubled. Even though the spot price is fairly low during peak under normal conditions and when the PV production is assumed doubled, the battery is not able to recharge itself due to the high load demand, and hence the import peak remains the same in these two cases. When the installed battery capacity is doubled, the import peak increases and the occurrence of the peak changes when applying the minimization of spot energy cost control strategy for both November test periods. The resulting import peak is significantly higher than the historical import peak of 2017. For November

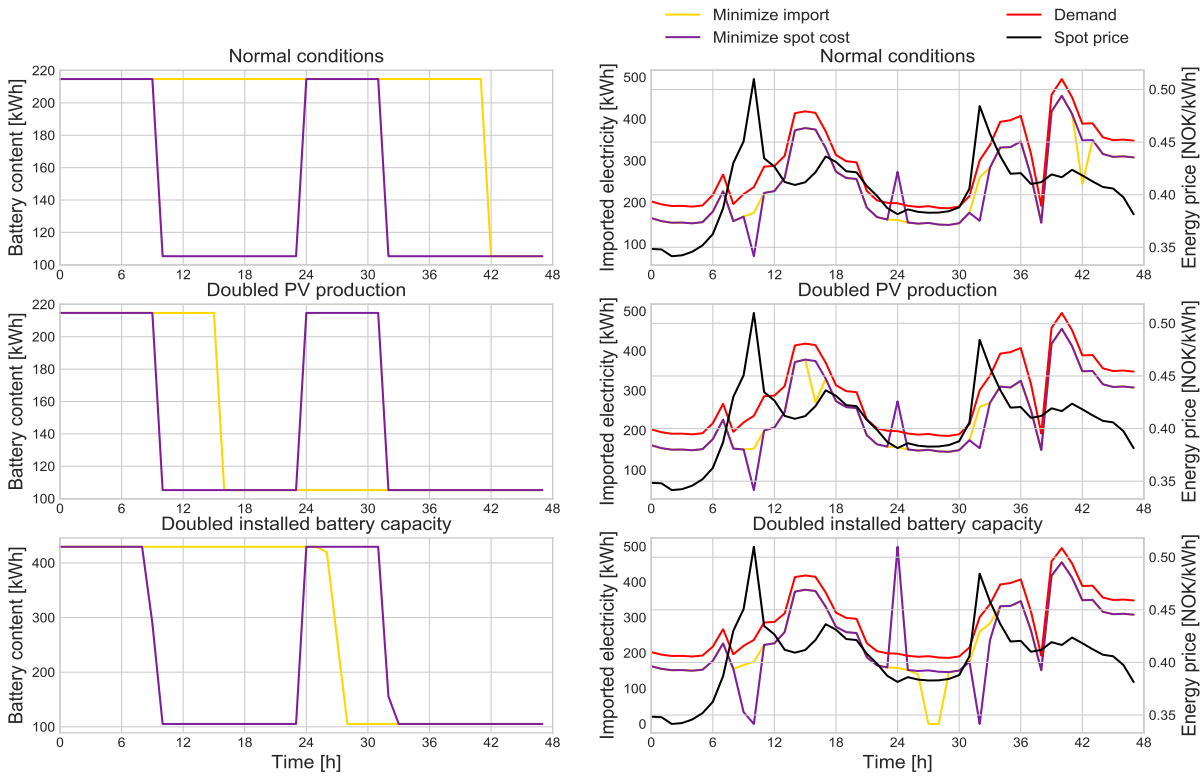

(A) 20th and 21st of November

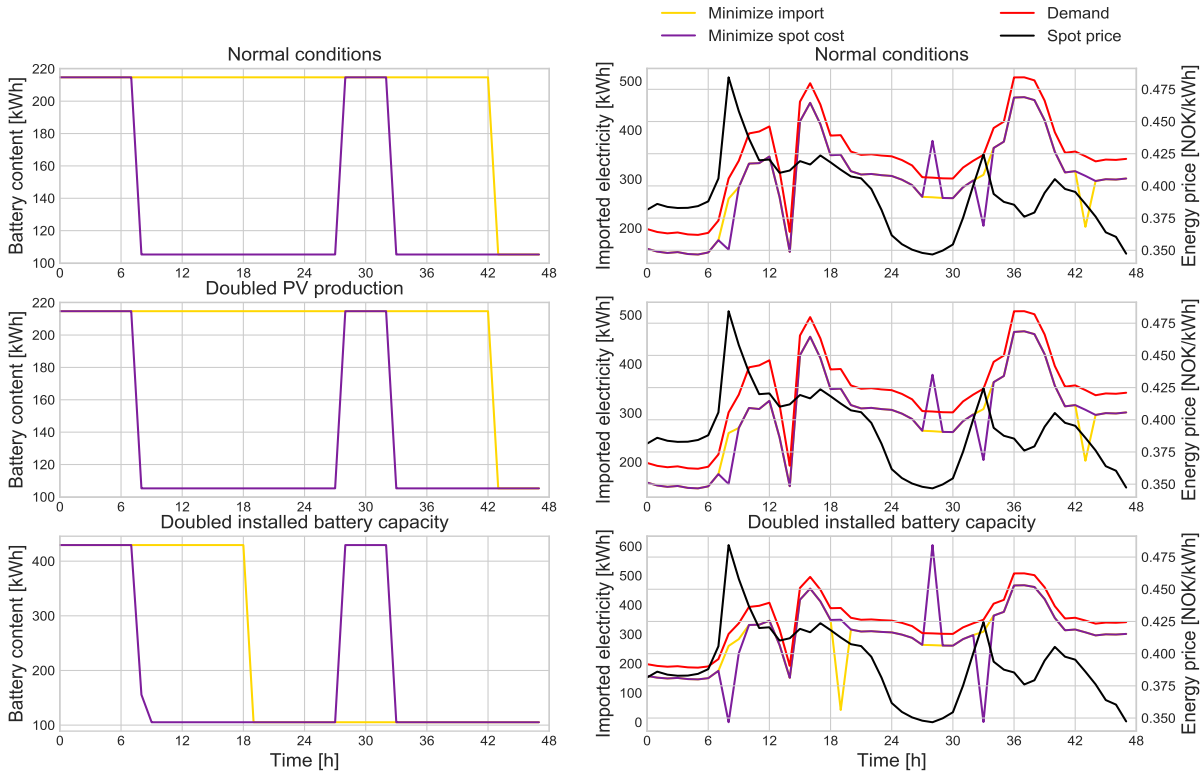

(B) 21st and 22nd of November

FIGURE 8.8: Optimization results of the 48-hour time periods in November 2017.

20 to November 21 in Fig. 8.8a, new import peak of 499.31 kWh/h. Due to the extremely low spot price between hours 24 and 30 on November 22 in Fig. 8.8b, import peak increases from 467.70 kWh/h to 604.18 kWh/h.

As seen in Fig. 8.8, the spot price is initially low before it starts to increase. The battery is, when applying the minimization of spot energy cost control strategy, set to recharge when the spot price is low. However, since the battery is assumed to be fully charged at the start of each test period, there is no available storage capacity at this time. If the initial battery content had been set to a lower value, the battery would initially charge. This is also the case for the 48-hour time periods in May.

8.2.2 Yearly Optimization Results

In the yearly simulations, the peak shave control strategy with the objective of minimizing the highest import peak is applied in addition to the other two control strategies. The size of the battery is a limiting factor when applying the peak shave control strategy. The installed capacity of the battery is 108 kW/204 kWh, and the battery is restricted to be able to deliver 100 kWh of usable energy at any given time to start up the CHP in case of power failure. This leaves a peak shaving potential of 104 kWh/h. The power peak typically occurs in winter, and as the PV production in winter is much lower than in summer, the realistic peak shaving potential becomes even smaller than 104 kWh/h.

Results of the minimization of total imported electricity control strategy are illustrated graphically in Fig. 8.9. Figure 8.10 shows the results when the total imported energy is minimized. The results of the peak shaving control strategy are presented in Fig. 8.11. For the peak shaving control strategy, the first, second and last iteration are plotted for each case. The iterations of the peak shaving control strategy were stopped when the resulting peak was higher than the restricted maximum. Each control strategy is tested for the same three cases as the 48-hour time periods: normal conditions, doubled PV production, and doubled installed battery capacity. For each case, and for each control strategy, the total yearly spot energy cost and grid tariff are calculated. For comparison, the total cost of import prior to the battery installation is also calculated. As historical import values from 2017 are only available from the 8th of February, the resulting cost estimation is lower than the expected cost of import. For consistency, the same time period, i.e., from 08.02.2017 to 31.12.2017, is used for all cases. The cost results are presented in Table 8.9.

TABLE 8.9: Calculated cost of imported electricity in 2017

Control Strategy	Energy Cost [NOK]	Grid Tariff [NOK]	Total Cost [NOK]
Initial import	362 305	523 379	885 684
Normal conditions			
Minimize import	360 547	522 019	882 566
Minimize energy cost	358 938	543 914	902 852
Peak shaving	360 591	505 899	866 490
Doubled PV production			
Minimize import	341 559	507 805	849 364
Minimize energy cost	339 929	529 625	869 554
Peak shaving	341 571	491 034	832 605
Doubled installed battery capacity			
Minimize import	360 484	521 962	882 447
Minimize energy cost	356 046	651 190	1 007 236
Peak shaving	360 493	487 208	847 701

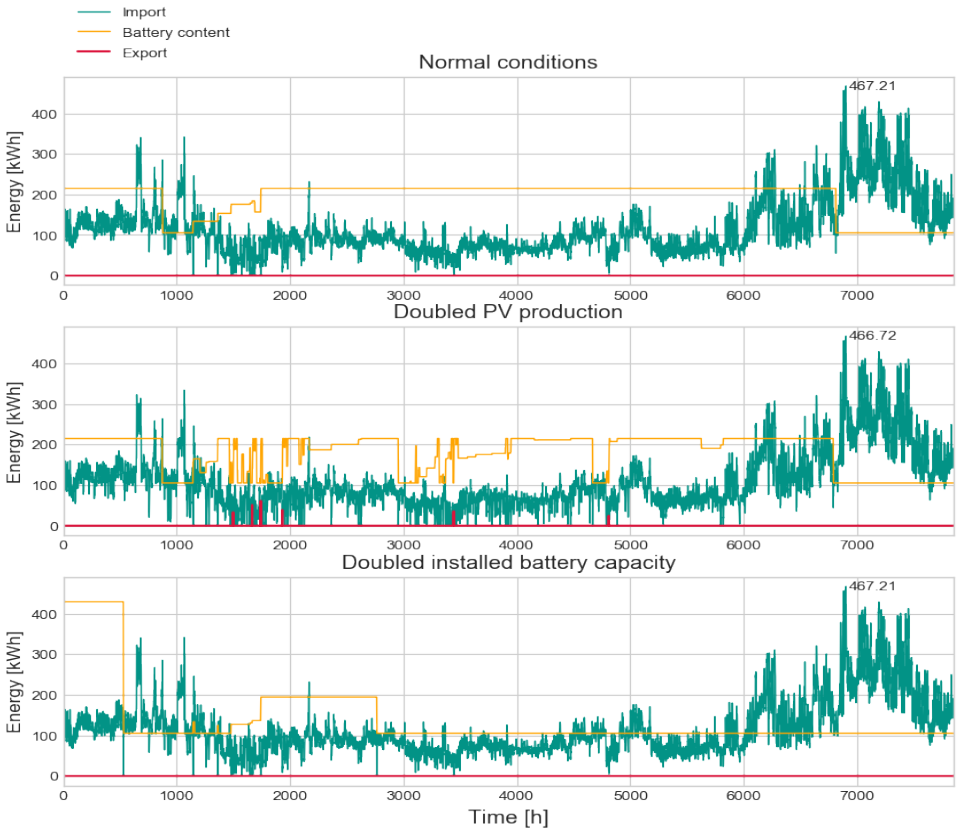

FIGURE 8.9: Control strategy result: Minimization of total import.

For the control strategy of minimizing the total imported electricity, the battery is not frequently utilized, just like the 48-hour optimization results showed. Some recharging of the battery takes place, especially when the PV production is assumed doubled. As the objective of this control strategy is to minimize the total import, the recharge of the battery is solely

a result of high PV production and low demand. Some energy is exported to the grid as a result of the doubled PV production. The total cost of imported energy when applying the minimization of import control strategy is lower than the total cost calculated for the historical import for all cases. As seen from Table 8.9, the savings potential of this control strategy is biggest when the PV production is assumed doubled.

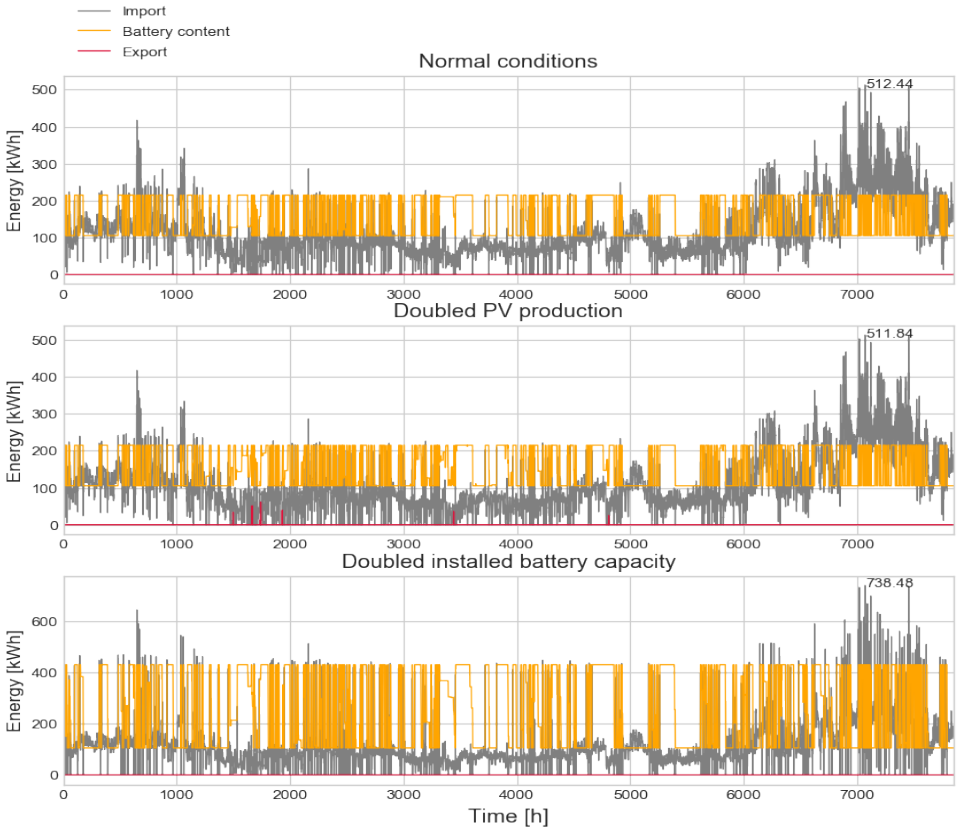

FIGURE 8.10: Control strategy result: Minimization of spot energy cost.

When the objective of the optimization model is set to minimize the total energy spot price, the battery is rapidly charged and discharged throughout the whole year as seen in Fig. 8.10. In the first two cases, under normal conditions and when the PV production is assumed doubled, the import peak is nearly constant at just over 500 kW. When the battery capacity is doubled, the import peak increases significantly to 738.48 kW. Recall that the historical import peak in 2017 was 467.70 kW, i.e., this control strategy leads to a higher import peak in all cases. As seen in Table 8.9, the minimization of spot energy cost control strategy, named *"Minimize energy cost"* in the table, results in the lowest total energy cost in all cases. However, due to the increased power peak that this control strategy results in, the grid tariff is high and hence is also the total cost of imported electricity higher compared to the other two control strategies. Especially when the installed battery capacity is doubled, the total

cost of import is extremely high. The combination of large battery capacity and low spot prices, results in large amounts of import, increased import peak, and hence high grid tariff costs. Also with the implementation of this control strategy, some energy is exported when the PV production is assumed doubled.

The peak shaving control strategy results in the lowest total import cost. As seen from Table 8.9, the energy cost of this control strategy is similar to that of the minimization of total import control strategy, and hence, as expected, the largest savings potential of the total import cost lies with the grid tariff. Under normal conditions and when the PV production is doubled, the peak reduction potential is approximately 34 kW. The minimum import peak was found after four and five iterations, respectively. Although doubling the installed battery capacity results in a greater peak reduction (72.81 kW), the total cost of import is higher than when the PV production is doubled. This is due to the increased storage capacity allowing for more import of electricity as long as the peak is not increased. When doubling the installed battery capacity, the peak shaving control strategy is significantly less efficient than for the first two cases. Seen from Fig. 8.11c, 26 iterations were needed to find the minimum possible peak.

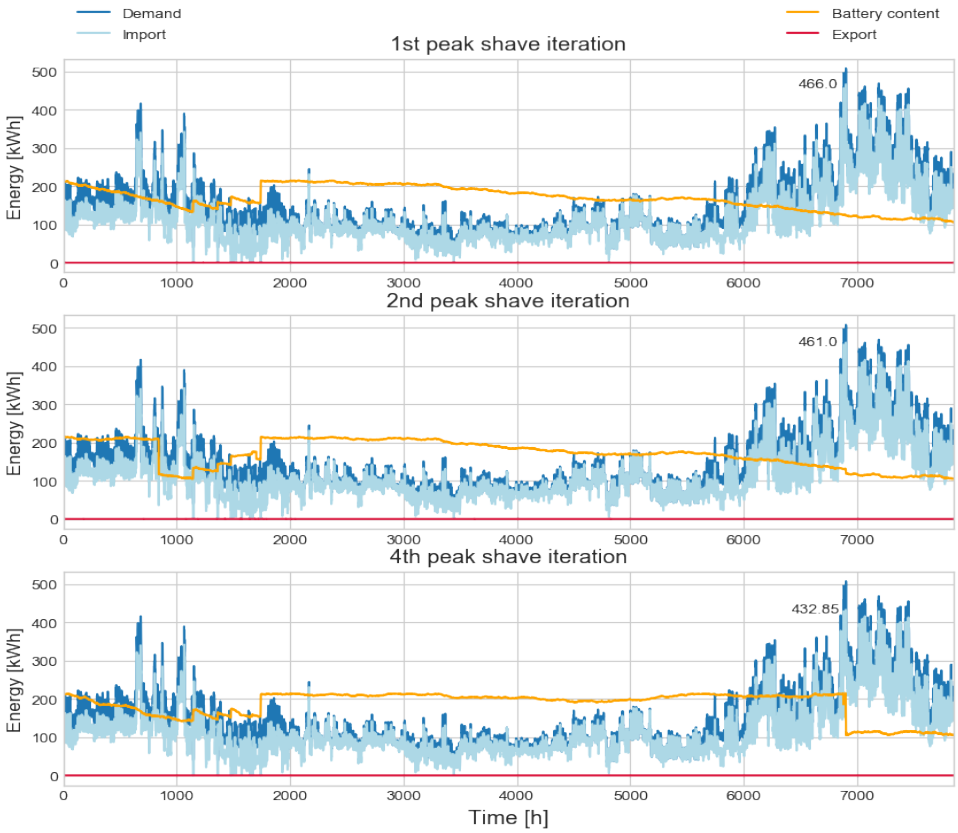

(A) Normal conditions

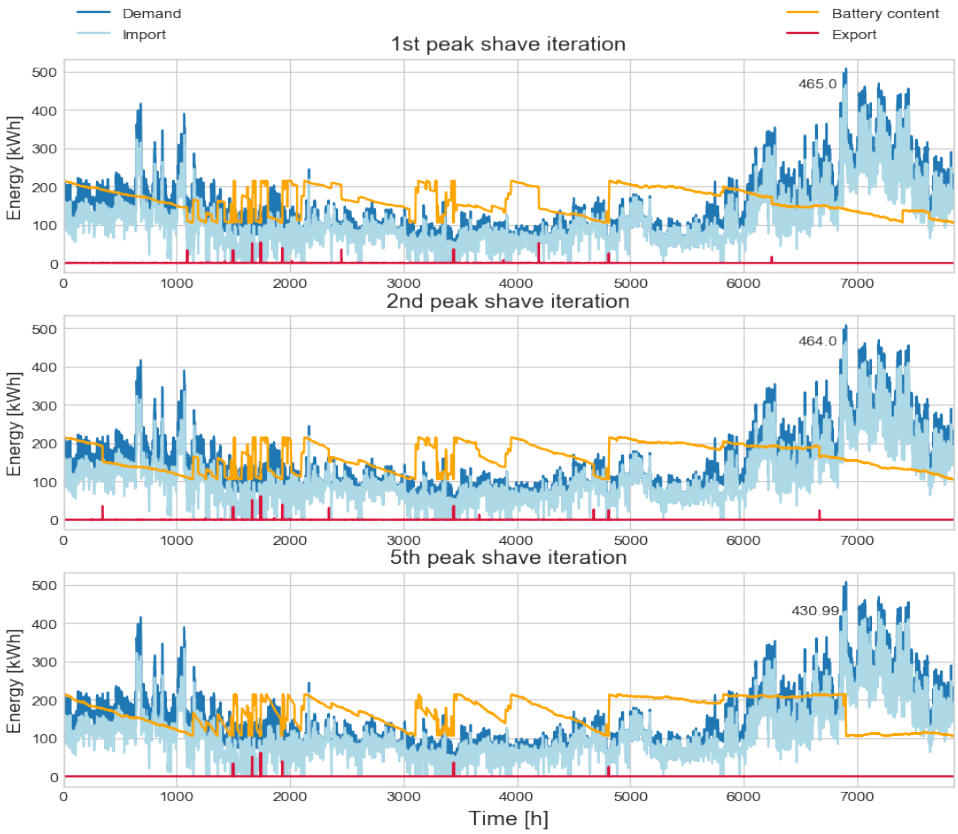

(B) Doubled PV production

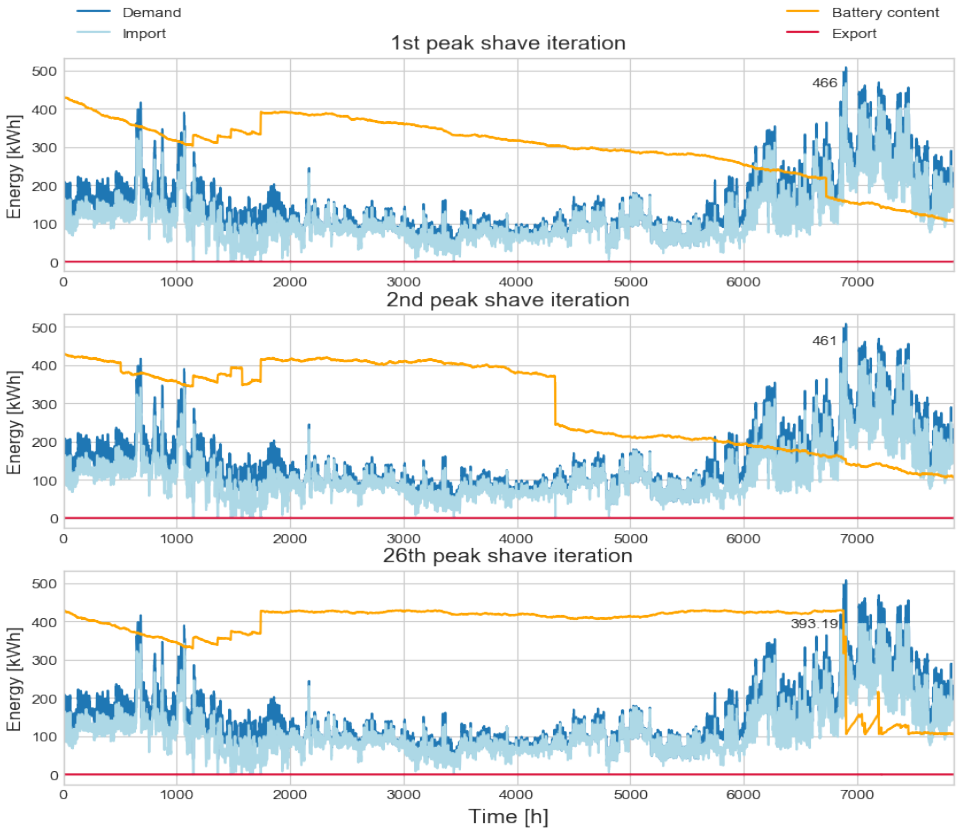

(C) Doubled installed battery capacity

FIGURE 8.11: Control strategy result: Peak shaving.

As seen from the plots in Fig. 8.11, the battery is more actively used when the PV production is doubled as high levels of PV production together with low load demand results in a recharge of the battery. Some energy is exported to the grid when the PV production is doubled, and as seen from Fig. 8.11b, the amount of exported electricity decreases with the number of iterations, i.e., the more the peak is reduced, more of the on-site generated electricity is used internally instead of being exported.

8.2.3 Notes and Comparisons of the Optimization Results

The goal of implementing different control strategies is not necessarily to find the optimal use of the battery. In this sense, the name *"optimization model"* is misleading. The battery utilization is optimized based on the given objective. The chosen battery control strategies may not be realistic, but they illustrate the main principles of different ways that the battery can be used. The main observations of the optimization model results from Section 8.2 are listed below:

Control Strategies

- Minimizing the total import was chosen as one of the control strategies due to the long-term vision of Statsbygg that Campus Evenstad would become 100% self-sufficient with electricity. The results show that the battery is not frequently used when applying this control strategy; the battery is simply discharged to reduce the total import. Any recharging of the battery is due to high PV production in times of low load demand.
- The minimization of spot energy cost control strategy results in rapid charge and discharge of the battery. As stated in Section 4.3, the lifetime of the battery is highly dependent on the number of charge and discharge cycles that the battery undergoes and the DoD of the battery. The deeper the battery is discharged, the more battery capacity is lost, and hence the battery lifetime is reduced. Based on this, the implementation of the minimization of spot energy cost control strategy could possibly impact the lifetime of the battery at Campus Evenstad. However, due to the small size of the battery and the restriction that the battery must at all times be able to deliver 100 kWh usable energy, the DoD of the battery is only approximately 50% which is considered low. The minimization of the spot energy cost control strategy reduces the energy cost of the imported electricity, but low spot prices result in higher peaks, which in turn results in

higher total costs. From the 48-hour time period results in Section 8.2.1, it is evident that the occurrence of the peak may also shift as a result of implementing this control strategy. As long as the new import peak does not exceed the initial import peak, it will not impact the grid tariff cost.

- Using the battery to perform peak shaving may significantly reduce the grid tariff. Even though spot prices are not considered in this control strategy, the total cost of imported electricity is reduced compared to the other control strategies. Reducing the import peak may also lead to that more of the self-generated electricity is used on-site instead of being exported to the grid.

Cases

- Doubling the PV production naturally has a bigger impact of the battery use in summer than it does in winter. The total import costs of all control strategies are lower when the PV production is doubled compared to the other cases. Doubled PV production also leads to some export of energy to the grid. The exportation of electricity represents a source of income that is not included in the cost calculations. However, exporting electricity at one price and importing it again at a later time at a higher price is not economically beneficial. As the installed PV capacity at Campus Evenstad is small compared to the load demand, it could be interesting to see how tripling the PV production would impact both the use of the battery and the grid tariff costs. However, as the PV production in November is very low due to few sunlight hours and small levels of solar radiation, a tripling of the PV production is not expected to impact the import peak significantly.
- Doubling the installed battery capacity enabled a greater peak reduction which in turn leads to lower grid tariff. However, due to the large energy storage potential that the battery holds under this assumption, more electricity is imported to recharge the battery, hence resulting in higher total costs. Both when the objective is to minimize the total import and when the objective is to perform peak shaving, the battery is infrequently used when the installed battery capacity is doubled.

It is important to emphasize that uncertain data is used in the optimization. For instance, the load demand is estimated based on historical data, and the PV production is estimated from the constructed PV model. In addition, the CHP plant, which contributes to the on-site electricity generation, is not modelled but set to be running on maximum in winter and completely cut off in summer as stated in Section 7.2.2. However, although the input data may be inaccurate, the main principles of the different control strategies and cases will still apply.

Chapter 9

Conclusion

This thesis represents a building block for future model predictive control of a battery system coupled with a grid-connected PV system. The aim of this thesis was to (a) develop a PV model to predict the PV system performance, and (b) test and analyze various control strategies of the battery.

Some built-in functions in the PVLIB library in Python were used in the handling of the input solar radiation, to decompose and transpose measured GHI into POA irradiance. Based on the testing and validation of the developed PV model in this thesis, the PV model proved to give accurate estimations of the PV performance of the PV system at Campus Evenstad in summertime. In wintertime, the built-in irradiance functions proved to be inaccurate. This shows the complexity of decomposing and transposing global solar radiation measured on a horizontal plane into POA irradiance for a specific tilt angle, especially in Northern countries. The PV model was tested with two irradiance decomposition methods, various overall PV system efficiencies, and surface types representing different albedo values. The `dirindex` irradiance decomposition method together with an overall system efficiency of 74% and surface type *asphalt* resulted in the most accurate PV estimations compared to historical measured PV performance.

Three control strategies were implemented in the optimization model of the battery: minimization of total importation of electricity, minimization of spot energy cost, and peak shaving. The intention of the optimization model was not to find the optimal use of the battery at Campus Evenstad. Rather, the goal was to investigate different ways a battery in a complex energy system could be used based on various optimization objectives. The main findings of tested control strategies are as following:

- Optimizing the utilization of the battery with the objective of minimizing total import results in an inactive use of the battery. The battery is only recharged when the PV production is higher than the load demand.
- Minimizing the spot energy cost, the battery is frequently charged and discharged. Using the battery for this purpose may result in an increased import peak, and the occurrence of the import peak may change.
- The peak shaving control strategy leads to a reduction of the total cost of imported energy. However, the way the peak shaving control strategy is implemented in the optimization model is not very efficient as several iterations are necessary to reach the optimal result.

Both the minimization of total import and the peak shaving control strategy resulted in a rather inactive use of the implemented battery when simulating for a whole year. Naturally, if the utilization of the battery was optimized for shorter time periods, e.g., 24 or 48 hours, the hourly battery content curve would look different than in the yearly simulations.

Suggestions to further work, both with regards to the improvement and further testing of the developed PV model and the optimization model, and with respect to performing model predictive control of the battery in the future, are given in Chapter 10.

Chapter 10

Further Work

This thesis represents a building block for future model predictive control of a battery connected to a PV system. In order to determine the hourly utilization of the battery, the hourly load demand and the hourly on-site electricity generation must be known. In this thesis, a model, predicting the PV performance based on measured meteorological data, has been developed. The model is solely tested with historical meteorological data, but forecasted meteorological data may also be used. Campus Evenstad has been used as a case study in this thesis. A CHP plant also contributes to the on-site electricity production at Campus Evenstad. The CHP plant at Campus Evenstad is heat driven, and as this thesis solely focuses on the electrical energy flow, it was considered out-of-scope to model the CHP plant. In order to predict the use of the battery, all on-site energy sources should be accounted for. Further work in order to achieve model predictive control of the battery should therefore include:

1. Load demand forecasting.
2. Heat demand forecasting, which in turn determines the electricity generation of the CHP plant.
3. Manipulation of the weather forecast to extract expected site-specific GHI values.

As illustrated and discussed in Section 8.1, the developed PV model highly overestimates the PV production in winter when solar radiation is low. An overestimation of the PV production would indicate that less import of electricity is needed than what is the actual case. In order to get accurate estimations of the PV performance in all periods of the year, the developed PV model should be improved. As previously discussed, the largest source to error in the PV model is the decomposition and transposition of input GHI into POA irradiance. In

this thesis, built-in functions in the PVLIB library were used to estimate the POA irradiance for the PV system at Campus Evenstad. Improving the accuracy of the developed PV model includes testing other irradiance decomposition and transposition methods - methods that adapt better to high latitudes and colder climates.

With regards to the control of the battery, three control strategies have been tested and analyzed in this thesis. These three control strategies may not be ideal for determining the operation of the battery in the specific case of Campus Evenstad, but they illustrate the flexibility that the battery provides for the end-user. It could be advantageous to test other control strategies than the ones presented in this thesis, or, perhaps even more interesting, to combine the different control strategies. When introducing the peak shave control strategy in Section 7.2.4, the benefit of performing peak shaving in times of grid peak was briefly discussed. An alternative control strategy of the battery could be to reduce the peak in times where the grid normally experiences their peak. In practice, a time range for when the peak should be reduced would have to be specified in the model. As described in Section 5.7, the typical power peaks that are often found in residences, do normally not take place in tertiary industries (Campus Evenstad goes under the category tertiary industry based on its operation). However, the grid itself will still experience peak periods. Optimizing the utilization of the battery to minimize grid peaks could, therefore, be an interesting control strategy to analyze.

Bibliography

[1] REN21. *Renewables 2018. Global Status Report*. Tech. rep. REN21 Secretariat, 2018. URL: http://www.ren21.net/wp-content/uploads/2018/06/17-8652_GSR2018_FullReport_web_-1.pdf (visited on 06/16/2018).

[2] Norsk Solenergiforening. *Om solenergi - Solceller*. URL: https://www.solenergi.no/solstrm/ (visited on 06/17/2018).

[3] Accenture and Word Wilde Fund for Nature. *Mot lysere tider. Solkraft i Norge - Fremtidige muligheter for verdiskaping*. Tech. rep. URL: http://awsassets.wwf.no/downloads/solkraft_i_norge___fremtidige_muligheter_for_verdiskaping.pdf (visited on 06/16/2018).

[4] Q. Lin et al. "Optimal control of battery energy storage system integrated in PV station considering peak shaving". In: *2017 Chinese Automation Congress (CAC)*. Oct. 2017, pp. 2750–2754. DOI: 10.1109/CAC.2017.8243243.

[5] Multiconsult and Asplan Viak. *Solcellesystemer og sol i systemet*. Tech. rep. Solenergiklyngen, 2018. URL: https://static1.squarespace.com/static/597512eb579fb3d3de0207aa/t/5aaef19d562fa7d5c7274b84/1521414583385/Rapport_solkraft_markedsutvikling_2017.pdf (visited on 06/17/2018).

[6] Maren Haugland Hansen and Lene Marie Rognan. "Small-Scale Stand-Alone Photovoltaic Systems in Rural Areas". Specialization Project. 2017.

[7] Øystein Holm. *Energilagring ved Campus Evenstad*. Tech. rep. Multiconsult, 2017.

[8] Thomas Markvart. *Solar electricity*. eng. 2nd ed. Energy engineering learning package. Chichester: Wiley, 2000. ISBN: 0471988529.

[9] Gilbert M Masters. *Renewable and efficient electric power systems*. eng. 2nd ed. Hoboken, N.J: Wiley, 2013. ISBN: 9781118140628.

[10] John A. Duffie. *Solar engineering of thermal processes*. eng. 4th ed. 2013. ISBN: 1-118-67160-0.

[11] Øyvind Byrkjedal, Anne Line Løvholm, and Sónia Liléo. *Resource mapping of solar energy - An overview of available data in Norway*. Tech. rep. Kjeller Vindteknikk, 2013.

[12] Jan Kleissl. *Solar energy forecasting and resource assessment*. eng. 1st ed. Oxford: Academic Press, 2013. ISBN: 0-12-397772-X.

[13] John Boland, Jing Huang, and Barbara Ridley. "Decomposing global solar radiation into its direct and diffuse components". eng. In: *Renewable and sustainable energy reviews* 28 (2013), pp. 749–756. ISSN: 1364-0321.

[14] Matthew Lave et al. "Evaluation of Global Horizontal Irradiance to Plane-of-Array Irradiance Models at Locations Across the United States". eng. In: *Photovoltaics, IEEE Journal of* 5.2 (Mar. 2015), pp. 597–606. ISSN: 2156-3381.

[15] Deutsche Gesellschaft für Sonnenenergie (DGS). *Planning and Installing Photovoltaic Systems: A Guide for Installers, Architects and Engineers*. eng. 3rd ed. Planning and Installing. Florence: Taylor and Francis, 2013. ISBN: 9781849713436.

[16] Sudipta Chakraborty. *Power Electronics for Renewable and Distributed Energy Systems : A Sourcebook of Topologies, Control and Integration*. eng. Green Energy and Technology. 2013. ISBN: 1-4471-5104-6.

[17] *PVWatts Version 5 Manual*. Tech. rep. National Renewable Energy Laboratory (NREL), 2014. URL: https://www.nrel.gov/docs/fy14osti/62641.pdf (visited on 06/23/2018).

[18] Ned Mohan. *Power electronics : converters, applications, and design*. eng. 3rd ed. Hoboken, N.J: Wiley, 2003. ISBN: 0471226939.

[19] SMA Solar Technology AG. *Sunny Boy 3000TL/3600TL/4000TL/5000TL With Reactive Power Control*. URL: http://files.sma.de/dl/15330/SB5000TL-21-DEN1551-V20web.pdf (visited on 04/21/2018).

[20] Christian Julien et al. *Lithium Batteries : Science and Technology*. eng. 2016. ISBN: 3-319-19108-X.

[21] Shriram Santhanagopalan. *Design and Analysis of Large Lithium-Ion Battery Systems*. eng. Norwood: Artech House, 2014. ISBN: 1-60807-714-4.

[22] Paul Komor and John Glassmire. "Electricity Storage and Renewables for Island Power: A Guide for Decision Makers". In: *International Renewable Energy Agency (IRENA), Bonn, Germany* (2012).

[23] MIT Electric Vehicle Team. *A Guide to Understanding Battery Specifications*. Tech. rep. MIT - Massachusetts Institude of Technology, 2008. URL: http://web.mit.edu/evt/summary_battery_specifications.pdf (visited on 07/01/2018).

[24] Eva Thorin, Jan Sandberg, and Jinyue Yan. "Combined Heat and Power". eng. In: 2015.

[25] Therese Bjørånesset Åsheim. "Analysis of a Photovoltaic Power Plant at Evenstad". Master's Thesis. Norwegian University of Science and Technology (NTNU), 2017. URL: http://hdl.handle.net/11250/2454738.

[26] Bruno M. T. Malavasi and Igor Sartori. *PV Monitoring System. Assessment for Økern sykehjem project*. Tech. rep. SINTEF Building and Infrastructure, 2014.

[27] M. Blumthaler, W. Ambach, and R. Ellinger. "Increase in solar UV radiation with altitude". In: *Journal of Photochemistry and Photobiology B: Biology* 39.2 (1997), pp. 130–134. ISSN: 1011-1344. DOI: https://doi.org/10.1016/S1011-1344(96)00018-8. URL: http://www.sciencedirect.com/science/article/pii/S1011134496000188.

[28] Sunny Portal. *2322 Evenstad-Hoiskolen-Laven PV System Profile*. URL: https://www.sunnyportal.com/Templates/PublicPageOverview.aspx?page=998f37a6-50bd-4d84-837e-183c9336c88b&plant=225ab166-58fb-4816-8fa0-9e34e7377b3d&splang=en-US (visited on 04/23/2018).

[29] Government.no. *Electricity certificates*. URL: https://www.regjeringen.no/en/topics/energy/renewable-energy/electricity-certificates/id517462/ (visited on 06/27/2018).

[30] Velaug Amalie Mook, Rebecca Norrie-Moe, and Anne Glomnes Rudi. *Status of NVE's work on network tariffs in the electricity distribution system*. 2016. URL: http://publikasjoner.nve.no/rapport/2016/rapport2016_62.pdf (visited on 02/25/2018).

[31] Eidsiva Nett. *Nettariff i distribusjonsnettet*. URL: https://www.eidsivanett.no/globalassets/dokumenter/priser/priser_bedrift_effektmalt2.1.pdf (visited on 07/03/2018).

[32] Eidsiva Energi. *InnlandsSpot*. URL: https://www.eidsivaenergi.no/stromavtaler/innlandsspot/ (visited on 06/28/2018).

[33] Nord Pool. *Historical Market Data*. URL: https://www.nordpoolgroup.com/historical-market-data/ (visited on 07/03/2018).

[34] Eisa Almeshaiei and Hassan Soltan. "A methodology for Electric Power Load Forecasting". In: *Alexandria Engineering Journal* 50.2 (2011), pp. 137–144. ISSN: 1110-0168. DOI: https://doi.org/10.1016/j.aej.2011.01.015. URL: http://www.sciencedirect.com/science/article/pii/S1110016811000330.

[35] Torgeir Ericson and Bente Halvorsen. *Hvordan varierer timeforbruket av strøm i ulike sektorer?* Tech. rep. Statistisk sentralbyrå, 2008. URL: https://www.ssb.no/a/publikasjoner/pdf/oa_200806/ericson.pdf (visited on 06/28/2018).

[36] Linda Pedersen, Jacob Stang, and Rolf Ulseth. "Load prediction method for heat and electricity demand in buildings for the purpose of planning for mixed energy distribution systems". In: *Energy and Buildings* 40.7 (2008), pp. 1124–1134. ISSN: 0378-7788. DOI: https://doi.org/10.1016/j.enbuild.2007.10.014. URL: http://www.sciencedirect.com/science/article/pii/S0378778807002381.

[37] R. W. Andrews et al. "Introduction to the open source PV LIB for python Photovoltaic system modelling package". In: *2014 IEEE 40th Photovoltaic Specialist Conference (PVSC)*. 2014, pp. 0170–0174. DOI: 10.1109/PVSC.2014.6925501.

[38] W. F. Holmgren and D. G. Groenendyk. "An open source solar power forecasting tool using PVLIB-Python". In: *2017 IEEE 44th Photovoltaic Specialist Conference (PVSC)*. June 2017, pp. 1–4. DOI: 10.1109/PVSC.2017.8366167.

[39] Richard Perez et al. *The development and verification of the Perez diffuse radiation model*. Tech. rep. Sandia National Labs., Albuquerque, NM (USA); State Univ. of New York, Albany (USA). Atmospheric Sciences Research Center, 1988.

[40] Douglas C Montgomery. *Introduction to Linear Regression Analysis*. eng. 5th ed. Wiley Series in Probability and Statistics. Hoboken: Wiley, 2013. ISBN: 1-119-18017-1.

[41] Tarald O. Kvålseth. "Cautionary Note about R 2". In: *The American Statistician* 39.4 (Nov. 1985), pp. 279–285. ISSN: 0003-1305.

[42] Pyomo. *About Pyomo*. URL: http://www.pyomo.org/about (visited on 02/23/2018).

[43] Gurobi Optimization. *Gurobi Optimizer*. URL: http://www.gurobi.com/products/gurobi-optimizer (visited on 03/15/2018).

[44] pvlib-python. *API reference*. URL: http://pvlib-python.readthedocs.io/en/latest/api.html# (visited on 05/28/2018).

[45] Ibrahim Reda and Afshin Andreas. "Solar position algorithm for solar radiation applications". eng. In: *Solar Energy* 76.5 (2004), pp. 577–589. ISSN: 0038-092X.

[46] D.G. Erbs, S.A. Klein, and J.A. Duffie. "Estimation of the diffuse radiation fraction for hourly, daily and monthly-average global radiation". eng. In: *Solar Energy* 28.4 (1982), pp. 293–302. ISSN: 0038-092X.

[47] Richard Perez et al. "A new operational model for satellite-derived irradiances: description and validation". eng. In: *Solar Energy* 73.5 (2002), pp. 307–317. ISSN: 0038-092X.

[48] Richard E. Payne. "Albedo of the Sea Surface". In: *Journal of the Atmospheric Sciences* 29.5 (1972), pp. 959–970. URL: https://doi.org/10.1175/1520-0469(1972)029%3C0959:AOTSS%3E2.0.CO;2.

[49] PVsyst. *Albedo coefficient*. URL: http://files.pvsyst.com/help/albedo.htm (visited on 05/10/2018).

[50] *Albedo*. URL: https://en.wikipedia.org/wiki/Albedo (visited on 05/10/2018).

[51] P.G. Loutzenhiser et al. "Empirical validation of models to compute solar irradiance on inclined surfaces for building energy simulation". eng. In: *Solar Energy* 81.2 (2007), pp. 254–267. ISSN: 0038-092X.

[52] Richard Perez et al. "A new simplified version of the perez diffuse irradiance model for tilted surfaces". eng. In: *Solar Energy* 39.3 (1987), pp. 221–231. ISSN: 0038-092X.

[53] R. Perez et al. "Modeling daylight availability and irradiance components from direct and global irradiance". eng. In: *Solar energy* 5 (1990), pp. 271–289. ISSN: 0038-092X.

[54] Moslem Uddin et al. "A review on peak load shaving strategies". In: *Renewable and Sustainable Energy Reviews* 82 (2018), pp. 3323–3332. ISSN: 1364-0321. DOI: https://doi.org/10.1016/j.rser.2017.10.056. URL: http://www.sciencedirect.com/science/article/pii/S1364032117314272.

[55] NVE - Norges vassdrags- og energidirektorat. *Network tariffs*. URL: https://www.nve.no/energy-market-and-regulation/network-regulation/network-tariffs/ (visited on 06/12/2018).